

Oligodendrocyte progenitor cells in 3D hyaluronic acid scaffolds

A Thesis

Presented to

the faculty of the School of Engineering and Applied Science

University of Virginia

in partial fulfillment
of the requirements for the degree

Master of Science

by

Deniz B Unal

December 2019

APPROVAL SHEET

This Thesis
is submitted in partial fulfillment of the requirements
for the degree of
Master of Science

Author Signature: _____

This Thesis has been read and approved by the examining committee:

Advisor: Kyle Lampe

Committee Member: Steven Caliari

Committee Member: Chris Highley

Committee Member: _____

Committee Member: _____

Committee Member: _____

Accepted for the School of Engineering and Applied Science:



Craig H. Benson, School of Engineering and Applied Science

December 2019

Abstract

Demyelinating disorders of the central nervous system have few solutions based primarily on immunosuppressive/modulatory therapies. Tissue engineering is known for providing localized treatments where cells in a supporting scaffold can be implanted with the advantage of adaptability to time and space inside the host. In this work, we seek to understand the applications of oligodendrocyte progenitor cells in supporting scaffolds as these may be crucial to understanding complex pathological phenomena associated with this cell type, such as myelination. Chapter 1 focuses on the broad biomaterials applications already developed with these precursor cells and their myelinating differentiated counterparts to elucidate therapies for several disease pathologies. Finding structure property relationships to understand the degree of myelination that occurs as a function of mechanical cues has its challenges, however emerging 3D models are advocated as bridging contributions to the 2D in vitro and in vivo models already devised. Chapter 2 presents the use of oligodendrocyte progenitor cells in hyaluronic acid scaffolds where stiffness in the range of brain tissue is the independent variable and proliferation, metabolic activity, and viability are the dependent variables. This experimentation is important to understand the potential for using hyaluronic acid in this application in comparison to other scaffolding materials. We conclude that the most compliant hydrogels result in the greatest metabolic activity per cell, but all stiffness hydrogels support cells adequately. Once these basic relationships are developed, future work can focus on incorporating axon mimics into these hydrogels and trying to induce myelination to occur starting with process extension to the axon mimics. Hyaluronic acid scaffolds with hyaluronic acid axon mimics have shown promise as a biomaterial combination that promotes oligodendrocyte progenitor cell process extension and increased metabolic activity per cell in comparison to hyaluronic acid without axon mimics.

Acknowledgments

I would like to thank the University of Virginia for providing the opportunity to pursue this MS degree. In particular, I would like to thank my advisors Kyle J. Lampe and Steven R. Caliari for all of the support and guidance they have provided.

I've had a great group of graduate student lab mates to work with. I would like to thank Nick Murphy for all the plates and stock cell solutions he provided when I was low on cells. I would like to thank Edi Meco for talking through day-to-day issues in the lab. I would like to thank James Tang for helping me to think critically about my work. Erica Hui was instrumental to my understanding of Caliari Lab protocols including methacrylated/thiolated coverslips and MeHA/NorHA synthesis. Bev Miller was an incredible sounding board for life in general and a cheerful, optimistic lab mate to have around. Ivan Basurto was a master of ANOVA and an all-around great person to discuss lab life with. I would like to thank Greg Grewal, Julia Tumbic, and Jack Whitewolf for being friendly, helpful, and courteous lab mates in the Caliari Lab. Finally I would like to specially thank Lauren Russell for the tremendous support in guiding the project I was taking over for her and going through special procedures with me like primary cell extraction.

I mentored an undergraduate student while I was here. I would like to thank Emily Zezas for giving me a chance to be her mentor. She was inquisitive and hard-working, and I wish her the best of luck in her college career.

Finally I would like to thank my family: my father Ali, my mother Canan, and my brother Cagin. I couldn't have made it this far without your continuous love and support. I hope that this thesis will make our family proud.

Table of Contents

Chapter 1: Engineering Biomaterial Microenvironments to Promote Myelination in the Central Nervous System..... 6

 Myelination, Remyelination, and Demyelination in the Central Nervous System 7

 Disease Models for Remyelination 11

 Cellular Events in Demyelinating and Remyelinating Lesions 14

 Lessons from Developmental Cues that Influence Myelination 18

 Biomaterial Strategies to Enhance Remyelination in the CNS 20

 Predecessors to biomaterials: cell transplantation techniques 21

 Extracellular matrix (ECM)-mimicking hydrogels as useful biomaterial strategies for regeneration 22

 The effects of hydrogel stiffness and degradation on oligodendroglial and neural fate..... 28

 Micro- and nano-fibers as instructive biomaterials 32

 The influence of peptide and protein sequences in regeneration..... 36

 Drug Delivering Biomaterials to Control Spatial and Temporal Release 39

 The Impact of Emerging 3D Models 40

 Conclusion and Outlook..... 42

Chapter 2: A 3D Hyaluronic Acid Hydrogel Model for Studying Oligodendrocyte Progenitor Cells in the Context of Demyelinating Disorders of the Central Nervous System 44

 Introduction: 45

 Materials & Methods:..... 46

 Results & Discussion 53

 Mechanical Properties of NorHA Hydrogels 54

 Effects of Mechanical Properties on Proliferation, Metabolic Activity, and Cell Morphology 57

 Conclusions: 68

Chapter 3: Future Work: Fiber Encapsulation Studies with Hyaluronic Acid Hydrogels . 69

 Introduction: 69

 Materials & Methods:..... 70

 Mechanics of hydrogels with fibers..... 71

 Effects of encapsulated fibers on OPC proliferation and metabolic activity 75

Appendix..... 80

Appendix 1: MeHA HNMR spectrum, HA-TBA, and NorHA HNMR spectrum.....	80
Appendix 2: Protocols.....	83
Appendix 2-1: Flask preparation for OPC MADM cells in the Lampe Lab:	83
Appendix 2-2: Passaging on T-75 flasks in the Lampe Lab:	84
Appendix 2-3: Freezing cells down:.....	86
Appendix 2-4: Seeding frozen cells:	86
Appendix 2-5: MeHA macromer synthesis in the Caliarì Lab:.....	87
Appendix 2-6: NorHA macromer synthesis in the Caliarì Lab:	89
Appendix 2-7: Hydrogel without fibers preparation for 3D encapsulations	92
Appendix 2-8: Hydrogel with fibers preparation for 3D encapsulations	94
Appendix 2-9: Fiber stock solution preparation (where cell viability was present).....	94
Appendix 2-10: Fiber stock solution preparation (where cell viability was not present).....	95
Appendix 2-11: Electrospinning.....	97
Appendix 2-12: Oscillatory shear rheology.....	98
Appendix 2-13: Alamar Blue	99
Appendix 2-14: Pico Green	100
Appendix 2-15: Cell Glo	102
Appendix 2-16: Spheroid Volume Measurements	105
Appendix 2-17: Primary OPC extraction	106
Appendix 2-18: Surface modification of glass substrates using trimethoxysilane-based coatings.....	111
Appendix 2-19: 2D NorHA experiments.....	113
Appendix 2-20: Fixing and staining of 2D hydrogels at end of experiment	115
Appendix 3: Supplemental Data	116
Works Cited	124

Table of Figures

Figure 1 - The process of de- and remyelination	9
Figure 2 - Biomaterial design parameters to promote oligodendrocyte maturation and myelination or remyelination	23
Figure 3 - Hydrogel crosslinking impacts oligodendrocyte progenitor cell (OPC) proliferation	26
Figure 4 - Axon-mimicking electrospun fibers promote oligodendrocyte progenitor cell (OPC) ensheathment and oligodendrocyte (OL) maturation.....	34
Figure 5 - Biomaterial-mediated gene delivery promotes oligodendrocyte-mediated myelination following spinal cord injury	38
Figure 6 - ~20% of the hyaluronic acid repeat units were modified with norbornene functional groups. Norbornene was crosslinked with DTT and LAP to form hydrogels with PBS as the solvent. Hydrogels were crosslinked under 4 mW/cm ² (365 nm) light for two minutes	54
Figure 7 - (A) average storage moduli for each sample type from three batches (B) individual batch trials	55
Figure 8 - MADM OPC line encapsulated at 1wt% (wt/v) NorHA, 1.5wt%, and 2wt% all proliferated over a period of 7 days.....	58
Figure 9 - MADM OPC line encapsulated at 1wt% (wt/v) NorHA, 1.5wt%, and 2wt% all showed increases in ATP concentration over a period of 7 days.....	59
Figure 10 - MADM OPC line encapsulated at 1wt% (wt/v) NorHA, 1.5wt%, and 2wt% all showed increases in ATP/DNA concentration over a period of 7 days.....	60
Figure 11 - MADM OPC line encapsulated at 1wt% (wt/v) NorHA, 1.5wt%, and 2wt% all showed increases in metabolic activity over a period of 7 days when the incubation time was 4 hours.....	61
Figure 12 - 10 μm slices of NorHA hydrogels at 1wt% - 2wt%.....	63
Figure 13 - MADM OPC line encapsulated at 1wt% (wt/v) NorHA, 1.5wt%, and 2wt% all showed increases in fraction of average spheroid volume over a period of 7 days.....	64
Figure 14 - Average live spheroid volume was determined by thresholding the images and automatically calculating the spheroid volume.....	65
Figure 15 - MADM OPC line encapsulated at 1wt% (wt/v) NorHA, 1.5wt%, and 2wt% all showed increases in total spheroid volume over a period of 7 days.....	66
Figure 16 - The ratio of total live spheroid volume to dead spheroid volume was taken for all sample types.....	67
Figure 17 - SEM imaging of fiber mats shows individual fibers with consistent cross section and no signs of webbing between fibers.....	71
Figure 18 - (A) Fiber mats were electrospun on aluminum foil, gently scraped off the aluminum foil, and suspended in solution. (B) Using the cryostat, the fibers are shorter and more uniform in shape.....	72
Figure 19 - 10 μm slices of NorHA hydrogels with 0.18wt% MeHA fibers.....	75
Figure 20 - Pico Green assay for experimentation with fibers shows inconclusive results. (n=3) for each sample type.....	77
Figure 21 - Alamar Blue assay on hydrogels with and without fibers. (n=3) for all sample types. Fraction reduction values about 1.00 may be due to over-exposure of samples to ambient light.....	78
Figure 22 - Cell Glo assay shows similar trends to no fiber experiments when referring to ATP concentration as a function of stiffness. (n=3) for all time points.....	78
Figure 23 - ATP/DNA shows similar trends to no fiber experiments when referring to ATP concentration as a function of stiffness. (n=3) for all time points.....	79
Figure 24 - MeHA HNMR spectrum for 90% methacrylation efficiency.....	80

Figure 25 - HA-TBA HNMR spectrum.	81
Figure 26 - NorHA HNMR spectrum.	82
Figure 27 - Representative 2D experiment images with NorHA hydrogels.	118
Figure 28 - Process extensions were measured after 72 hours of culture in 2D coverslip experiments. ...	119
Figure 29 - Number of processes per cell were counted manually.	119
Figure 30 - NeuronJ plugin in Fiji was used to trace process extensions and measure their lengths.	120
Figure 31 - (A) Cells were counted as primary objects in Cell Profiler using the appropriate module. It was hypothesized that the best way to count process extensions would be as secondary objects (B) that were based on the profiles of the cell bodies. There is a separate module for counting secondary objects.	122
Figure 32 - GFP+ transfected MADM OPC cells with F-actin stain (red) and DAPI stain (blue). Large process extension was not observed after fixing these cells even though before fixing the cells seemed healthy and active.	123

Chapter 1: Engineering Biomaterial Microenvironments to Promote Myelination in the Central Nervous System

Deniz B. Unal¹, Steven R. Caliari^{1,2}, Kyle J. Lampe¹

¹Department of Chemical Engineering, ²Department of Biomedical Engineering, University of Virginia, Charlottesville, Virginia 22903, United States

Keywords:

Oligodendrocyte, myelin, biomaterial, tissue engineering, stem cell, central nervous system

Abstract:

Promoting remyelination and/or minimizing demyelination are key therapeutic strategies under investigation for diseases and injuries from multiple sclerosis (MS) to spinal cord injury, stroke, and virus-induced encephalopathy. Myelination is essential for efficacious neuronal signaling. This process is originated by oligodendrocyte progenitor cells (OPCs) in the central nervous system (CNS). Resident OPCs are capable of both proliferation and differentiation, and also migration to demyelinated injury sites. OPCs can then engage with these demyelinated axons and differentiate into myelin-forming oligodendrocytes (OLs). However this process is frequently incomplete and often does not occur at all. Biomaterial strategies can now be used to guide OPC and OL development with the goal of regenerating healthy myelin sheaths in formerly damaged CNS tissue. Growth and neurotrophic factors delivered from such materials can promote proliferation of OPCs or differentiation into OLs. While cell transplantation techniques have been used to replace damaged cells in wound sites, they have also led to poor viability, uncontrollable differentiation, and poor integration into the host. Biomaterial scaffolds made from extracellular matrix (ECM) mimics that are naturally or synthetically derived can improve transplanted cell

survival, support both transplanted and endogenous cell populations, and direct their fate. In particular, stiffness and degradability of these scaffolds are two parameters that can influence the fate of OPCs and OLs. The future outlook for biomaterials research includes 3D in vitro models of myelination / remyelination / demyelination to better mimic and study these processes. These models should provide simple relationships of myelination to microenvironmental biophysical and biochemical properties to inform improved therapeutic approaches.

Myelination, Remyelination, and Demyelination in the Central Nervous System

Myelination is the process of covering neuronal axons with a lipid-rich wrapping called the myelin sheath and is carried out by oligodendrocytes (OLs) in the central nervous system (CNS). This process increases the transmission rate and efficiency of electrical signal conduction through axons.¹ Myelination occurs from cell-cell interactions between glia and neurons, with the long-term result being a symbiotic relationship between an axon and oligodendrocytes.² Axons with diameters larger than 0.2 μm are selectively wrapped while smaller axons are not.³ Most studies of myelin membrane assembly have focused on the major myelin proteins: myelin basic protein (MBP) and myelin proteolipid protein (PLP), as these proteins compose 80% of the total myelin protein.⁴

OLs clearly provide axonal support via insulating myelin, but they also serve a broader role. Recent studies highlight the role of OLs in providing trophic support to axons, possibly through metabolic coupling.⁵ A PLP1-null mouse model,⁶ which leads to normal-looking CNS myelin sheaths but development of axonal swellings and degeneration at 6-8 weeks,^{7,8}

showed axonal pathology that is similar to mitochondrial diseases. This raises the question as to whether oligodendroglial trophic support is needed for mitochondrial energy metabolism in axons.⁹ It is possible that OLs provide metabolic support to axons all along their length.⁹ In contrast to astrocytes, which have small axonal points of contact with the nodes of Ranvier,¹⁰ OLs engulf long axonal segments. The diffusion barrier to metabolites posed by the myelin, as well as an absence of glycogen in OLs rules out an isolated glycolysis support mechanism, however the coupling of astrocytes and OLs in gap junctions^{11,12} could provide a route for metabolites through the blood-brain barrier to myelin and the glial cytoplasm.⁹

Some diseases and injuries cause disruption of the myelin sheath in a process known as demyelination (**Figure 1**). The most common disease with this pathology is multiple sclerosis (MS). Demyelination is debilitating for motor function, which relies on quick, efficient transmissions of electrical impulses to transmit messages throughout the nervous system. As demyelination progresses, neurons undergo continuous conduction in place of normal saltatory conduction due to increases in conductance and intra-axonal sodium ion concentration.¹³ This leads to protease activation and axonal degradation, and ultimately neuronal loss.¹⁴ In myelin-related diseases, demyelination and axon loss are thought to be preceded by inflammation, excitotoxicity, and oligodendroglial injury.⁹ The order of events is debated depending on the type of model used. Experimental autoimmune encephalitis (EAE) is a common model of demyelination and frequently compared to multiple sclerosis. The EAE model reflects the prevailing opinion that inflammatory mechanisms and products of antibodies, T cells, and macrophages lead to demyelination in the majority of patients.¹⁵ In contrast, lesions from early MS patients show that OL damage and myelin destruction are the primary events followed by local microglia activation and proliferation and later by invasion of inflammatory cells.^{16,17}

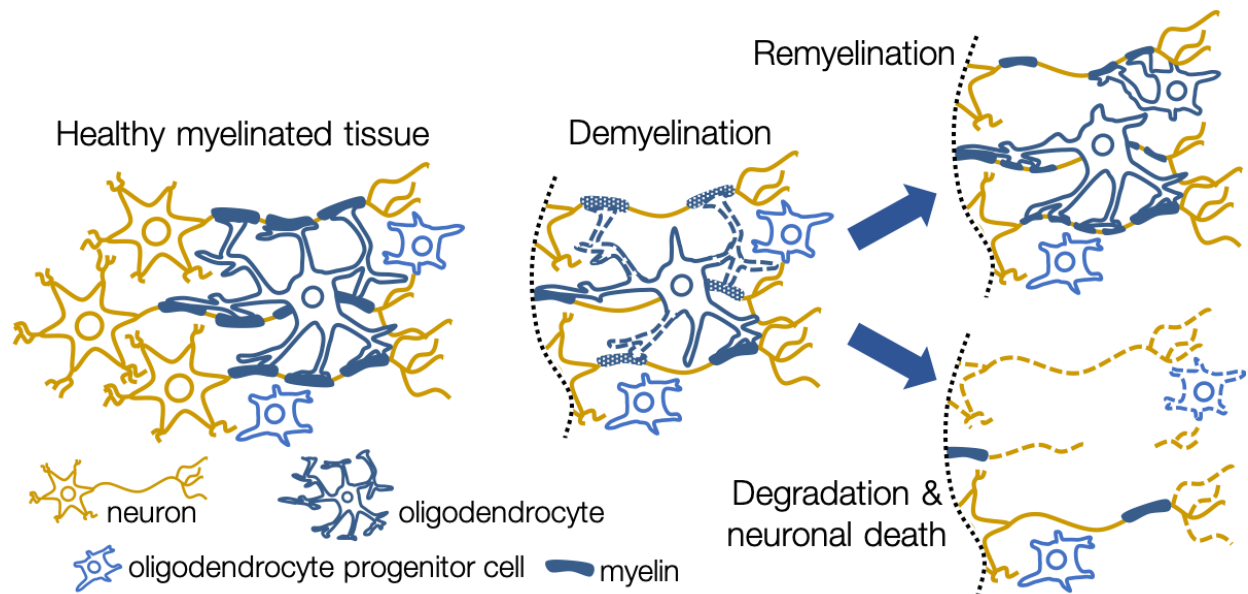


Figure 1 - The process of de- and remyelination

Healthy CNS tissue is full of oligodendrocytes (OLs) and oligodendrocyte progenitor cells (OPCs) as well as neurons (yellow) and astrocytes (not shown). Oligodendrocytes form an insulating myelin sheath, in discrete segments, covering mature neuronal axons. Typically a single oligodendrocyte is responsible for myelinating several neurons. During demyelination, myelin segments are degraded and lost, and the oligodendrocytes are damaged in the process. Unhealthy tissue can be remyelinated, as local OPCs move into the lesion, differentiate, and form new myelin, although new myelin sheaths are typically less robust (thinner and shorter) than the native healthy myelin. Alternatively, in clinical manifestations such as multiple sclerosis, remyelination often fails. In this case, demyelination can lead to complete loss of myelin in the lesion, death of oligodendrocytes, and ultimately axonal fragmentation and neuronal death. Preventing the loss of myelin and regenerating new myelin are strategies that could improve clinical outcomes. Therefore biomaterials that guide the fate of OPCs, direct OL maturation, and drive remyelination are clear targets to stimulate regeneration and functional recovery.

It has been known since the 1960s that remyelination occurs naturally.¹⁸ In fact, in the 1980s, the term “shadow plaque” was coined for MS lesions with areas of remyelination.¹⁹ To remyelinate axons, oligodendrocyte progenitor cells (OPCs) need to establish contact with the axons, express myelin genes, form myelin membranes, and ensheath the neuronal axons.²⁰ In the 1980s, studies showed that OLs up-regulate major myelin genes when neurons are present.²¹ At the time it was believed that while OLs could be provoked to form lipid-rich sheets containing myelin proteins in the absence of neurons, spirally wrapped sheaths only formed in the presence of neurons. Recent research over the past two decades has shown that neurons are not strictly required for myelination, as will be addressed further in this review. The control of myelination

through axonal maturity and connectivity to targets is a topic that is beginning to be addressed.²² For instance, blocking ion channels²³ and glutamate receptors²⁴ is being evaluated as a potential treatment technique by promoting axonal integrity through remyelination, or the process of forming new myelin in previously demyelinated tissue occurs spontaneously in some cases. The composition of myelin, synthesis method, and transcriptional regulators between developmental myelination and remyelination are similar,²⁵⁻²⁸ with the key difference being that remyelination produces layers that are thinner and shorter than expected.²⁹ Areas of remyelination can be identified by the abundance of thinly myelinated fibers³⁰ with shortened internodes (myelin segments) and widened nodes of Ranvier (the space between myelin segments) (Figure 1).³¹ The effect is most noticeable on large axons.¹⁴ Other characteristic features of remyelination include moderate reduction of axonal density,³¹ absence of macrophages with early myelin degradation products,¹⁹ and a low number of perivascular inflammatory infiltrates.¹⁹

Remyelination is mostly present in the early relapsing stages of MS and is rare in the late progressive stage of the disease.³² Remyelination starts to occur early after the onset of demyelination, while there are still macrophages loaded with myelin degradation products.^{33,34} Later studies suggested that such remyelination was transient³⁵ and periods of demyelination could negatively impact remyelinated shadow plaques.³⁶ Patient studies showed that subcortical white matter lesions in the cortex demonstrated more remyelination than periventricular lesions.^{19,37} The process of remyelination often localizes at sites of greater OL numbers, however the current consensus is that their precursors, OPCs, provide the remyelinating potential for mature OLs.^{29,38} Several lines of evidence support this theory stemming from cell transplantation studies after demyelination.³⁹⁻⁴¹ Following injury, OPCs are recruited through proliferative and possibly migratory mechanisms.²⁹ They enter an activated phenotype in response to a complex array of

signals initiated by the immune system.¹⁴ OPCs engage the demyelinated axons and differentiate into myelin-sheath-forming OLs.²⁹ Failure can occur at any stage, and clinical observations reveal that remyelination can gradually fail as demyelination progresses.⁴² In these scenarios, natural remyelination is unable to form strong, stable structures. As MS progresses, this lack of sufficient repair leads to irreversible losses in myelin and cell function.¹⁴ MS motivates the development of therapeutic approaches to permit or promote remyelination in lesion sites while minimizing demyelination. In addition to MS, remyelination is a critical process that is also inhibited after CNS injuries such as spinal cord injury.

Disease Models for Remyelination

The potential for recovery, in addition to the wide heterogeneity of patient outcomes in demyelinating diseases has motivated the development of multiple models for demyelination and remyelination. As a primary example, while remyelination occurs in a significant portion of lesions in MS,^{19,43} there is generally high variability in the level of remyelination seen across MS patient populations due to differences in genetics as well as immunological and growth factor profiles.⁴⁴ The common outcomes of these models include widespread primary demyelination that results in axonal degeneration, nerve cell loss, and dendritic/synaptic injury (Figure 1).⁴⁵ The demyelination models include toxin administration for regionally specific demyelination in the CNS and virus induced pathology tailored to resemble MS or any particular demyelinating disorder being studied.

The most widely used model based on the production of demyelinating lesions by toxins is the cuprizone model. This model has been used in mice, rats, and guinea pigs to induce primary demyelination that specifically occurs in the corpus callosum and superior cerebellar

peduncles^{46,47} to investigate the differentiation and maturation of OPCs in the early stages of remyelination.^{46,48,49} The copper chelating properties produce copper deficiency that inhibits oligodendroglia specifically for reasons that are not fully understood.⁵⁰ Myelin removal is reported via several pathways including stripping by microglial cells followed by phagocytosis, as well as translocation of all or parts of the myelin, creating naked axons.⁴⁶ Remyelinating OLs and precursors are found only around active sites of remyelination once the animals no longer receive a cuprizone-containing diet.⁴⁶ The processes of astrogliosis and demyelination are synchronized and astrogliosis progresses until maximal demyelination.⁵⁰ Studies in the corpus callosum did not find quantifiable structure-property relationships between the G ratio (the circumference of the axon divided by the circumference of the myelin sheath)⁵¹ and the axonal diameter.⁴⁹ Skripuletz et. al. studied the effects of astrocyte ablation in the cuprizone model, and found that there was a decreased regeneration of OLs after five to six weeks of cuprizone treatment and delayed myelin clearance in the corpus callosum.⁵² The effect on myelin clearance was eliminated when astrocyte ablation started at the peak of microglia activation.⁵² Remyelination was prevented in the astrocyte-ablated mice, indicating that clearance of myelin debris is necessary before remyelination can occur.⁵² Acute axonal damage occurred in greater amounts early after the cuprizone-diet cessation,⁵² but it was also present after long-term remyelination,⁵³ indicating that demyelination could still be detected during the remyelination phase.

In the lysolecithin model, the lipid lysolecithin produces demyelination when injected into the spinal cord or cerebellar peduncle myelinated fiber tracts. There is likely a two-pronged effect, where lysolecithin acts as a detergent that compromises the integrity of cell membranes (for which OLs are particularly susceptible as they are unable to metabolize lysolecithin, leaving concentrations in the cell membrane)⁵⁴ and furthermore activates monocytes,

macrophages, microglia, and lymphocytes to strip axons of their myelin.⁵⁵⁻⁵⁷ One of the key advantages of this model is that demyelination and remyelination phases can be separated; for example, the positive contribution of innate immune system to remyelination can be observed which is obscured in other models by myelin damage,⁵⁸ and there is only minimal axonal damage upon injection.⁵⁹ As an example of the model, Nogo-A neutralization enhanced spontaneous remyelination both three days after treatment and two weeks after treatment following a demyelinating insult in the adult rat spinal cord.⁶⁰ There was no effect on OPC proliferation, migration, or differentiation or on reactive astrocytes.⁶⁰ In SJL/J mice injected with lysolecithin in the spinal cord, spontaneous remyelination increased steadily over a period of 5 weeks but never reached the thickness observed in normal axons.⁶¹ Corticosteroid treatment with polyclonal IgG and anti-SCH Ig did not improve remyelination statistically, however mAb SCH94.03 and methylprednisolone showed a factor of 1.9 to 2.6 increase in the number of remyelinated axons per square millimeter of lesion area after 3 weeks.⁶¹ This suggests that increasingly specific Ig preparation increased remyelination.⁶¹ Interestingly, no decrease in macrophages was observed between the 94.03-treated group that enhanced remyelination and the anti-SCH Ig and poly-IgG groups which did not enhance remyelination, indicating different mechanisms of enhanced remyelination between methylprednisolone and 94.03.⁶¹ The antibody mAB SCH94.03 is found naturally in the serum of humans and mice and is polyreactive with a wide range of antigens without specific somatic mutations, indicating that certain natural autoantibodies can be promote a healing response to CNS injury even in nonimmune demyelination.⁶¹ The positive effects of immune responses in demyelinating disorders has been present throughout the decades with the lysolecithin model. In the cuprizone model, remyelination proceeds to completion in an age-dependent manner.^{48,62}

Other models use viral infections to include the role of adaptive immunity and mimic the pathology of diseases such as MS. Since viral infection has been suggested as a possible cause of MS,⁶³ this creates opportunities for immunotherapy development and testing. A collection of models that induce immune responses from CD4⁺ T cells have been created to mimic parts of MS pathology. These are known as experimental autoimmune encephalomyelitis (EAE) models.⁴⁵ In EAE models of MS, the chemokine and receptor combination CXCL12/CXCR4 are necessary for proper migration and survival⁶⁴ of OPCs. Blockade of this signaling limits OPC maturation during remyelination.⁶⁵ The EAE models have been useful for pre-clinical testing of immunomodulatory MS drugs, however they are not well suited for studying remyelination. The location of lesions is random and locating the lesions can be challenging.⁶⁶ The exact age of a single EAE lesion cannot be determined without continual magnetic resonance imaging.⁶⁶ Additionally, the evidence of remyelination following drug treatment in EAE is a secondary phenomenon of reducing inflammation.⁶⁶

Cellular Events in Demyelinating and Remyelinating Lesions

Engineering cell- and biomaterial-based therapies to treat myelin-related injuries and disease requires understanding of the native cellular events in demyelinating lesions and the discrete roles specific cell populations play in these events. The first responding cells to lesion sites are macrophages and microglia from the surrounding tissue that clean debris such as degraded myelin.⁶⁷ The activated microglial phenotype occurs when microglia are exposed to cell necrotic material, accumulated debris, and excess aberrant protein, but their phenotype reverts to non-reactive when these stimuli are removed.^{68,69} This phagocytic removal of degraded myelin occurs

slowly, for up to several months.⁶⁷ The myelin debris is characterized by inhibitory molecules such as NI250 and myelin-associated glycoprotein (MAG).⁶⁷

Microglia are well known for clearing debris after programmed cell death in the development of the CNS, as this process is necessary to maintain CNS homeostasis.⁷⁰ Clearance of debris and phagocytic phenotype is also critical for proliferation of OLs, differentiation of OPCs, and recruitment of new OPCs to the wound lesion site in MS to begin the remyelination process.⁷¹ In the lysolecithin mouse model, the depletion of macrophages reduced remyelination.⁷¹ Knocking out the microglial chemokine receptor CX3CR1 results in impaired remyelination because of the ineffective functioning of microglia and macrophages.^{71,72} In the EAE model, these positive effects of microglial recruitment and activation are mixed with detrimental autoimmune functions such as antigen presentation and proinflammatory cytokine production.⁷³ Microarray gene expression studies from the corpus callosum in the mouse cuprizone model showed evidence of microglial trophic support in remyelination, where microglia scavenge and reutilize sequestered cholesterol.⁷⁴ The significant upregulation of lysozyme in phagocytic microglia and wide abundance of Oil red O positive microglia shows the ingestion of tissue debris, corroborating this phenotype.⁷⁵ However, evidence of two distinct phenotypes for demyelination and remyelination has not been demonstrated.⁷⁵ The few significant changes in microglia phenotype were transiently induced during the demyelination phase.⁷⁵

After microglial activation, astrocytes are activated with a rapid increase in glial fibrillary acidic protein (GFAP) expression followed by the formation of fully stellarized, fibrillary astrocytes.⁴⁵ GFAP is a major intermediate filament protein (IFP) representing mature astrocytes and its upregulation is a prominent feature of reactive astrocytes. In addition to MS, this microglial activation occurs in many forms of brain injury including ischemia, traumatic brain injury, and

hypoxia. The formation of tightly interwoven fibrillary astrocytes creates a physical barrier between damaged and healthy tissue⁶⁸ known as a glial scar.^{67,76} Glial scarring occurs to limit the size of the injury, re-establish the blood-brain barrier, and reduce inflammation.⁷⁷ The activation of astrocytes is known to occur up to 1 cm from the injury in rats.⁶⁷ Degenerative axons and dying terminals have been suggested to be a trigger for such extracellular matrix production of GFAP by astrocytes.⁷⁸ A study in 2019 on patients with neuromyelitis optica (a perivascular inflammatory demyelinating disease historically considered as a form of MS but now regarded as a separate disease entity⁷⁹) has brought new evidence to light that astrocytes are destroyed together with myelin and oligodendrocytes in newly formed demyelinated lesions.⁸⁰ Ruptured astrocyte foot processes (extensions that form tight junctions with endothelial cells and regulate water, ion, and soluble factor diffusion in the blood brain barrier) are stained for aquaporin 4 (AQP4).⁸¹ In contrast to the prevailing current opinions of astrocyte pathology in MS, this study found that in post-phagocytic MS plaques, astrocytes undergo regressive changes through generation of aquaporin AQP4-negative gemistocytic astrocytes with large homogeneous milk-like cytoplasm descriptive of extreme but circumscribed neural degeneration.⁸⁰ These astrocytes are abnormal and not fully differentiated, and they contribute to changes in nerve conduction that accompany the onset of a clinical relapse of MS as well as the recovery of nerve conduction associated with remission.⁸² After stab wound,⁸³ spinal cord injury to the dorsal root,⁸⁴ and general spinal cord injury,^{83,85,86} astrocytes in their reactive state produce chondroitin sulfate proteoglycans (CSPGs) such as brevican, neurocan, neuron-glia antigen 2 (NG2), and tenascin,⁸⁷ major inhibitory components of glial scars.⁸⁸ Anti-NG2 antibody treatment prevents inhibition of axonal growth in vitro.⁸⁹ CSPGs can severely affect cytoskeleton and membrane components of growth cones as well as interfere with pathways that mediate inhibition such as the GTPase RhoA pathway.⁹⁰ Time-lapse images of

the dystrophic endings (bizarrely shaped growth cones that are incapable of robust regeneration and do not extend lamellopodia) show repeated attempts at endocytosis attempts at forming supportive membranes.⁹¹ CSPGs from the glial scar inhibit OPC migration as well as the morphological differentiation of OLs.⁸⁹ OPCs, OLs, meningeal cells (if the injury penetrates the meningeal surface of the brain or spinal cord), astrocytes, and multipotent progenitor cells are all recruited to the lesion site as well and can produce MAG and oligodendrocyte myelin glycoprotein (OMGP) that inhibit axon regrowth.^{87,67,92}

It has been thought since the mid-twentieth century that glial scarring is only detrimental to neuronal growth, preventing axonal regeneration.⁹³ Recent research suggests otherwise for ascending sensory tracts (ASTs) in mice. Ablating or attenuating the astrocytic scars fails to enable spontaneous axon regrowth in these studies.⁹⁴ A diverse array of cells including pericytes, fibroblasts, and inflammatory cells can produce CSPGs even when the astrocytic glial scar is removed. Conversely, the glial scar may include stimulatory molecules that promote regeneration in some unknown way.⁹⁴ The dual nature of the glial scar could be time-dependent, with beneficial effects during the acute phase of injury but prevention of axon growth in chronic or later stages. Attenuating astrocyte scar formation through blocking of integrin signaling two weeks after spinal cord injury leads to improved locomotor performance.⁹⁵ In contrast, ablation of reactive astrocytes five weeks after spinal cord injury did not promote axonal growth.⁹⁴ Unfortunately, neither study characterized the effects of scar ablation on other cells in the damaged CNS, so it is difficult to interpret whether microglia or macrophages are confounding factors.⁹⁶

Lessons from Developmental Cues that Influence Myelination

Biomaterials strategies for promoting (re)myelination represent a potentially promising approach. The recapitulation hypothesis has emerged in recent years with the notion that developmental myelination and remyelination should have similar processes in theory.⁹⁷ These strategies may be inspired by CNS developmental processes. While originally it was thought the OLs were homogeneous with origin in the neural tube, it is now widely believed that the OPC population is heterogeneous^{98–100} and specified based on domains distributed along the germinal neuroepithelium of the neural tube.¹⁰¹ There is an overproduction of OLs based on redundant sets of OPC populations with competition for targets resulting in significant OL death.¹⁰² Initial induction of OPC fate is regulated by the neural patterning cue sonic hedgehog (Shh) and antagonized by bone morphogenetic protein (BMP).^{103,104} Key transcription factors expressed include Olig1, Sox10, and Nkx2.2¹⁰⁵ while there is repression of negative regulators of fate such as Sox6 and Hes5.^{106,107} Many of these factors are upregulated both in development and after injury to the white matter.¹⁰⁸ Also in development, OPCs in the white matter express glutamate receptors^{109,110} and receive synaptic input^{109,111–113} from unmyelinated axons^{112,113} which allows them to receive and respond to neuronal activity. Using biomaterials to support an overabundance of OPCs with support from encapsulated transcription factors could provide the environment needed to form mature OLs in developmental-like cell concentrations.

After development in the ventricular zone of the embryonic brain and spinal cord, OPCs migrate significant distances using embryonic blood vessels as guide rails.¹¹⁴ Migratory OPCs are defined by the expression of PDGFR α .¹¹⁴ They are elongated along blood vessels with their cell bodies on the endothelial surface while having a single, long leading process along the vessel.¹¹⁴ Guidance cues are needed (such as an endothelial vascular scaffold) for migration

throughout the developing CNS.¹¹⁴ The endothelium expresses the chemokine/receptor combination CXCL12/CXCR4 throughout OPC developmental migration.¹¹⁴ Upon inactivation of CXCR4, Wnt-associated OPCs reverse their vessel-associated clustering behavior, demonstrating a Wnt-activated, CXCR4 dependent mechanism for OPC attraction to the vascular scaffold.¹¹⁴ Loss of function of CXCR4 leads to diminished migratory ability in the CNS, and CXCR4 is downregulated in the Wnt pathway where OPCs differentiate into OLs.¹¹⁴ Therefore it is through Wnt activation that OPCs mediate attraction to the vascular scaffold during migration while blocking differentiation, with the downregulation of these events leading to endothelial dissociation and differentiation.¹¹⁵ Migration proceeds through retraction of processes and repelling of cells from each other via contact-mediated cues, creating unique independent regions for each cell (sometimes referred to as “tiling”), while also responding to attractive and repellent biochemical cues such as Shh, Semaphorin 3A and 3F, Netrin-1, CXCL1, PDGF-AA, and tenascin-C.¹¹⁶ Despite these cues, migration seems to be stochastic¹¹⁶ and highly dependent on self-repulsion of OPCs through contact-mediated inhibition.¹¹⁷ Given appropriate mesh sizes in biomaterial scaffolds, migration to form organized cell clusters can be facilitated with polymer crosslinks acting as guidance rails.

Myelination occurs through sequential steps in maturation of the oligodendroglial lineage. Enrichment of specific immature OL populations in certain regions of the adult mouse brain¹¹⁸ suggests that differing mechanical properties of these regions can influence regional diversity of OL populations¹¹⁹ and explain why certain regions of the CNS are myelinated as opposed to others. Hughes et. al. found a positive correlation between OL differentiation, death, and proliferation of neighboring OPCs.¹²⁰ OPCs govern their cell density¹²¹ and local cell-cell interactions. During remyelination the OPCs differentiate into mature OLs, generate a myelin

membrane to ensheath local exposed axons, and then concentrically wrap and tightly compact to form the myelin sheath.⁵¹ An early strategy for promoting remyelination could be through enhancing OPC repopulation using factors like basic fibroblast growth factor (bFGF) and PDGF which are known to contribute to OPC proliferation.¹²² The ethidium bromide demyelination model (comparable to the lysolecithin model) found overproduction of OLs and controlled apoptosis similar to in development.¹²³ Remyelination tends to occur more effectively in areas with greater numbers of OLs.¹²⁴ The majority of signals that promote proliferation of OPCs also inhibit differentiation into OLs, and this phenomenon occurs naturally to ensure proper timing of axonal network distribution and proper distribution of myelinated white matter.⁴² Therefore, biomaterial strategies must be carefully tuned with regard to their ability to stimulate proliferation and/or differentiation: we might focus on selectively incorporating OPCs and then guiding their development to mature OLs.

Biomaterial Strategies to Enhance Remyelination in the CNS

Generally speaking, spontaneous remyelination is hindered by limited availability of OPCs, rate of proliferation of OPCs, migratory capacity of OPCs, limited differentiation into OLs,^{29,125} and myelinating ability of OLs in the later stages of wound healing. Human studies show divergent remyelination depending on the location of the lesion, the age of the patient, and the type of MS present.¹⁹ For example, in relapsing-remitting MS, two-thirds of all plaques were active in comparison to only one-third with secondary progressive MS. However, the failure of remyelination is a complex issue which is unlikely to be explained by dysregulation of a single factor. One reason for remyelination failure could stem from findings in ethidium bromide-induced demyelination lesions where glutamatergic synaptic are blocked. Remyelination is partially

regulated by glutamatergic synapses which keep OPCs in a proliferative state and prevent them from differentiating.¹²³ While cell transplantation techniques using OPCs have achieved some remyelination, the fate of transplanted cells is strongly influenced by the type of injury and the local microenvironmental signals (biomechanical and biomolecular). Additionally, the formation of scar tissue impedes the survival and directed differentiation of OPCs in the spinal cord injury lesion sites.¹²⁶ To achieve control over cell trafficking, survival, proliferation, and differentiation in vivo, the use of biomaterial systems can create supportive niches for the transplanted cells to include signaling molecules, cell-cell contacts, and cell-matrix adhesions.²⁰ In the following sections we discuss the use of various biomaterial strategies to enhance remyelination in the CNS.

Predecessors to biomaterials: cell transplantation techniques

The lack of recovery from disease and injury in the CNS originally encouraged the conclusion that repair via the generation of new cells was limited (at best) in the adult brain.⁸⁸ However, over a span of three decades, neurogenesis was found to occur in the hippocampus,¹²⁷ olfactory bulb,¹²⁸ and forebrain.^{129,130} The brain also has resident glia that can repopulate lost astrocytes and oligodendrocytes.^{131,132} When the endogenous repair processes are lacking or disrupted, cell transplantation may be a suitable strategy. For instance, numerous attempts have been made to integrate various cells after spinal cord injury: neural stem/progenitor cells (NSPCs),^{133,134} embryonic stem cells (ESCs),^{135,136} induced pluripotent stem cells (iPSCs),¹³⁷ mesenchymal stromal cells (MSCs),^{138,139} Schwann cells,¹⁴⁰ olfactory ensheathing glia,^{141,142} central glia, and differentiated progeny of these stem cell types.

Recently, ESC-derived NG2⁺ OPCs were shown to support axonal outgrowth for a week after implantation in the spinal cord post-injury, challenging the assertion that NG2 expression is always inhibitory (particularly in the acute phase of spinal cord injury).¹⁴³ Functional

clearance of CSPG to make room for axon growth coincided with matrix metalloproteinase 9 (MMP-9) expression.¹⁴³ iPSCs derived from skin fibroblasts of primary progressive MS patients successfully differentiate into OPCs.¹⁴⁴ These cells were sorted for O4 and injected in vivo where they achieved mature OL differentiation, and formed compact myelin resembling the natural tissue.¹⁴⁴ The immunomodulatory role of MSCs makes them a candidate for MS treatment. Human bone marrow-derived MSCs can alter the endogenous neural responses to demyelination through production of a variety of neurotrophic factors^{145,146} that have neuroprotective functions.¹⁴⁷ Localization to the area of damage is likely to enhance suppression of inflammation and reduction of demyelination and axonal injury¹⁴⁸; such cell localization can be readily achieved by combining cell delivery with a material that assembles after injection. While cell-based therapies have shown some promise, downsides include lack of control over differentiation, poor survival, and ineffective integration into the host tissue.¹⁴⁹ Biomaterials may help localize transplanted cells to the desired target site and aid host tissue integration. Furthermore, biomaterials applied as cell-instructive templates for either transplanted or endogenous cells can help support sustained cell viability and promote lineage specification of stem cells.

Extracellular matrix (ECM)-mimicking hydrogels as useful biomaterial strategies for regeneration

The CNS extracellular matrix (ECM) contains CSPGs, glycosaminoglycans (GAG) like hyaluronic acid (HA), and proteins such as laminin, fibronectin, and sometimes collagen.¹⁵⁰ These molecules are involved in regulating cellular proliferation, differentiation, and migration. Biomaterial strategies can help elucidate native cell-ECM interactions by allowing experiments to test specific, isolated interactions in a reductionist approach. Furthermore, engineered materials provide a great deal of design flexibility so that properties can be tuned to influence, and potentially

control, biological phenomena including progenitor cell proliferation, differentiation, and maturation (**Figure 2**).

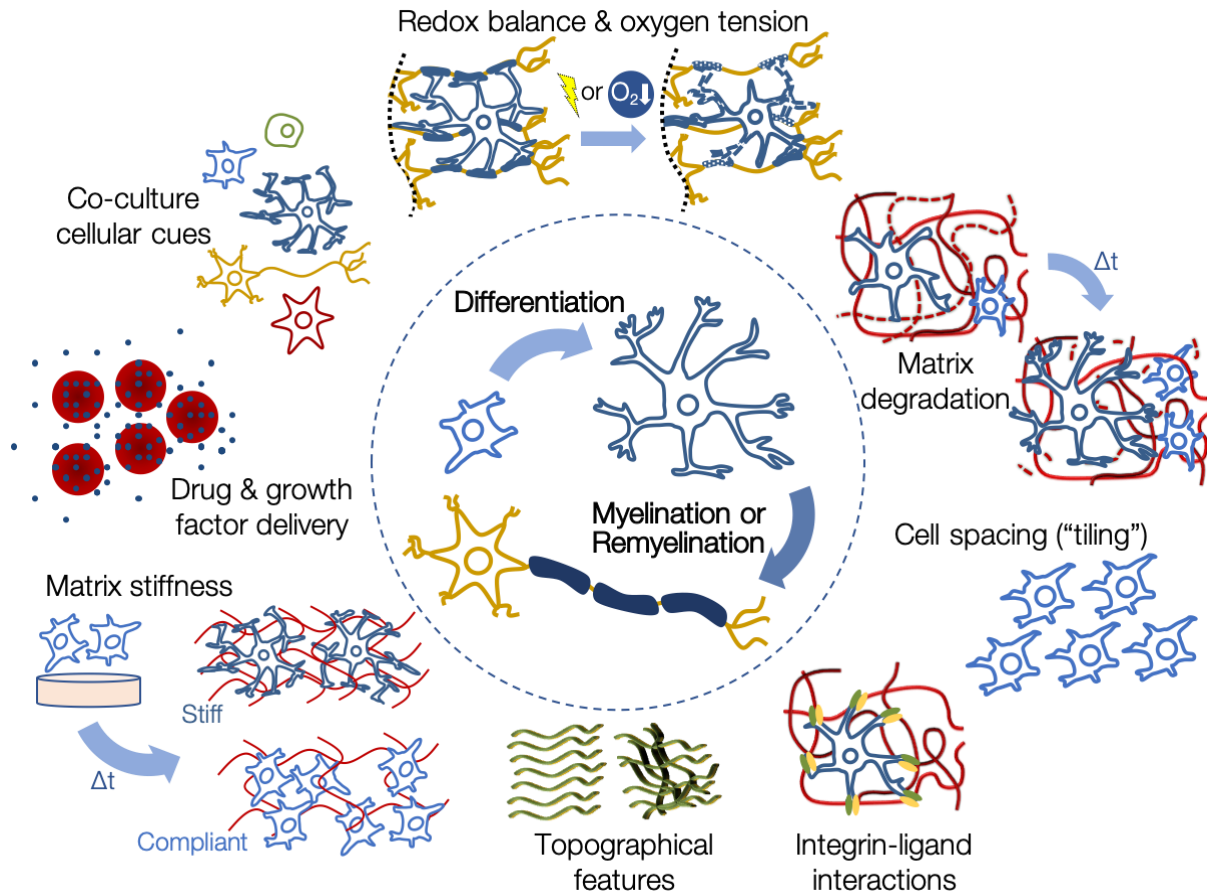


Figure 2 - Biomaterial design parameters to promote oligodendrocyte maturation and myelination or remyelination

Moving clockwise from top: *Redox balance & oxygen tension* can be controlled with materials designed to protect cells and scavenge superphysiological reactive oxygen species (ROS) during or after hypoxic (ultra-low oxygen) conditions and/or an influx of ROS produced during inflammation which negatively affect cell health. *Matrix degradation* can be engineered through hydrolytic and/or enzymatic mechanisms as well as external triggers such as light and affects cellular growth/phenotype, proliferation, and migration. *Cell spacing* can be controlled in a 3D matrix by encapsulating cells at a controlled density or placing cells in specific locations through advanced biomanufacturing technologies such as bioprinting and stereolithography. *Integrin-ligand interactions* are governed by biomaterial biochemistry and can be specified through controlled presentation of extracellular matrix (ECM)-derived domains known to activate cellular integrin receptors. *Topographical features* such as axon-mimicking fibers can promote myelination by emulating native physical structures, but orientation is clearly an important feature in guiding cellular outgrowth. *Matrix stiffness* is tuned through adjusting polymer content as well as crosslinking mode/density and affects cellular mechanotransduction, morphology, and overall phenotype. *Drug & growth factor delivery* vehicles can promote cell proliferation, migration, maturation, and scavenging of ROS by presenting factors with controlled release profiles in both space and time. *Co-culture cellular cues* are introduced through the various cell types used to promote myelination including neural stem/progenitor cells, oligodendrocyte progenitor cells, mature oligodendrocytes, neurons, astrocytes, and other CNS cells.

Natural brain tissue is enriched with sulfated GAGs rather than fibrous proteins¹⁵¹ and is non load-bearing and thus considerably softer than most other tissues. Brain has an elastic modulus, or stiffness, of about 200-1000 Pa, compared to 10^4 Pa for muscle and 10^9 - 10^{10} Pa for bone.¹⁵² Hydrogels, water-swollen polymeric networks, are particularly useful for CNS applications because they mimic the compliant environment while maintaining physical structure and facilitating cell migration as well as biomolecule transport.¹⁵³⁻¹⁵⁵ Hydrogels may be crosslinked using covalent or physical mechanisms, and can be created from a variety of sources: matrix harvested from animals or cells, synthetic polymers, yeast- or bacterial-produced GAGs, recombinant engineered proteins, and synthetic peptides. Furthermore, these materials are frequently combined in various ways to achieve a desired outcome.

In situ gelling hydrogels have been used extensively in the CNS because they are biocompatible, biodegradable, mechanically tunable, porous, permeable to diffusion of ions, nutrients, and waste products, and moldable to the shape of patient defects.¹⁵⁶ Many types of in situ gelling materials have resulted in desirable cell behavior in vivo. For instance, hyaluronic acid methyl cellulose hydrogels (HAMC) modified with RGD, a fibronectin-derived peptide promoting integrin-mediated cell adhesion, and PDGF-A showed enhanced OPC survival when compared to HAMC with only PDGF-A or HAMC alone in vitro.¹⁵⁷ These results were complemented by in vivo data demonstrating improved migration of OPCs from the injection site to the lesion site at two weeks post rat spinal cord injury with the RGD-modified biomaterial,¹⁵⁷ consistent with previous fibronectin studies of cell migration.^{143,158} This is encouraging, as the effectiveness of ECM-derived peptides like RGD in vivo has been questioned.¹⁵⁹⁻¹⁶¹ MBP expression was increased in the HAMC-RGD/PDGF-A group as well,¹⁵⁷ but mostly the positive effect was on host cells as opposed to engrafted cells which supports similar previous observations.¹⁶² Fibrin-based

hydrogels loaded with MSCs improved functional recovery and survival of transplanted cells in acute hemisection rat spinal cord lesions.¹⁶³ Remyelination occurred when OPCs were cultured in hyaluronic acid and gelatin hydrogels crosslinked with polyethylene glycol (PEG), however there were no direct relationships formed between hydrogel properties and survival of transplanted cells.²⁰ Poly(2-hydroxypropyl methacrylamide) (PHPMA) functionalized with RGD and transplanted into chronic balloon compression injured spinal cord, reduced tissue atrophy, improved migration of astrocytes and Schwann cells into the scaffold, and increased angiogenesis.¹⁶⁴

Commonly used hydrogels such as Matrigel (derived from mouse sarcoma) are complex and variable in composition¹⁶⁵ while fully synthetic hydrogels provide a chemically-defined environment with elegant control of chemical and physical properties. In between these options, hydrogels made from single ECM components can promote more specific cell-substrate interactions. In these hydrogels, the formation of native ECM structures such as fibers, pores, and ridges can provide important structural support for cellular organization, as well as physical cues for cellular interactions.^{166,167} ECM hydrogels derived from tissue at specific injury sites contain bioactive components that could uniquely benefit OPC and OL repair and remodeling. For instance, sulfated GAG concentrations are significantly reduced in spinal cord ECM compared to brain.¹⁶⁸ Like injury site-derived ECM from the brain and spinal cord, fibrin, a fibrillar protein found in blood plasma, can be polymerized to form a matrix comparable to the brain and spinal cord. Fibrin has been used as a scaffold for differentiation of endometrial stromal cells into OPCs,¹⁶⁹ support of axonal ingrowth after spinal cord injury,¹⁷⁰ and as a scaffold comparison to dosage-dependent cell transplantation studies after spinal cord injury.¹⁷¹

Hydrogels made of synthetic materials such as poly(ethylene-glycol) (PEG) have been widely used to mimic hydrated, compliant CNS tissue. However, these materials require modification with cell-instructive ligands to possess bioactivity. Two different OPC lines have been encapsulated in 3D covalently-crosslinked, nondegradable PEG hydrogels. N20.1 and MADM OPCs proliferate in a wide array of PEG hydrogel stiffnesses, but larger increases in ATP and greater amounts of proliferation were observed in hydrogels with lower PEG macromer concentrations or higher macromer molecular weight correlating to lower stiffnesses and larger mesh sizes (**Figure 3**).¹⁶⁹ PEG is also commonly used to deliver growth factors^{172,173} and steroids¹⁷⁴ into the CNS in pre-clinical rodent models.

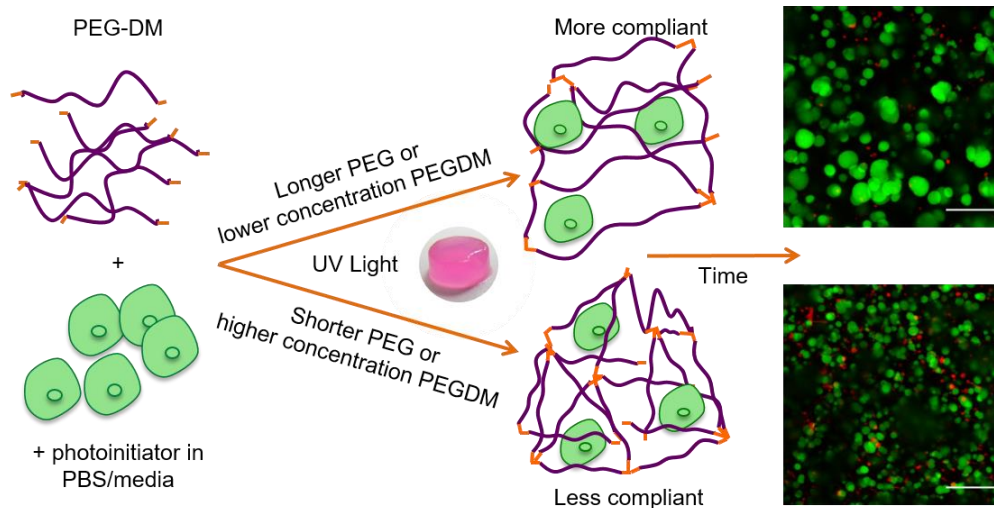


Figure 3 - Hydrogel crosslinking impacts oligodendrocyte progenitor cell (OPC) proliferation

OPCs can be combined with poly(ethylene)glycol-dimethacrylate (PEG-DM) macromer and a photoinitiator in cell culture media and briefly exposed to UV light to create a 3D hydrogel with cells distributed uniformly throughout. The hydrogel crosslinking and stiffness are readily controlled by adjusting the PEG molecular weight or concentration during crosslinking. These hydrogels are designed to approximate the mechanical stiffness of native tissue ranging from approximately 200-2000 Pa (storage moduli). Less crosslinked hydrogels have lower shear moduli and lead to greater proliferation of OPCs in the 3D culture system, observed via confocal microscopy as large multicellular spheroids. This strategy is advantageous in elucidating OPC response to matrix physical properties. Scale bars indicate 200 μ m. Figure reproduced from Russell, Lampe (2017) *ACS Biomaterials Science and Engineering*.

HA is a natural, degradable, non-immunogenic GAG found in the CNS ECM. Its functions are diverse and based in part on the molecular weight of the polymer, which ranges from thousands to millions of Daltons.¹⁵¹ HA is involved in forming perineuronal nets as well as regulating development, inflammation, angiogenesis, and regeneration.¹⁵¹ In general, the HA found in normal CNS tissues is high molecular weight (> 500 kDa) and is believed to help maintain NSC stemness^{151,175} and quiescence.^{175,176} Low molecular weight HA (< 30 kDa) may promote differentiation,¹⁷⁷ and mid molecular weight HA (~ 65 kDa) has demonstrated inhibition of OPC maturation and myelination.¹⁷⁸ High molecular weight HA decreases proliferation of astrocytes using non-integrin cell surface receptors including CD44, the receptor for hyaluronan-mediated motility (RHAMM), lymphatic vessel endothelial hyaluronan receptor 1 (LYVE-1), intracellular adhesion molecule 1 (ICMA-1), and toll-like receptors (TLR) 2 and 4.¹⁵¹ HA hydrogels have also been implemented in CNS repair. Crosslinked high molecular weight HA hydrogels implanted in rat spinal cords with dorsal hemisection injury reduced astrocyte proliferation and attenuated the inflammatory response and gliosis in the surrounding tissue.¹⁷⁹ CD44 and RHAMM can also promote cell adhesion and survival.¹⁸⁰ Evidence suggests that HA hydrogels support a vastly higher number of neurons in culture when compared to cultures maintained on standard collagen,⁹³ although this has yet to be tested in the context of OPC and OLs. HA is hydrophilic and polyanionic, and HA-based materials are typically modified with laminin-derived¹⁸¹ or fibronectin-derived¹⁶⁴ peptide sequences to support cell adhesion and growth.

Hydrogels formed from self-assembling peptide sequences also improve oligodendrocyte outcomes. For instance self-assembling peptide amphiphile hydrogels injected in a model of spinal cord injury resulted in increased numbers of oligodendrocytes at the injury site.¹⁸² A hydrogel based on the repeating RADA amino acid sequence (also known as Puramatrix) led to

improved remyelination after SCI as well, although this was attributed to an increase in Schwann cells, as OLs were not examined.¹⁸³ Recently developed hydrogels using a short AYFIL peptide sequence also show suitability for OPC culture.¹⁸⁴ These RAPID (for rapidly assembling pentapeptides for injectable delivery) hydrogels may be particularly conducive for delivery of viable OPCs to an injury or disease site as they attenuate the cell membrane damage caused when injecting a suspension of cells in media (a Newtonian fluid).^{184,185} Importantly, all of these peptide hydrogels are self-assembling physical hydrogels, with stiffness approximating that of native tissue.

The effects of hydrogel stiffness and degradation on oligodendroglial and neural fate

Stiffening of brain tissue occurs during development and maturation with mechanics varying by anatomical region and age. While there is some dependence on subregion, the overall trend clearly indicates a significant increase in stiffness with age.¹⁸⁶ Testing methods, loading conditions, and sample morphology all have impact on the measured mechanical properties, with many results in the literature contradicting each other.¹⁸⁷⁻¹⁹¹ In studies of human brain tissue, the elastic and viscous responses are regional-dependent but not directionally-dependent.¹⁸⁷ Indentation tests on the bovine brain show gray matter elastic modulus doubles from 310 ± 20 Pa prenatally to 680 ± 20 Pa postnatally, while white matter stiffness tripled from 450 ± 180 Pa prenatally to 1330 ± 640 Pa postnatally.¹⁹² At the same time, there is a wide variety of results in the literature reporting gray matter being substantially stiffer than white matter,¹⁹³ both having equal stiffness,¹⁹⁴ and white matter being stiffer.¹⁹⁵ The white matter contains high densities of myelinated axons, OLs, astrocytes, and microglia, and the local stiffness of white matter is highly correlated to the regional myelin content.¹⁹⁶

Changes in tissue stiffness in adults usually occurs as a result of injury or disease. For instance, MS acute demyelination leads to decreased tissue stiffness.¹⁹⁷ However chronic demyelination instead leads to increased tissue stiffness which is correlated with augmented ECM deposition.¹⁹⁷ This tissue stiffening often causes cells to behave abnormally.¹⁹⁸ Cellular integration and translation of mechanical cues to biochemical signaling (known as mechanotransduction) affects myriad cell behaviors including spreading, motility, and traction force generation¹⁹⁸, all critical processes for OPCs and OLs to reach a demyelinated site and generate or regenerate myelin. Matrix stiffness is also an important regulator of both differentiated and un-differentiated cell types in the nervous system, including OPCs and OLs.^{199,200} OLs are strong contributors to the load-bearing cellular microstructure,²⁰¹ however the possibly significant contribution of neurons, astrocytes, and microglia is not known.¹⁹²

Hydrogels that allow deformation and spreading to occur readily in 3D environments are desirable²⁰² since brain and spinal cord matter are the most compliant human tissues. For instance, the material effects of PEG-based hydrogels have been investigated on neural stem/progenitor cells (NSPCs) and their differentiation into neurons.²⁰³ NSPCs encapsulated in low concentration PEG-dimethacrylate (PEG-DM) hydrogels that have lower stiffness have higher metabolic activity, greater neuronal differentiation, less astrocytic differentiation, reduced indicators of glial scarring, and lower apoptotic activity.¹⁷³ Mechanical properties, most notably elastic modulus (stiffness), that best mimic the nature of brain tissue induce neuronal differentiation of MSCs and embryonic stem cells.²⁰⁴

Mechanical properties are useful for directing cell morphology. HA/gelatin hydrogels of 120 Pa supported the highest number of sprouting processes per OPC.²⁰ Higher stiffnesses (312 Pa and 624 Pa) resulted in more rounded cellular morphologies. These actin-based

processes culminate in the formation of myelin-like sheet lamella. Similarly in polyacrylamide / Matrigel hydrogels of ~ 1500 Pa and ~ 30000 Pa, less complex branching morphology was found in the stiffer substrates in both proliferating and differentiating media conditions.²⁰⁵ Collagen may also work well to drive OPC proliferation and differentiation according to recent studies. After culturing OPCs for three days in proliferation media, it was found that OPCs expressing A2B5 antigen developed short processes.²⁰⁶ When OPCs were cultured with dorsal root ganglia (DRG) for eight days, OPCs differentiated and formed multiple processes, and wrapped myelin sheath around the neurites of the DRG neurons.²⁰⁶ OPCs maintained round morphology after three days, but changed to an irregular morphology after eight days when differentiated, which suggests that OPCs can reconstruct the environment in the collagen microspheres.²⁰⁶ Other studies have shown that ECM components tend to enhance the biological properties of OPCs compared to non-ECM substrates,¹⁴³ and collagen and fibronectin are potential advocates for treating the injured spinal cord.

Mechanical properties can also be used to direct cell proliferation and differentiation. HA/gelatin hydrogels demonstrated the highest levels of OPC proliferation at an elastic modulus of 120 Pa, which is close to native CNS tissue.²⁰ The expression of Olig1 in the cytoplasm, necessary for membrane expansion and maturation,²⁰⁷ was higher in rigid matrices.²⁰⁵ The expression of differentiation and maturation markers (MBP and PLP) as well as cellular area and morphology were assessed in 6500 Pa polyacrylamide substrates with and without merosin, a factor known to promote differentiation of OPCs to OLs.²⁰⁸ Cells differentiated for 5 days displayed larger PLP area and MBP fluorescence intensity when cultured on polystyrene tissue culture plates coated with poly-D-lysine/merosin (PDLMN) as opposed to bare polystyrene plates.²⁰⁹ OPC migration efficiency on 2D polyacrylamide hydrogels was found to be greatest at

700 Pa.²¹⁰ Methacrylamide chitosan (MAC) hydrogel elastic moduli of less than 1000 Pa promote NSPC differentiation into astrocytes and neurons, while stiffnesses of 7000 Pa and greater drive oligodendrocyte differentiation.²¹¹ Analysis of MOG gene expression shows increased OL maturation and myelination on <1000 Pa MAC surfaces.²¹¹ In the developmental CNS, high MOG mRNA levels correspond to increased myelin deposition in the white matter where axons form and mature during development.²¹¹ Intermediate stiffnesses of 3500 Pa were best for proliferation.²¹¹

Hydrogels crosslinked to encapsulate cells can have fixed mechanical properties, but truly mimicking the ECM requires changes in mechanical properties on the time and length scales of cellular development, which is why degradation rates are often studied.¹⁵⁴ Tuning bulk properties and degradation rates is more straightforward with synthetic hydrogels compared to ECM-derived materials. The use of poly(α -hydroxy acids) such as lactic and glycolic acid to promote material degradation work well since they are biocompatible and metabolically recyclable by the body.²¹² In a potential side benefit, lactic acid has shown antioxidant properties, reducing the level of reactive oxygen species and the intracellular redox state,²⁰³ an important aspect in regulating OPC fate. More oxidized cellular states have led to differentiation of OPCs where more reduced states have led to self-renewal of these cells.²¹³ Biomaterial degradation is primarily engineered to proceed via either hydrolytic or enzymatic mechanisms. While hydrogels composed of natural biopolymers like collagen and fibrin degrade enzymatically,²⁰² synthetic materials must be designed to have this capability. A common way to achieve this is through the inclusion of matrix metalloproteinase (MMP)-cleavable crosslinkers. Cell-secreted MMPs cleave crosslinks in the hydrogel network, leading to local degradation that enables increased cell contractility and migration.

Micro- and nano-fibers as instructive biomaterials

Electrospun fibers can be produced in the nano- and micro- scale in random or aligned orientations. They provide a variety of useful advantages including high porosity, high surface area to volume ratio, and better mimicry of fibrillar protein architectures which are often necessary for representing the mechanical behavior of the ECM.¹⁵⁴ Nanofibers of 200-300 nm diameter are useful for OL culture since they accurately represent native axon diameters.²¹⁴ When cultured with nanofibers of 283 nm average diameter, NSPCs showed a 3-fold increase in OLs and 40% drop in NSPCs compared to tissue culture polystyrene.²¹⁴ In contrast, fibers with an average diameter of 749 nm showed the highest levels of neuronal differentiation.²¹⁴ The topographical cues of the ECM can also be mimicked through the fiber surfaces, and this will influence cell behavior through short and long-range biochemical cues.²¹⁴ For example, graphene-nanofiber scaffolds can lead to selective differentiation of neural stem cells into mature OLs without requiring culture media differentiation cues.²¹⁵

Self-assembling peptide (SAP) nanofiber scaffolds can simulate a true 3D environment with fiber dimensions 10-100 times smaller than cells.^{182,184,197} The most widely used SAP is RADA16-I, composed of 16 residues of alternating hydrophilic arginine, hydrophobic alanine, and hydrophilic aspartic acid.¹⁹⁷ When formed into a hydrogel, RADA16 has fiber widths of 10-15 nm and pores of 5-200 nm wide. This size range, combined with the compliant stiffness and physical gelation mechanism, allows cells to remodel the matrix, allowing migration, differentiation, and proliferation of NSPCs.¹⁹⁷ Functionalized 3D SAPs of RADA16-BMHP1 (laminin-derived motif), RADA16-BMHP2 (laminin-derived motif), and RADA16-RGD supported higher NPSC proliferation rates when SAP concentration was minimized, but 2D cultures still had higher proliferation overall.¹⁹⁷

Recently, electrospun fibers have been used to create *in vitro* systems that represent the spinal cord. Initial studies demonstrated that neural stem cells adhered more strongly on poly(L-lactic acid) PLLA fibers than on the PLLA 2D film controls.²¹⁶ Then, that same group showed that aligned fibers guided neurite extension along the length of the fibers.²¹⁷ Glass microfibers²¹⁸ and/or Vicryl²¹⁹ nanofibers were permissive to OL ensheathing and wrapping. Other recent work utilized electrospun fibers as artificial axons to study the role of fiber (axon) diameter on OPC myelination (**Figure 4**).²²⁰ Polystyrene fibers from 0.4 – 4.0 μm diameter showed increased concentric wrapping of fibers as well as increased expression of MBP and PDGFR α , markers of myelinating OLs and OPCs respectively.^{220,221} It was shown that fiber diameter was sufficient to initiate concentric wrapping by rat primary oligodendrocytes, and a minimum fiber diameter threshold of 0.4 μm was observed.^{220,221} Both OPCs and mature OLs showed similar relationships to the fiber diameter, and OPCs can ensheath the fibers before expression of differentiation markers like MBP.^{220,221}

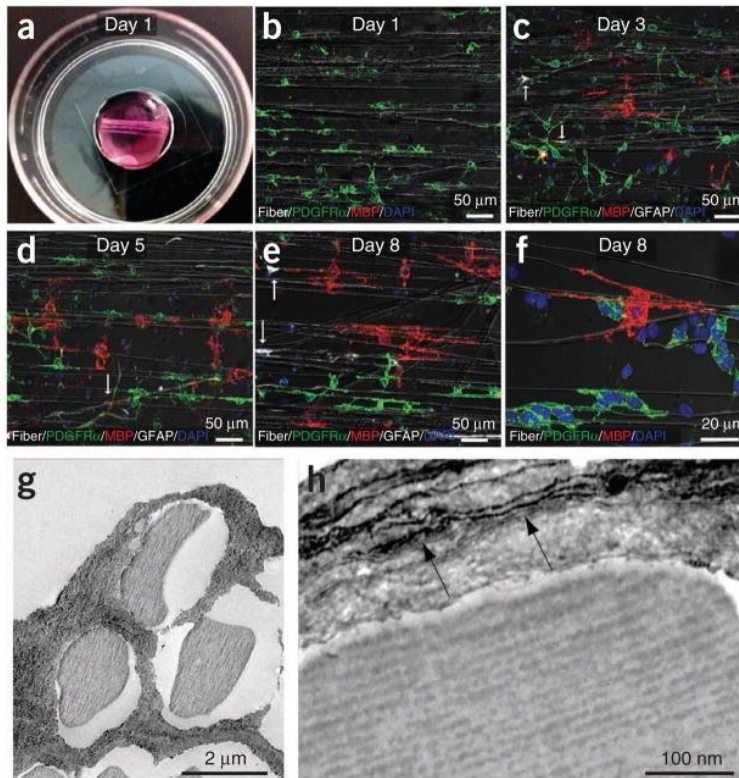


Figure 4 - Axon-mimicking electrospun fibers promote oligodendrocyte progenitor cell (OPC) ensheathment and oligodendrocyte (OL) maturation

Engineered biomaterials offer a path toward better understanding of the biophysical environmental cues that drive OPC maturation and myelination. In this work, primary rat OPCs were cultured on electrospun poly-L-lysine-coated polystyrene fibers with diameters that approximate the diameter of mature axons (2-4 μm). A) Suspended fibers were initially seeded with OPCs in platelet-derived growth factor (PDGF)-containing media. B) Immunostaining illustrates initial conformation of PDGF receptor α (PDGFR α , green)-positive OPCs to contact guidance cues provided by the fibers. C-F) Over the 8 days of culture, OPCs gradually extend processes toward neighboring fibers and express myelin basic protein (MBP, red), a marker of mature oligodendrocytes. G) Electron micrographs show ensheathment of fibers by OPCs on day 3 which later H) differentiate into OLs and deposit multiple layers of membrane (arrows) around a fiber. Together, these results suggest that engineered biophysical cues, namely fiber architecture/diameter, can drive OPC proliferation, organization, and maturation. Figure reproduced from Lee et al. (2013) *Nature Protocols*.

Soon after the work with OPCs on PLLA fibers in 2013, controlled delivery of microRNAs (miRs) was studied for its potential to affect OL lineage progression regulated OL development.²²²⁻²²⁴ Overexpression of miR-219 and miR-338 enhanced OPC differentiation and blockage of their expression inhibited OL maturation.²²⁵ These miRs were incorporated onto poly(ϵ -caprolactone) (PCL) electrospun fibers using a mussel-inspired bio-adhesive 3,4-dihydroxy-L-phenylalanine (DOPA) coating.²²⁶ Fiber topography alone (in the absence of miR

delivery) enhanced OPC differentiation.^{226,227} MiR-219/miR 338 cocktail treatment enhanced RIP expression (a marker of OPC differentiation), but its influence was higher on aligned small diameter (300 nm) fibers.²²⁶ Regardless of miR treatment, large-diameter fibers (2 μm) induced more MBP expression than small fibers (an indicator of OL maturation).²²⁶ Alignment also plays a role with MBP⁺ expression increasing by 3-5 fold on the aligned fiber groups (small vs. large) as opposed to 1-2 fold on the random fiber groups (small vs. large).²²⁶ Also similar to previous reports, fiber diameter and orientation affected gene uptake and gene silencing.²²⁸ The efficacy of miR-219/miR-338 cocktail in enhancing OPC differentiation and maturation under both proliferative and pro-myelinogenic conditions was similarly demonstrated by an aligned poly(caprolactone-co-ethyl ethylene phosphate) (PCLEEP) fiber scaffold stabilized by collagen embedment.²²⁹

In addition to electrospinning, 3D printing may also be used to create topographical templates for OPC growth, OL differentiation, and myelination. In one example, 3D printing was used to create an aligned scaffold for reliable identification of full circumferential wrapping. OPCs adhere to, engage and migrate along fibers and fiber bundles (PDMS, polyHEMA, and poly(HDDA-co-starPEG)) surface-functionalized with laminin and poly-D-lysine.²³⁰ A three-fold increase in myelination was observed on axons surface-coated with laminin as opposed to the nonspecific cell adhesion surface coating of poly-D-lysine.²³⁰ About three-fold OL engagement was observed with 140,000 Pa fiber stiffness than 400 Pa fiber stiffness for laminin-coated pillars of diameter 16 μm .²³⁰ Artificial axon diameters of 20 μm were infrequently engaged, which indicates that there is a maximum diameter above which myelin-rich wrapping does not occur efficiently.²²⁰ Future studies are focused on the effect of mechanical stiffness on remyelination in

axons less than $\sim 1 \mu\text{m}$ in diameter, as it is understood that axons in this range can either provide a permissive or restrictive cue for engagement and wrapping of axons.²²⁰

The influence of peptide and protein sequences in regeneration

Limited regeneration in CNS diseases is attributed to multiple factors including insufficient trophic factor support and up-regulation of axonal growth inhibitors.^{231,232} For instance, after spinal cord injury, there are many destructive processes including neuron and OL cell death, demyelination, inflammation, and deposition of a glial scar.^{231,232} Even in the developing brain and optic nerve, 20-50% of OPCs undergo apoptosis as they mature into OLs, which shows their dependence on limited mitogenic/survival factors.⁴² Promoting regeneration requires a multi-faceted approach.

The use of cell-instructive peptides takes advantage of native cell-ECM interactions to promote regeneration. Materials functionalized with thiolated YIGSR and IKVAV peptides support increased neurite outgrowth.²³³ Self-assembling peptide amphiphiles form cylindrical nanofiber hydrogels that inhibit glial scar formation, enhance differentiation of neural progenitor cells, and promote axon elongation when implanted in vivo in mice.¹⁸² Full length proteins can also be used to modify material bioactivity. Elastin-like proteins (ELPs) are engineered polymers mimicking the functionalities of tropoelastin and are characterized by the VPGXG pentapeptide repeat unit (where the guest residue, X, is any amino acid except proline) as well as their lower critical solution temperature (LCST) behavior. ELPs can be engineered to contain bioactive sequences such as RGD motifs and have been coated on PLGA scaffolds to improve adhesion-mediated proliferation and differentiation of NSPCs.²³⁴ Surfaces modified with higher amount of ELP matrix promoted higher cell adhesion and growth.²³⁴ ELPs can also be crosslinked into a hydrogel themselves. With a family of bioactive sequences, multiple ELPs can be combined to

work synergistically to induce differentiation of NSPCs. Elastin-mimetic polypeptide hydrogels showed increased dorsal root ganglia neurite outgrowth with RGD functionalization²³⁵ as well as being supportive of NSPC proliferation²³⁶ and this can now be applied in culturing other cells of the CNS.

Growth factors are known to regulate proliferation, differentiation, and migration of resident CNS cells. Some of the most well-studied growth factors and molecules to promote differentiation of OPCs to OLs are Shh, brain-derived neurotrophic factor (BDNF), neurotrophin-3 (NT-3), and thyroid hormone 3,3',5-triiodothyronine (T3). In particular, gradients of NT-3 and Shh during development have been suggested to contribute to recruitment and differentiation of progenitor cells within the spinal cord.²³² Shh enhances proliferation and differentiation of OPCs into OLs both in vitro and in vivo (**Figure 5**).²³² NT-3 promotes neuronal survival, sprouting of spared axons, and regeneration of injured axons after injury. The combined lentiviral delivery of NT-3 and Shh via a macroporous PLGA scaffold promoted axon extension and myelination with Shh specifically increasing oligodendrocyte-mediated myelination.²³² PDGF and fibroblast growth factor 2 (FGF-2) inhibited myelination while increasing the numbers of pre-myelinating OLs.²³⁷ These OLs are unable to myelinate until the PDGF is removed.⁴² There was no increased proliferation/differentiation in co-cultures of rat neurons and OPCs in response to neuregulin 1 (Nrg1).⁴²

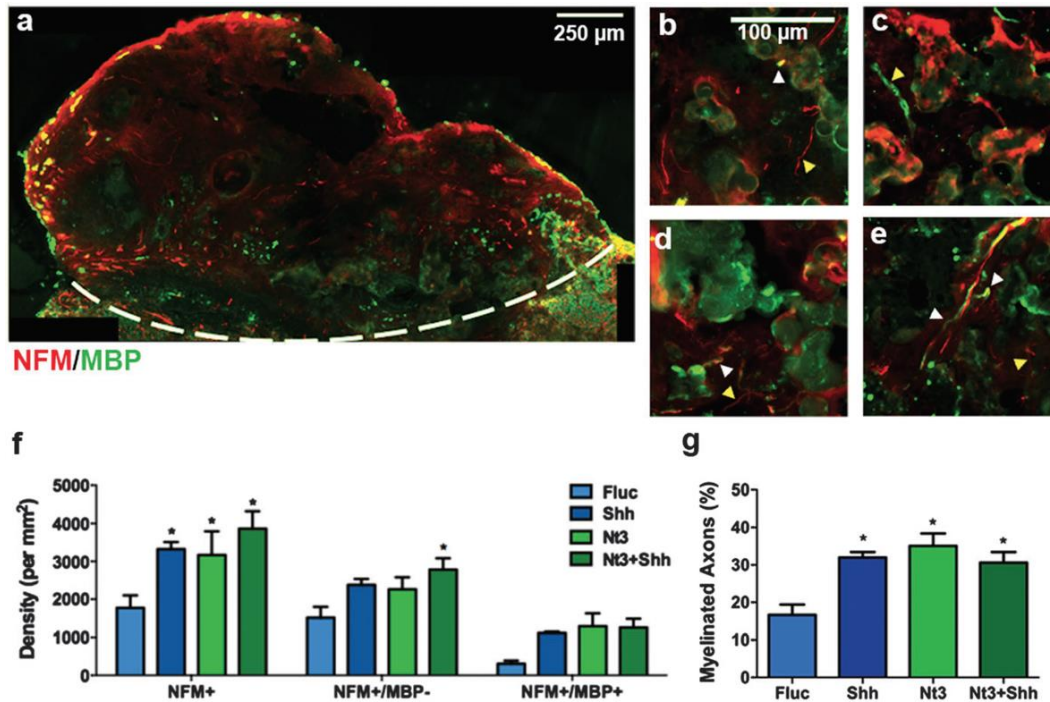


Figure 5 - Biomaterial-mediated gene delivery promotes oligodendrocyte-mediated myelination following spinal cord injury

Biomaterial-driven controlled delivery of small molecule drugs, proteins, RNA, and/or genetic information is a promising strategy for promoting tissue repair. In this work, heparin-modified poly(lactic-co-glycolic acid) (PLGA) constructs delivering lentivirus encoding for neutrophin-3 (Nt3) and/or sonic hedgehog (Shh) were applied in a mouse model of spinal cord injury. Notably, this biomaterial leveraged the following design considerations: i) highly porous, aligned microstructure to direct cell infiltration and organization, ii) gene delivery to promote sustained, localized benefits to tissue repair, and iii) translation of Nt3 and Shh, two proteins known to promote oligodendroglial proliferation and differentiation. A) Constructs delivering Shh show presence of myelin (MBP, myelin basic protein, green) on neuronal axons (NFM, neurofilament, red) along with groups delivering B) Firefly luciferase (Fluc), C) Shh, D) Nt3, or E) Nt3 + Shh. F) Quantification of axon density and G) Myelination in experimental groups. Figure reproduced from Thomas et al. (2014) *Integrative Biology*.

Brain-derived neurotrophic factor (BDNF) regulates oligodendrogenesis in the CNS.²³⁸ Treatment with other neurotrophins has been suggested to reduce disease burden in the EAE model by possibly enhancing oligodendrocyte survival. Transplanted NSPCs or MSCs may have trophic effects on the host CNS that enhance cell survival²³⁹ and endogenous remyelination.^{240–242} Interferon- γ ²⁴³ and glial cell-line derived neurotrophic factor (GDNF)²⁴⁴ have demonstrated neuroprotective functionality and promoted axonal growth respectively following spinal cord injury. Growth factors including ciliary neurotrophic factor (CNTF), Shh,²⁴⁵ vascular

endothelial growth factor-165 (VEGF₁₆₅), and epithelial growth factor (EGF),²⁴⁶ have been photopatterned into hydrogels such as agarose, HA, and PEG. The fact that NSPCs cultured on a GRGDS-modified agarose hydrogel migrated into the hydrogel along a Shh concentration gradient²⁴⁵ demonstrates that photopatterning can be used to control spatial orientation of growth factors and peptides to create 3D environments.

Drug Delivering Biomaterials to Control Spatial and Temporal Release

Polymeric drug delivery biomaterials such as micro- and nano-spheres, liposomes, and colloids can deliver biomolecules and cells in significant and sustained dosages. For example, agarose hydrogels with embedded lipid microtubules were used as a slow-release delivery mechanism to deliver brain derived neurotrophic factor (BDNF) to dorsal hemisection injuries of the spinal cord, reducing the reactivity of astrocytes and CSPG production while also allowing more regenerative fibers to enter the hydrogel 6 weeks after injury.²⁴⁷ Since OPCs require at least 14 days to differentiate into OLs, ensheath axons, and form compact myelin according to previous observations,²⁴⁸ polymeric drug delivery systems that release their payloads over prolonged periods at a relatively constant rate are desirable. The rate of degradation is important to consider since rapid degradation can lead to undesired burst release.²⁴⁹ Slow-degrading polymers are tolerated well in the CNS,²⁵⁰ however the immune system can react to these polymers depending on how they are presented.²⁴⁹ Highly soluble proteins allow for more uniform distribution of protein within the particles. The conjugation of active ingredients with biomaterials like conjugated dextran-nerve growth factor (NGF) enhances the penetration of the active ingredient as the biomaterial is degraded and eliminated slowly.²⁴⁹ Microspheres prepared by a spontaneous emulsification technique released less than 10% of the total amount of loaded protein over the first 5 days, but after about 8 weeks, over 75% of the total protein was released.²⁴⁹ Microspheres

produced by double emulsion method release almost 20% of the total protein loaded within the first 2 hours of incubation, followed by slow release of the remaining 70% during the period of 8 weeks.²⁴⁹ Few studies have applied this specifically to OPCs, but it appears that rapid withdrawal of PDGF-AA, rather than sustained release, promotes OL differentiation in a 3D culture system.²⁵¹ The potential of drug delivery to specifically affect OPC and OL fate via the growth factors mentioned above remains to be seen.

The Impact of Emerging 3D Models

Successful translation of biomaterials for CNS repair and disease therapies will depend on improved understanding of cell behavior in three dimensions. While the majority of what we know about cell behavior is derived from studies on standard 2D cultures, OPCs and OLs reside in dynamic 3D microenvironments presenting complex biophysical and biochemical instructive cues. 3D in vitro biomaterial models can bridge the gap between 2D models and in vivo animal models. More broadly, 3D models hold the potential to unlock relationships between myelination and microenvironmental signals such as ECM stiffness. As a recent example, tuning 3D PEG-dimethacrylate (PEG-DM) hydrogel stiffness over a range of storage moduli relevant to CNS tissue (230-1910 Pa) through alterations of polymer concentration or molecular weight led to varying levels of proliferation and PDGFR α expression in two different OPC lines.¹⁶⁹ The most compliant hydrogels permitted the most proliferation and PDGFR α expression, and in these hydrogels fewer cells were either committed to the oligodendrocyte lineage or dedifferentiated.¹⁶⁹ Additionally, laminin incorporation into the PEG-DM hydrogels did not significantly affect OPC proliferation or differentiation.¹⁶⁹ Collagen/hyaluronan hydrogels permit OPC proliferation and differentiation successfully, notably in the absence of growth factors.²⁵² Seidlits et. al. found that 3D human NSC cultures in HA-based hydrogels showed improved proliferation and differentiation

in comparison to 2D cultures.²⁵³ Differentiation was directed more towards neurons and OLs as opposed to reactive astrocytes, however mature OLs were not observed.²⁵³ In agreement with Russell et. al., the addition of laminin I adhesive peptide had no effect on proliferation and differentiation.²⁵³ 3D models can be multi-purpose, for example in the modeling of glioblastoma tumor (ie, a cell mass composed of OPCs proliferating indiscriminately) where ECM is composed of a soft, HA-rich, microporous 3D scaffold.²⁵⁴ A similar HA-based model was developed by Xiao et. al. to show how HA-CD44 and RGD-integrin αV interactions promote chemotherapy resistance.²⁵⁴

3D materials have also been used to interrogate the role of ligand presentation in promoting OL lineage specification. NSPCs were encapsulated in alginate hydrogels engineered using avidin-biotin interactions to present ligands engaging either $\alpha 3\beta 1$ and $\alpha v\beta 3$ integrins or the cell surface receptor CD44. Ultimately, $\alpha 3\beta 1$ engagement promoted OL maturation in both mouse and human NPCs as measured by elevated expression of MBP and O4 respectively.²⁵⁵

The potential of 3D materials to drive large-scale production of OPCs for treatment of demyelinating disease and injury has recently been explored using thermoresponsive PEG-poly(N-isopropylacrylamide) (PNIPAM) hydrogels. Taking advantage of PNIPAM's LCST behavior, human embryonic stem cells (hESCs) cultured in 3D PEG-PNIPAM were easily isolated by lowering the temperature below the LCST, leading to reverse gelation. PEG-PNIPAM hydrogel culture of hESCs in defined media containing Smoothened agonist (SAG) and retinoic acid (RA) led to a yield of around 30% O4+ cells.²⁵⁶

In addition to unstructured hydrogels, nanofibrous biomaterials replicating the architecture of CNS components (spinal cord, axons) have been studied. Poly(ϵ -caprolactone) (PCL) nanofibers successfully promoted alignment of human pluripotent stem cell (hPSC)-derived

neurons, astrocytes, and OPCs. When the PCL fibers were embedded in PuraMatrix, a commercially available SAP hydrogel, cells within 10 μm of fibers were still able to sense the presence of the fibrous contact guidance cues and orient themselves in the fiber direction. This work highlights the potential of hydrogel-fiber composite materials for fundamental CNS-related studies.²⁵⁷

Conclusion and Outlook

Demyelination and remyelination are competing mechanisms in the struggle for functional CNS regeneration. Biomaterials continue to find growing and diverse applications in CNS disease research, but the potential for elucidating and instructing oligodendroglial processes is largely unexplored. The search for therapeutic solutions to demyelination has expanded from cell transplantation techniques to biomaterials research in the form of hydrogels, fibrous scaffolds, and micro- and nano- particles. The ability to carefully tune the properties of these materials is critical to the success of such strategies. We have learned much over the past two decades about how these features impact processing of neurite outgrowth and NSPC differentiation, and some of these lessons are being translated to OPCs and oligodendrocytes. However, OPCs and OLs are unique from other CNS cell types in many aspects and thus the desired biomaterial properties may require different specific features or regimes. For instance, the control of the microenvironment in a hydrogel is necessary to direct cell behavior. It appears though that the specific range of hydrogel stiffness that biases NSPCs to differentiate into neurons is different than the range that drives OPCs into OLs. This should not be surprising given the processes that occur during development, where a wave of neurogenesis occurs followed by a wave of oligodendrogenesis.

A multi-faceted approach to therapeutic remyelination will likely be needed, including the use of hydrogels and oriented topographical features to deliver cells and bias differentiation as well as growth factors to enhance cell survival and/or promoting axon myelination. The timescales governing lesion progression will be a challenge for new therapies, as many cellular and biochemical influences are not stagnant, but ebb and flow in waves of de- and remyelination. OPC and OL injury mechanisms, natural OPC development mechanisms, and engineering properties of biomaterials all must be understood independently and combined strategically in order to provide a coordinated response on a spatial and temporal level. This will require collaboration between engineers, physicians, neuroscientists, biologists, and biochemists. Oligodendrogenesis is an understudied process, and both OPCs and differentiated OLs remain elusive in their regulatory mechanisms. How can OPCs be directed through the stages of remyelination effectively in vitro and in vivo? Are biomaterials researchers limiting their therapeutic strategies by not studying cues as a function of space and time? Could the right combination of biomaterial cues be sufficient to trigger endogenous remyelination, or will cellular therapy be required? Will therapies have to be customized to each individual patient? The search for these answers will continue to drive ongoing research efforts and the field is well-positioned to seek answers toward translational biomaterial therapies in pursuit of regenerative and restorative CNS myelination.

Acknowledgements

The authors wish to thank the University of Virginia for supporting this work (KJL, SRC), along with the Translational Health Research Institute of Virginia (THRIV) (KJL).

Chapter 2: A 3D Hyaluronic Acid Hydrogel Model for Studying Oligodendrocyte Progenitor Cells in the Context of Demyelinating Disorders of the Central Nervous System

Deniz B. Unal¹, Steven R. Caliari^{1,2}, Kyle J. Lampe¹

¹Department of Chemical Engineering, ²Department of Biomedical Engineering, University of Virginia, Charlottesville, Virginia 22903, United States

Keywords:

Oligodendrocyte progenitor cell, myelin, hyaluronic acid, tissue engineering, axon mimic, central nervous system

Abstract:

There are no clinical solutions for demyelinating disorders of the central nervous system which motivates the need for myelination models. In this work, we propose a 3D hyaluronic acid hydrogel model to study the effects of mechanical properties on oligodendrocyte progenitor cell (OPC) behavior and act as a foundation for a myelination model. Using oscillatory shear rheology we tuned the stiffness range of the hydrogels to that of brain tissue (200 – 2000 Pa) and studied the effects of stiffness on metabolic activity, proliferation, and cell morphology of OPCs over a 7 day period. OPCs in all hydrogels proliferated over the 7 day period, but of the three sample types the two lower stiffness hydrogel groups (169.8 ± 42.1 Pa and 793.9 ± 203.3 Pa) supported greater metabolic activity per cell than the highest stiffness hydrogels (2178.7 ± 127.2 Pa). Mesh sizes were also calculated with a trend of decreasing mesh size with increasing stiffness. All mesh sizes were sufficiently large for biomolecule transport and supported OPC proliferation to the same degree. We also studied spheroid volume as a function of stiffness and found that the lower

stiffness hydrogels supported greater average spheroid volume per gel volume than the highest stiffness hydrogels. Cell viability was greatest for the lowest stiffness hydrogels (85% viability) and decreased (to 71% viability) in the stiffest hydrogels on day 7. Future work involves studying metabolic activity, proliferation, and cell morphology of OPCs in hydrogels with encapsulated axon mimics that serve as the principal mechanical cues for studying myelination. Preliminary results show significant process extension in NorHA hydrogels with 0.18wt% fiber encapsulation at Day 7 of culture.

Introduction:

One of the major life-altering effects of central nervous system (CNS) disorders is demyelination, with multiple sclerosis being the most common disease pathology. Without the mostly lipid-based myelin sheath to insulate neuronal axons, these axons that rely on efficient node to node conduction revert to inefficient continuous conduction. In turn, this leads to protease activation, axonal degradation, and ultimately axonal loss.¹⁴ A key strategy in biomaterials research has been to promote “remyelination” or the regeneration of the myelin sheath after degeneration. Oligodendrocyte progenitor cells (OPCs) of the central nervous system are one of the most influential cell types in this research.²⁵⁸ OPCs are distributed through the white matter in the brain and differentiate primarily into mature oligodendrocytes.¹ Oligodendrocytes myelinate the axons of neurons in the central nervous system (counterparts to Schwann cells in the peripheral nervous system) to increase efficiency and precision of electrical impulse conduction.⁷⁷ Known as the recapitulation hypothesis, developmental myelination in the postnatal rat brain and remyelination after injury may have similar processes where OPC development and maturation can be leveraged in bioengineered solutions for multiple sclerosis.⁹⁷

Hydrogels are useful for CNS applications as they are compliant, facilitate cell migration, and permit biomolecule transport.¹⁵³ OPCs and their precursors (neural stem cells) have been studied in non-degradable polyethylene glycol (PEG) hydrogels¹⁷³ as well as collagen, agarose, chitosan, and fibrin hydrogels.^{259,260} We chose hyaluronic acid as a scaffolding material for OPCs. It is a good building block for an extracellular matrix (ECM) mimic. It is abundant in the CNS, highly polyanionic, and known for being the only non-sulfated glycosaminoglycan (GAG).^{151,177,178} It also aids in brain and spinal cord injury in rodents by decreasing inflammation.²⁶¹

With the use of any material as a 3D scaffold comes the need for studies of the effects of mechanical properties on OPC behavior. These foundational studies form the basis for more complicated fiber included experiments. Jagielska et. al. showed that OPCs are mechanosensitive, with proliferation being highest at 700 Pa on 2D substrata.²¹⁰ Russell et. al showed that OPC ATP fold changes were highest for polyethylene glycol (PEG) hydrogels of 240 ± 84 Pa (8000 MW) in comparison to 270 ± 87 Pa (6000 MW) and 630 ± 79 Pa (4600 MW) with all macromer concentrations at 6wt%.¹⁶⁹ In this work, we adjust the macromer concentration to demonstrate the effects of stiffness and mesh size on OPC proliferation, metabolic activity, and spheroid volume in 3D norbornene functionalized hyaluronic acid (NorHA) hydrogels. Future work looks at these same effects when crosslinked methacrylated hyaluronic acid fibers (MeHA) fibers are encapsulated in the hydrogels. This is one of the pioneering studies of incorporating fibers with OPCs in 3D hydrogels.

Materials & Methods:

Cell Culture:

Green fluorescent protein positive (GFP+) mosaic analysis with double markers (MADM) OPCs were expanded in vitro on T75 (Corning CellBind) treated tissue culture plates. MADM cells are derived from mouse glioma cells that express many OPC markers and are used to model loss of heterozygosity of tumor suppressor genes in cancers.^{169,262} Cells were expanded on polyornithione-coated tissue culture plates (10 µg/mL) and incubated at 37°C to establish hydrophilicity. Then tissue culture plates were rinsed thrice with Dulbecco's phosphate buffered solution (PBS) and filled with 8 mL OPC proliferation media. OPC proliferation media consisted of Dulbecco's modified Eagle's medium (DMEM, Life Technologies) with 4mM L-glutamine and 1mM sodium pyruvate (Life Technologies), with N2 supplement (Life Technologies) and B27 supplement (Life Technologies), and 1% penicillin-streptomycin (Life Technologies). Cells were seeded at 0.5×10^4 cells/cm² and passaging was done at 80% confluence. Media was changed every two days. Cryopreserved cells were passaged at least once before using in experimentation. Cells from passage numbers 10-25 were used.

MeHA Macromer Synthesis:

MeHA was manufactured according to an adaptation of Burdick et. al. protocol.²⁶³ Methacrylic anhydride (MA) was added dropwise to Research Grade Sodium Hyaluronate (Lifecore Biomedical, 65 kDa) at 1% w/v and stirred until homogeneous. The solution was kept on ice and the pH was maintained between 8-9 with 5 N NaOH. MA was added in a 1:1 molar ratio to MeHA with 12.3x excess to get a methacrylation efficiency of 90%. After all methacrylic anhydride was added, the solution was continually stirred overnight. The solution was then dialyzed (molecular

weight cutoff 6-8 kDa) for 5 days against deionized water. Macromer solution was frozen overnight at -80°C and then lyophilized for 3 days. ^1H NMR spectra can be found in Appendix 1.

NorHA Macromer Synthesis:

HA-TBA Synthesis: Research Grade Sodium Hyaluronate (Lifecore Biomedical, 65 kDa) was converted to its tetrabutylammonium salt (HA-TBA) to prepare for dissolution in DMSO.²⁶⁴ Sodium hyaluronate was dissolved in DI water at 2 wt% and Dowex resin (50W x 200) was added at the ratio of 3g resin/1g HA).²⁶⁴ The resin exchanges sodium ion for hydrogen ion, making the solution strongly acidic. The solution was stirred for ~2hrs. Stirring was stopped to allow the resin to settle to the bottom of the flask. The solution was then filtered with #2 filter paper by vacuum filtration. Filtration was repeated to ensure the solution was clear. The solution was titrated to pH of 7.02-7.05 with TBA-OH. The HA-TBA solution was then frozen at -80 C and lyophilized. Tubes were purged with N_2 and stored at -20 C . ^1H NMR spectrum can be found in the appendix (Appendix 1).

NorHA Synthesis: In a dried and stoppered round bottom flask, the HA-TBA and Nor-amine (5-Norbornene-2-methylamine) were added. Nor-amine was added assuming 20% of molar HA-TBA units modified, ~50% reaction efficiency, and 1:1 molar ratio with regard to HA-TBA moles of repeat units. The mixture was stirred at 350 RPM. Anhydrous DMSO was added via cannulation to the flask (~5mL per 0.1g). (Benzotriazol-1-yloxy)tris(dimethylamino)-phosphonium hexafluorophosphate (BOP, VWR) was added at a 1:1 molar ratio with regard to HA-TBA moles of repeat units. Once the HA-TBA was fully dissolved, the BOP was added separately via cannulation with the BOP dissolved in ~20mL of anhydrous DMSO. The reaction was allowed to proceed for ~2hrs, and then it was quenched with ~10 mL of DI water. The solution was transferred

to dialysis tubing and put on dialysis for 5 days, the first three of which included ~5g of NaCl in ~5gal of DI water. Through filtration, the side-products from the BOP coupling were removed. Then the solution was returned to dialysis for 3-5 days. Finally, the solution was transferred to 50 mL tubes, frozen at -80 C and lyophilized to dry. ¹H NMR spectra can be found in the appendix (Appendix 1).

Hydrogel Preparation:

Hydrogel precursors solutions (without fibers) were prepared with 1–2wt% NorHA macromer, 0.0328wt% lithium phenyl-2,4,6-trimethylbenzoylphosphonate (LAP), DL-Dithiotreitol (DTT, Sigma-Aldrich) at a 0.315 thiol-norbornene ratio, cell solution, and solvent of PBS. LAP is the photoinitiator and DTT is the crosslinker. OPC MADM cells were encapsulated at 5×10^6 cells/mL. Gel precursor solutions (with fibers) had identical composition except fiber solution was included at 0.18wt%.

Oscillatory Shear Rheology:

NorHA macromer solution was created using 1–2wt% NorHA macromer, 0.0328wt% LAP, 0.315x thiol group/norbornene group ratio of DL-Dithiothreitol, and solvent of PBS. 50 μ L aliquots were pipetted onto a UV-configured plate of an Anton Parr rheometer. A 25mm diameter smooth cone and plate with a 0.505° angle was used to perform a time sweep. Hydrogels were cured in-situ at 0.1% oscillatory strain, 10rad/s oscillation frequency, and 4mW/cm² UV light intensity (365 nm). After 30s of pure oscillatory motion, light exposure was introduced underneath the plate for 2min.

Swelling Studies:

The tapered section of 3mL syringes were cut off. 360 μ L hydrogel precursor solutions matching those used in the hydrogel preparation section were pipetted into the tops of the 3mL syringes. The solutions were cured under 4mW/cm² UV light (365 nm) for 2 minutes. Samples were then soaked in PBS at 37°C. At time points 0hrs, 24hrs, and 48hrs, three samples each per sample type were weighed (removing excess liquid). These samples were then lyophilized, and the dry mass was recorded. Flory-Rehner calculations were used²⁶⁵ to determine mass and volumetric swelling ratios, molecular weight between crosslinks, and mesh size. First the molecular weight between crosslinks was determined through the equilibrium swelling theory for crosslinked polymers²⁶⁶:

$$\frac{1}{M_{c,S}} = \frac{2}{M_n} - \frac{v/V_1[\ln(1-v_{2,s})+(v_{2,s})+\chi(v_{2,s})^2]}{(v_{2,r})[(\frac{v_{2,s}}{v_{2,r}})^{\frac{1}{3}} - \frac{v_{2,s}}{2v_{2,r}}]} \quad (1)$$

Where $M_{c,S}$ is the molecular weight between crosslinks estimated from swelling (g/mol), M_n is the molecular weight of the macromer (g/mol), v is the specific volume of the macromer (mL/g), V_1 is the molar volume of the solvent (mol/cm³), χ is the polymer solvent interaction parameter, $v_{2,r}$ is the volume fraction of polymer in the relaxed state, and $v_{2,s}$ is the volume fraction of polymer in the swollen state. Multiple sources state that the polymer solvent interaction parameter can be taken as 0.473 because of the similarities between hyaluronic acid and dextran.^{265,267} The effective crosslinking density and mesh size calculations are then adapted from Leach et. al.²⁶⁷

$$v_e = \frac{\rho_p}{M_{c,S}} \quad (2)$$

Where v_e is the effective crosslinking density (mol/cm³), and ρ_p is the density of the dry polymer (g/mL).

$$\xi = 0.1743(v_{2,s})^{-\frac{1}{3}}(M_{c,S})^{\frac{1}{2}} \quad (3)$$

Where ξ is the mesh size (nm).

Alamar Blue:

In Alamar Blue, the chemical compound resazurin is reduced to resorufin through cellular respiration. The metabolic activity is represented by percent reduction and can be measured through absorbance or fluorescence intensity. The Beer-Lambert law is used when measuring absorbance values. Equations 4, 5, and 6 describe the phenomena.

$$\varepsilon_{RED}\lambda_1 C_{RED} + \varepsilon_{OX}\lambda_1 C_{OX} = A \lambda_1 \quad (4)$$

$$\varepsilon_{RED}\lambda_2 C_{RED} + \varepsilon_{OX}\lambda_2 C_{OX} = A \lambda_2 \quad (5)$$

$$C_{RED/C} = \frac{(\varepsilon_{OX}\lambda_2 A \lambda_1) - (\varepsilon_{OX}\lambda_1 A \lambda_2)}{(\varepsilon_{OX}\lambda_2 P \lambda_1) - (\varepsilon_{OX}\lambda_1 P \lambda_2)} \quad (6)$$

Where $\varepsilon\lambda$ is the molar extinction coefficient (oxidized or reduced form) at excitation or emission wavelength (570nm = λ_1 , 600 nm = λ_2), $A\lambda$ is the absorbance value of the sample at excitation or emission wavelength, C is the concentration of Alamar blue (oxidized or reduced form) and $P\lambda$ is the absorbance of the control wells (excitation or emission). Alamar Blue cell viability reagent (ThermoFisher) was mixed with OPC proliferation media at 10% reagent by volume. Each MeHA gel with encapsulated cells was incubated in 400 μ L of this pre-made solution for 4 hours at 37°C. Hydrogels were then removed from solution. Remaining solution for each sample was pipetted into three 100 μ L replicates along with three 100 μ L replicates of blank 10% by volume mixed Alamar Blue solution. Absorbance was read in a BMG Clariostar monochromator microplate reader.

Live/Dead Assay:

Each hydrogel was suspended in 1 mL of PBS plus glucose (PBSG) with the same concentration of glucose as in OPC proliferation media. Each stain consisted of 4 μ M ethidium homodimer with

incubation at 37°C for 60 minutes followed by rinsing 2x with PBSG. Live/dead images were collected using a Zeiss LSM 510 confocal microscope with ~500 μm z-stacks having an interval of 10 μm for each frame (We acknowledge the Keck Center for Cellular Imaging at the University of Virginia for the usage of the Zeiss 510 microscopy system, grant # RR021202).

Cell Glo:

A standard curve for ATP was made using the manufacturer's protocol. Cell Glo reagent was prepared by adding 10 mL of CellTiter-Glo buffer to the CellTiter-Glo substrate to reconstitute the lyophilized enzyme mixture. Solution was gently mixed through inversion. Once completely dissolved, the solution was stored in the -20°C in 1 mL aliquots. A white 384-well plate was used for the assay. 25 μL of each standard was added with three pipetting replicates. 20 μL of PBS were added to separate wells and then 5 μL of sample was added for each well to represent a sample. To all wells (standards and samples), 25 μL of CellGlo reagent was added. The plate was added to equilibrate for about 10 minutes. Luminescence was measured in a BMG Clariostar monochromator microplate reader. A standard curve was plotted relating luminescence values to ATP concentrations. Sample ATP concentrations were determined based on that standard curve.

Pico Green:

A standard curve for DNA was made using the manufacturer's protocol. A black 384-well plate was used for the assay. Standards were pipetted at 20 μL with three pipetting replicates. Samples were pipetted with three pipetting replicates and three sample replicates at 5 μL sample volume and 15 μL 1x TE buffer. The Pico Green reagent was diluted to 50 μL dye/10mL 1x TE Buffer. 20 μL of dye was added to all the standards and samples. Fluorescence was measured in a BMG

Clariostar monochromator microplate reader. A standard curve was plotted relating fluorescence values to DNA concentrations. Sample DNA concentrations were determined based on that standard curve.

Spheroid Volume measurement:

Z-stacks of ~500–1500 μ m thickness were loaded in ImageJ, and the GFP and ethidium homodimer channels were separated. GFP images were analyzed using the “3D object counter” module in ImageJ which thresholded the image and then provided spheroid volume on all individual spheroids. Average spheroid volume was calculated for each gel, normalized to the gel volume, and then averaged between three hydrogels per sample type per trial. Spheroid volume was summed for each gel, normalized to the gel volume, and then averaged between three hydrogels per sample type per trial. A total of 3613–14870 spheroids were measured per image. Spheroid volume varied between sample types depending on ratio of live to dead cells and size of spheroids in sample. Three images were taken per trial per sample type and a total of 5 trials were used. Two of these experiments had images from only two sample types.

Statistical Analysis:

ATP, DNA, metabolic activity, and spheroid volume data were analyzed using two-way ANOVA followed by the Tukey post-hoc test with α -value of 0.05.

Results & Discussion

The NorHA hydrogels were formed through the crosslinking of norbornene functional groups with a dithiol crosslinker (DTT) and a photoinitiator that absorbs strongly at 365

nm UV light (LAP) (Figure 6). Norbornene groups preferably crosslink with the DTT instead of with themselves, creating what is known as an orthogonal system where the degree of crosslinking can be tuned by the molar ratio of thiol groups to norbornene groups.²⁶⁴ The functionalization efficiency of the NorHA is kept low (~20-28%) so as to minimize crosslinking, encourage swelling, and permit diffusion of biomolecules to and from the hydrogel. Gramlich et. al. demonstrated the positive correlation between storage modulus and thiol to norbornene group ratio up to 0.8.²⁶⁸ The molar ratio of thiol to norbornene groups was kept low at 0.315 again to minimize crosslinking while at the same time forming a strong enough polymer network to keep the hydrogel from eroding substantially in media.

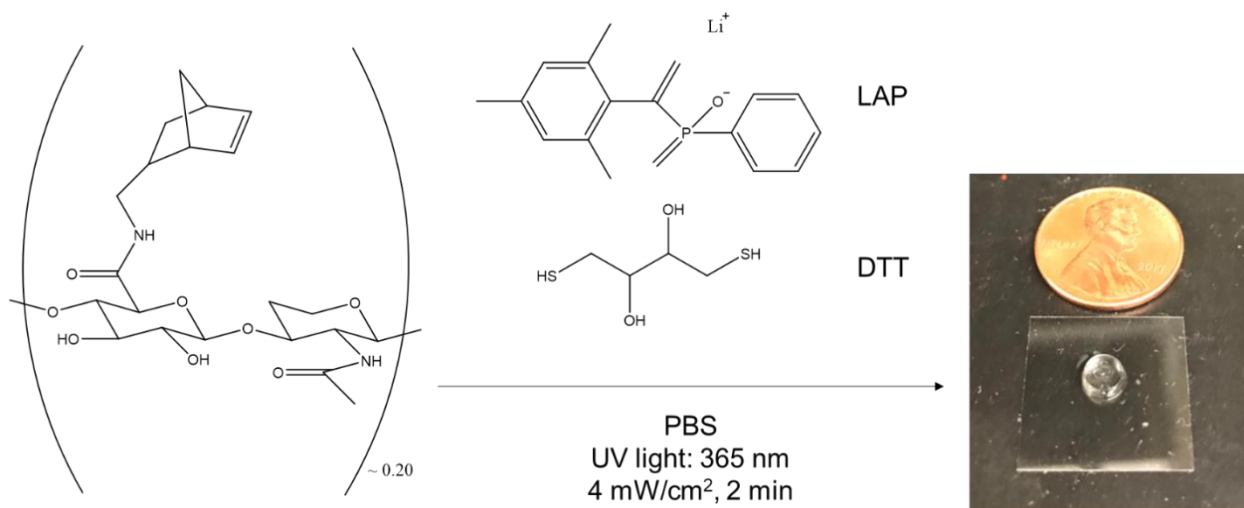


Figure 6 - ~20% of the hyaluronic acid repeat units were modified with norbornene functional groups. Norbornene was crosslinked with DTT and LAP to form hydrogels with PBS as the solvent. Hydrogels were crosslinked under 4 mW/cm² (365 nm) light for two minutes

Mechanical Properties of NorHA Hydrogels

Cells sense mechanical cues and respond to them through changes in morphology, metabolic activity, and proliferation. Storage modulus and mesh size are key properties affecting these cell traits.¹⁶⁹ Storage modulus dictates the stiffness of the material. Mesh size dictates the

spacing between crosslinks and availability for cell colony growth and biomolecule diffusion.

Storage modulus can be measured through oscillatory shear rheology (Figure 7).

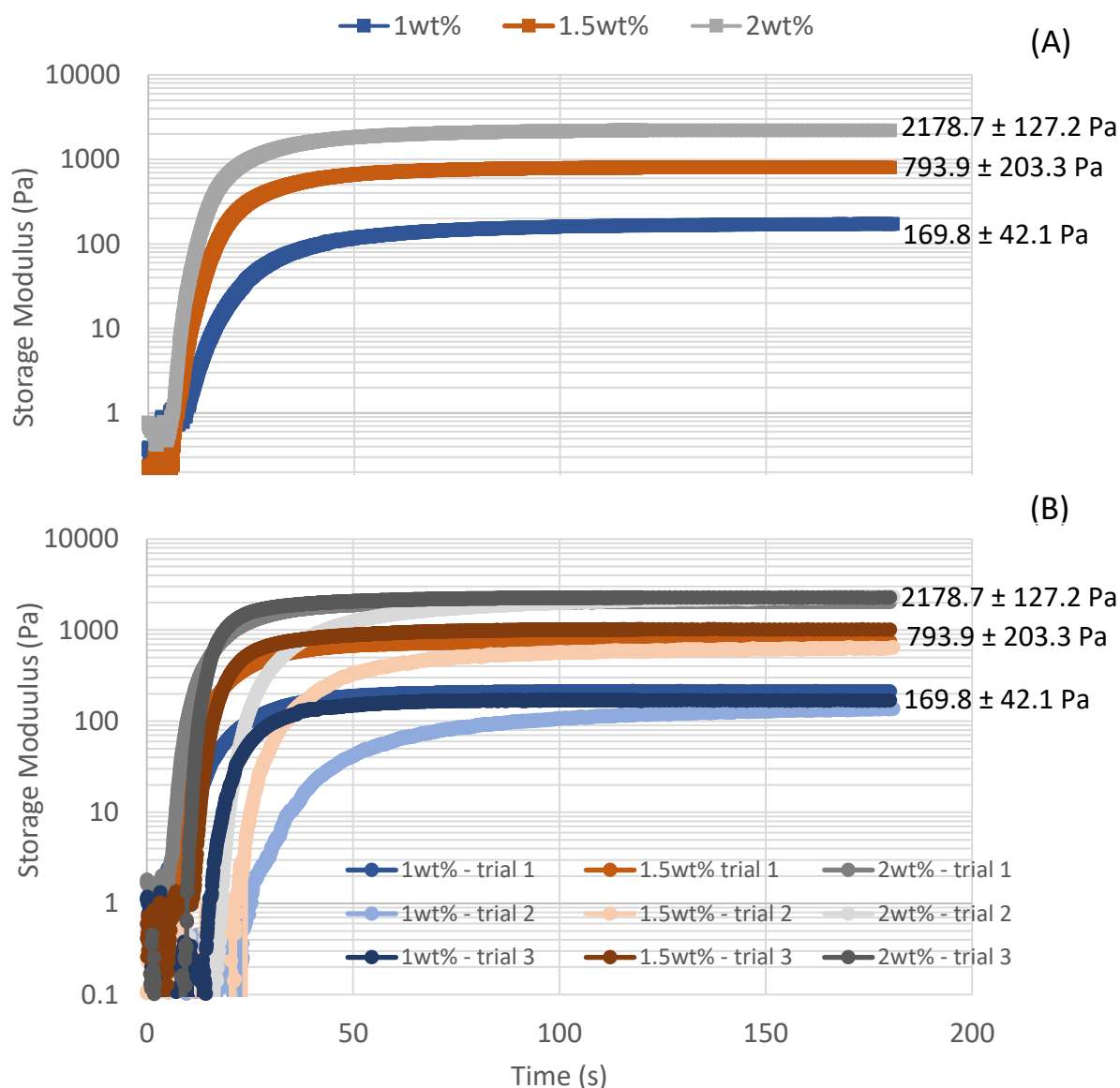


Figure 7 - (A) average storage moduli for each sample type from three batches (B) individual batch trials

Oscillatory shear rheology was performed on NorHA hydrogels in-situ at 1wt% (wt/v) NorHA, 1.5wt%, and 2wt% in three different batches each with $n = 3$. Hydrogels were formed by exposure to UV light from 0 to 120 seconds. Storage modulus was calculated from the average of 150–180s for each trial. All storage moduli are reported with standard deviation as the error. Loss moduli fluctuate around 1 Pa and do not significantly change amongst the weight percentage samples since the hydrogels are elastic.

Formulations of NorHA hydrogels were adjusted to match the range of brain tissue stiffness (i.e. 200-2000 Pa)¹⁵² with 1wt% corresponding to 169.8 ± 42.1 Pa, 1.5wt% corresponding to 793.9 ± 203.3 Pa, and 2wt% corresponding to 2178 ± 127.2 Pa. Mesh sizes were determined through Flory polymer theory (Materials and Methods). In comparison to previous studies with PEGDM hydrogels, the NorHA hydrogels show 6-7 fold increase in mesh size with notably higher stiffness values, suggesting that the NorHA hydrogels could allow for greater cell activity while still mimicking CNS tissue appropriately. Methacrylation efficiency of polyethylene glycol dimethacrylate (PEGDM) hydrogels was 82-86%¹⁶⁹ while functionalization efficiency of NorHA hydrogels was 20-28%, and the resulting mesh sizes indicate an advantage in cell encapsulations studies for lower functionalization efficiency materials. Leach et. al. performed swelling studies with glycidyl methacrylate-HA (GMHA) that is two orders of magnitude greater in molecular weight but only 5-11% functionalized with methacrylate groups. Molecular weight between crosslinks was also found to be two orders of magnitude greater (not reported here) in comparison to NorHA hydrogels.²⁶⁷ Consequently, mesh sizes were an order of magnitude greater than those of NorHA hydrogels. Stiffnesses were comparable to NorHA and PEGDM hydrogels. Stiffness does correlate inversely with mesh size, however the primary relationship is that mesh size results from the functionalization efficiency, the molecular weight of the polymer, and the degree of crosslinking. Moreover, stiffness is not always an indication of mesh size.

Molecular Weight (g/mol)	Functionalization Efficiency (%)	Sample Type	Stiffness (Pa)	Mesh Size (nm)
65,000	20-28	1wt% NorHA	169.8 ± 42.1	85.6 ± 2.7
65,000	20-28	1.5wt% NorHA	793.9 ± 203.3	75.6 ± 3.6
65,000	20-28	2wt% NorHA	2178.7 ± 127.2	73.2 ± 3.5
8,000	82-86	6wt% 8000 MW PEG	240 ± 84	12.5
6,000	82-86	6wt% 6000 MW PEG	270 ± 87	9
4,600	82-86	6wt% 4600 MW PEG	630 ± 79	8.2
2,000,000	5	1wt% GMHA	109.4 ± 16.3*	644
2,000,000	7	1wt% GMHA	131.3 ± 6.4*	619
2,000,000	11	1wt% GMHA	154.5 ± 28.2*	539

Table 1 - Comparison of NorHA hydrogel mesh sizes with PEGDM hydrogel mesh sizes¹⁶⁹ and GMHA hydrogel mesh sizes²⁶⁷

Swelling studies were performed by taking wet mass / dry mass to obtain mass / volumetric swelling ratios. Equilibrium swelling ratios were reached after 48 hrs in PBS with (n=8) per sample type. * indicates complex shear modulus.

Effects of Mechanical Properties on Proliferation, Metabolic Activity, and Cell Morphology

After characterizing the mechanical properties and mesh sizes of our hydrogels, we encapsulated OPCs and tracked their numbers over a 7 day culture as measured by DNA content. The change in DNA concentration over time is indicative of the changes in cell population. The assay resulted in weight percentage of macromer and day of culture combining additively to influence DNA concentration. DNA values from 1wt% and 1.5wt% hydrogels are similar and together they are statistically different from 2wt% ($\alpha < 0.05$). DNA concentration significantly increased in all hydrogel conditions over the culture period. These results are comparable to

Russell et. al. findings with PEGDM hydrogels, where a statistically significant difference ($\alpha < 0.05$) was found only between 270 ± 87 Pa and 240 ± 84 Pa hydrogels.¹⁶⁹

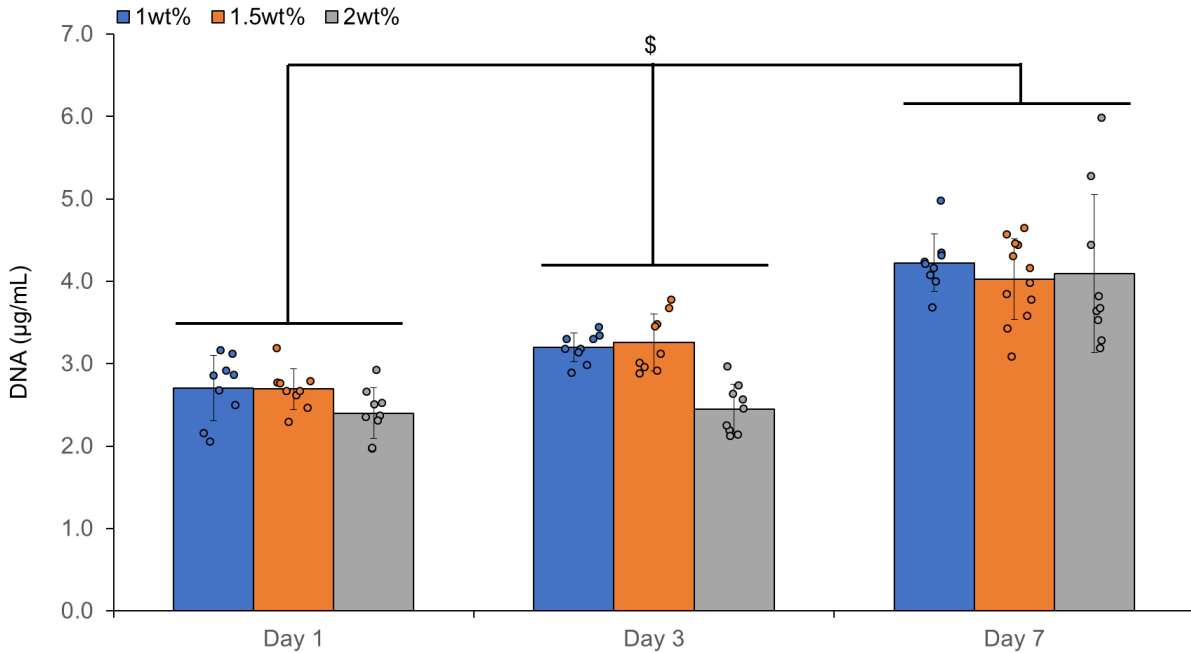


Figure 8 - MADM OPC line encapsulated at 1wt% (wt/v) NorHA, 1.5wt%, and 2wt% all proliferated over a period of 7 days.

\$ indicates statistically different DNA concentrations at each time point ($\alpha < 0.05$). (n=9) for 1wt%, (n=12) for 1.5wt%, (n=9) for 2wt%

ATP concentration is a measure of how metabolically active the total cell population is in the hydrogels. ATP concentration (Figure 9) was influenced by a non-additive combination of weight percentage and day of culture, with all time points different from each other ($\alpha < 0.05$) and all weight percentages different from each other ($\alpha < 0.05$). The hydrogels of lowest stiffness demonstrated the highest ATP concentrations and values decreased with increasing stiffness. This agrees with Russell et. al.¹⁶⁹

ATP concentration normalized to DNA concentration provides a measure of average metabolic activity per cell, which allows the direct comparison of sample types with any inherent heterogeneities. After normalization of ATP to DNA (Figure 10), it was found that the weight percentage and day of culture combine in a non-additive way to affect ATP/DNA. All time points are significantly different from each other ($\alpha < 0.05$) and all weight percentages are different from each other ($\alpha < 0.05$).

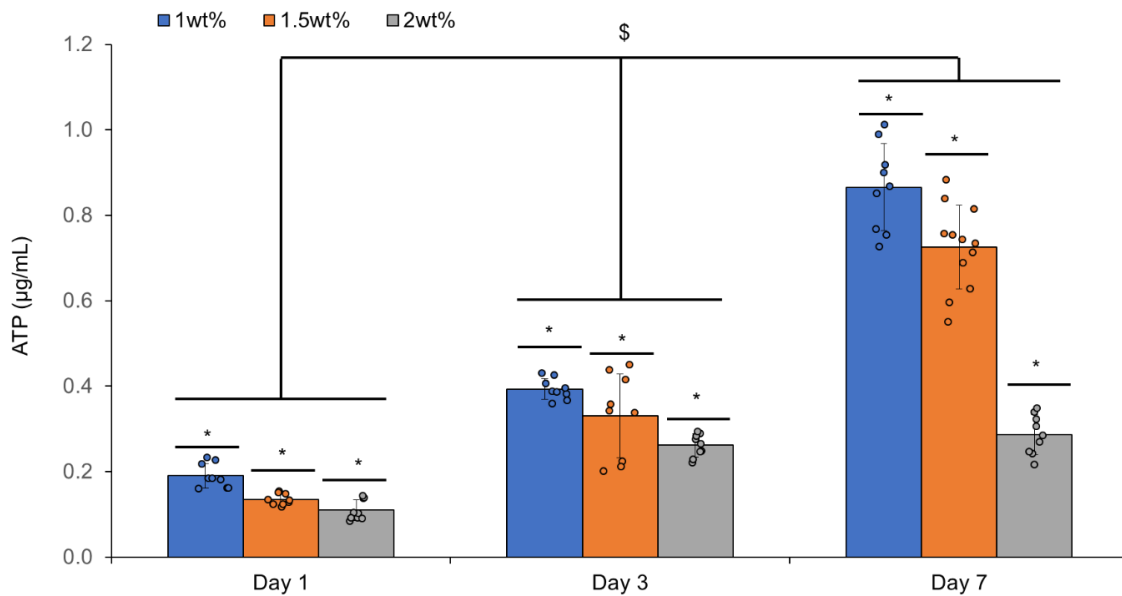


Figure 9 - MADM OPC line encapsulated at 1wt% (wt/v) NorHA, 1.5wt%, and 2wt% all showed increases in ATP concentration over a period of 7 days.

\$ indicates increase in ATP at each time point ($\alpha < 0.05$). * indicates that all weight percentage sample types are significantly different from the other two sample types ($\alpha < 0.05$). (n=9) for 1wt%, (n=12) for 1.5wt%, (n=9) for 2wt%

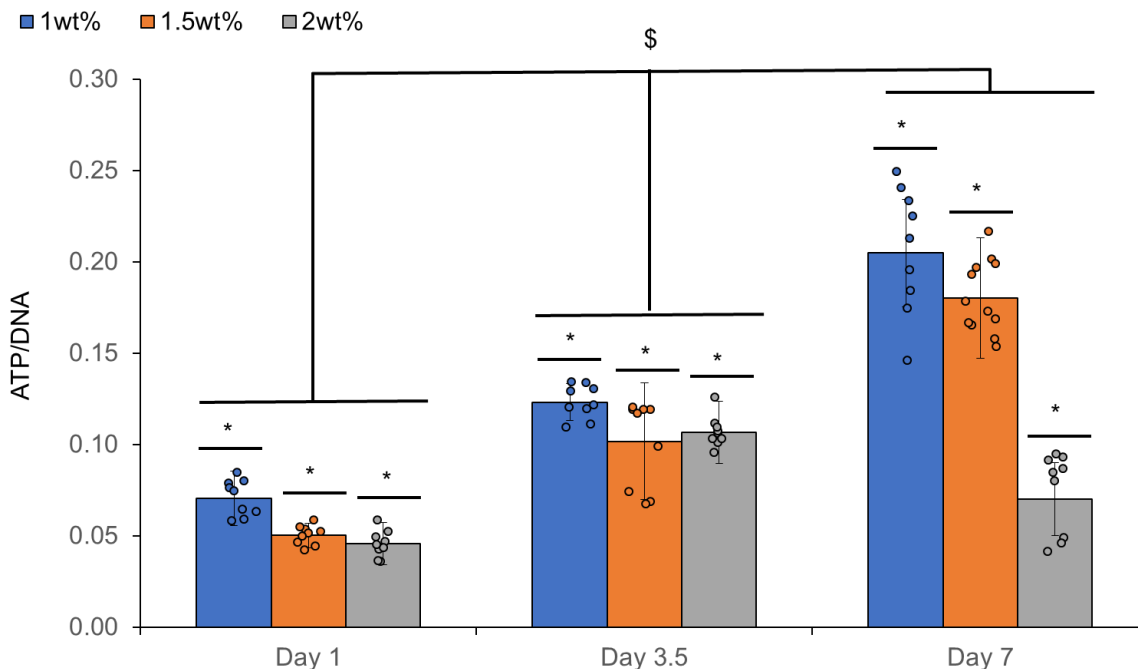


Figure 10 - MADM OPC line encapsulated at 1wt% (wt/v) NorHA, 1.5wt%, and 2wt% all showed increases in ATP/DNA concentration over a period of 7 days.

\$ indicates increase in ATP/DNA at each time point ($\alpha < 0.05$). * all weight percentage sample types are significantly different from each other ($\alpha < 0.05$). (n=9) for 1wt%, (n=12) for 1.5wt%, (n=9) for 2wt%

The Alamar Blue assay can be used to assess the total metabolic activity in hydrogel samples over an extended period of time by introducing a dye that is reduced in the electron transport chain without interfering with it.²⁶⁹ The dye is reduced before oxidative phosphorylation, and requires $2H^+$ and $2e^-$ from the Krebs cycle per molecule to be reduced.²⁷⁰ The Cell Glo assay only monitors ATP, so that includes the 2 molecules of ATP produced by glycolysis and 30 molecules produced through oxidative phosphorylation.²⁷¹ The mechanistic differences between these assays suggests that Cell Glo will provide sharper differences in energy metabolism between hydrogel sample types since there are 32 ATP molecules per cycle in comparison to 1 molecule of $FADH_2$, 2 molecules of NADH, and 1 molecule of GTP. That trend is observed when comparing Figure 9 with Figure 11. In Alamar Blue metabolic activity studies (Figure 11), it was found that

weight percentage and day of culture combine in an additive way to influence metabolic activity. Metabolic activity increased at all time points with all weight percentages ($\alpha < 0.05$). All hydrogel sample types were indistinguishable from each other.

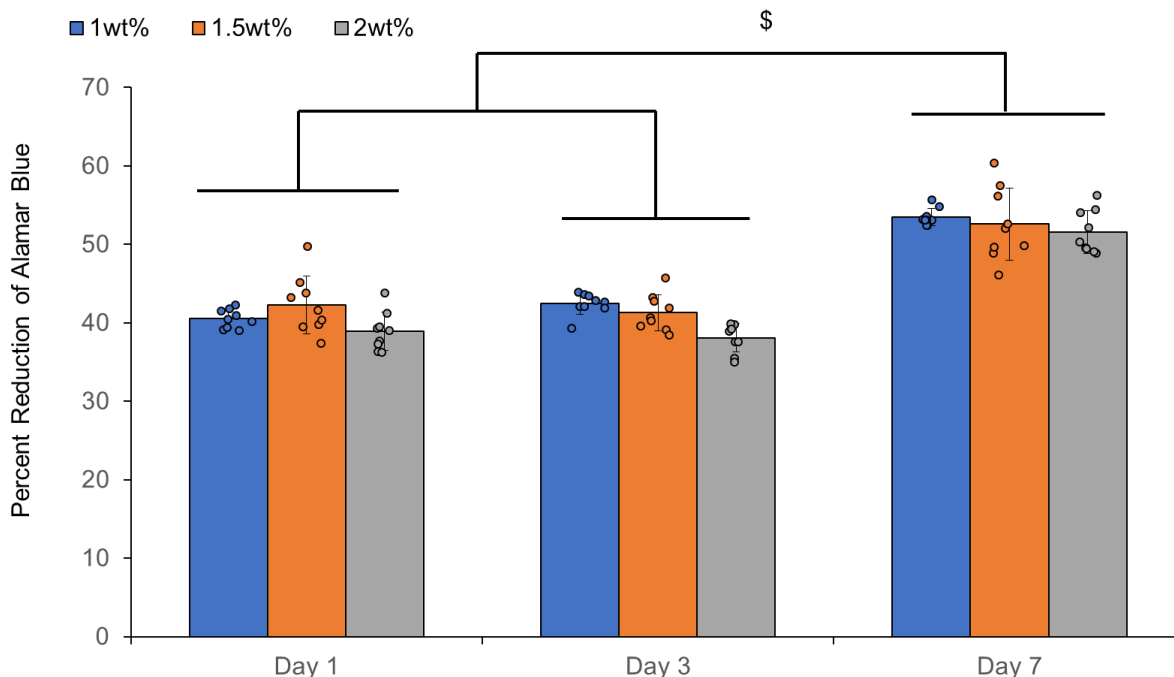


Figure 11 - MADM OPC line encapsulated at 1wt% (wt/v) NorHA, 1.5wt%, and 2wt% all showed increases in metabolic activity over a period of 7 days when the incubation time was 4 hours.

\$ indicates increase in metabolic activity at each time point ($\alpha < 0.05$). (n=9) for 1wt%, (n=12) for 1.5wt%, (n=9) for 2wt%.

Metabolic activity followed the same statistical trends as DNA concentration. Since the Alamar Blue assay was not normalized, it was expected that heterogeneities in hydrogel samples would be present as was the case in the Pico Green assay.

Collectively as a concentration of cells in a hydrogel, the 1wt% and 1.5wt% were identical, however when looking at the per cell level, the 1wt% hydrogels outperformed the 1.5wt% hydrogels. The 2wt% hydrogels were outperformed in both cases. This suggests that there is another non-linear effect occurring between 1wt% and 1.5wt% in addition to culture time and

stiffness. A 4.6x increase in stiffness (1.5wt% in comparison to 1wt%) corresponds to a ~11.6% reduction in mesh size (Table 1). A 12x increase in stiffness (2wt% in comparison to 1wt%) corresponds to a ~14.5% decrease in mesh size (Table 1). This is indeed a non-linear relationship. A comparable observation was made by Russell et. al. where a 2.6 fold increase in stiffness led to a mesh size change from 9.47nm to 6.61nm (30%) and the increases in ATP concentration were significant.¹⁶⁹ The evidence from this study and Russell et. al. hints that every formulation of curable polymer solution has a non-linear stiffness to mesh size curve which affects OPC metabolic activity per cell. Considering the hydrodynamic radii of most model proteins is on the order of 1-6nm,²⁷² all stiffness hydrogels were adequately supportive of diffusion of necessary biomolecules. If the NorHA hydrogels have larger mesh sizes, we would expect the spheroid volumes (or diameters) to be larger in these hydrogels in comparison to the PEGDM hydrogels.

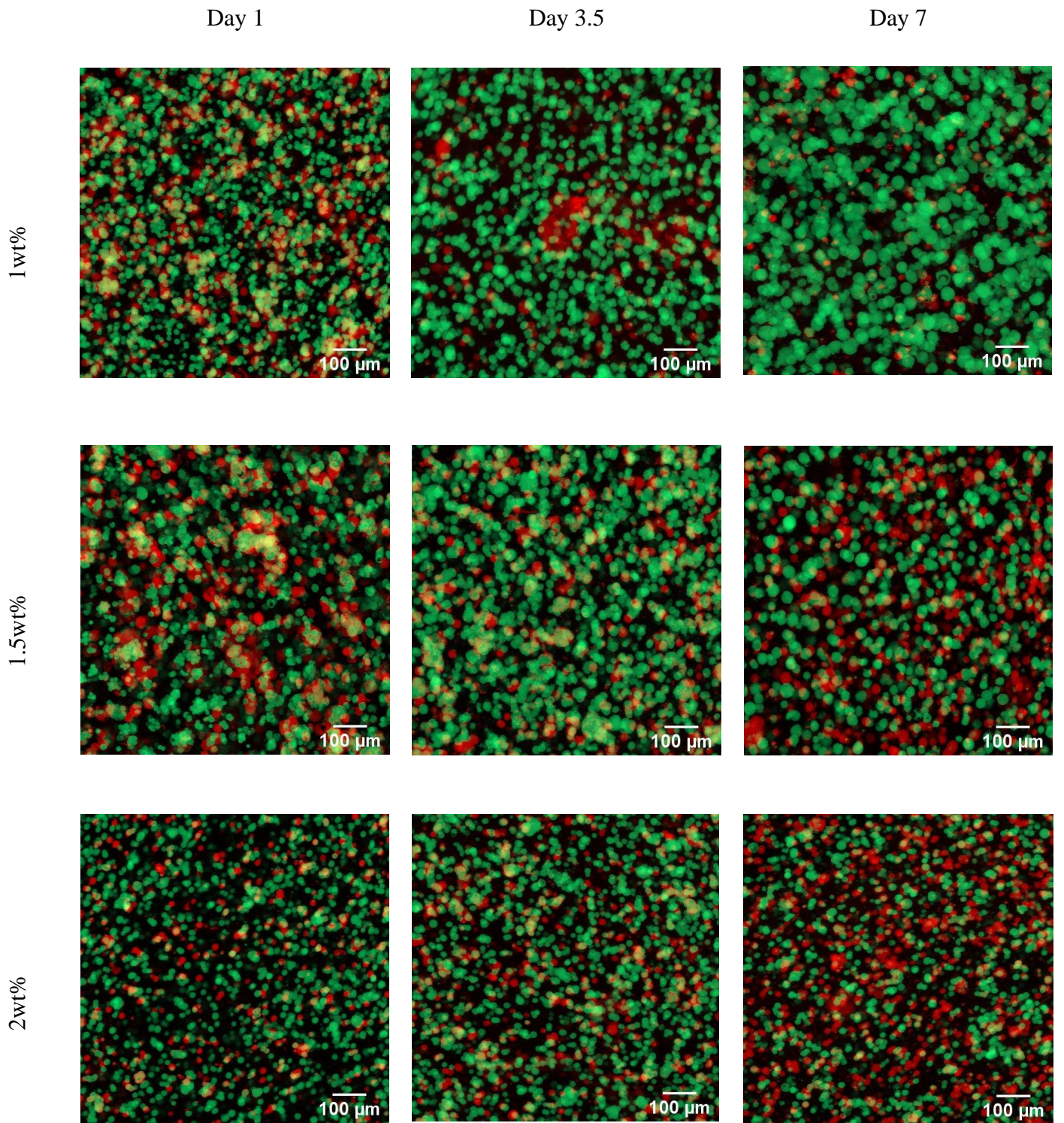


Figure 12 - 10 μm slices of NorHA hydrogels at 1wt% - 2wt%.

Portrait (1,1) 930 um depth (1,2) 770 um depth (1,3) 1700 um depth (2,1) 876 um depth (2,2) 1200 um depth (2,3) 1930 um depth (3,1) 810 um depth (3,2) 900 um depth (3,3) 1710 um depth.

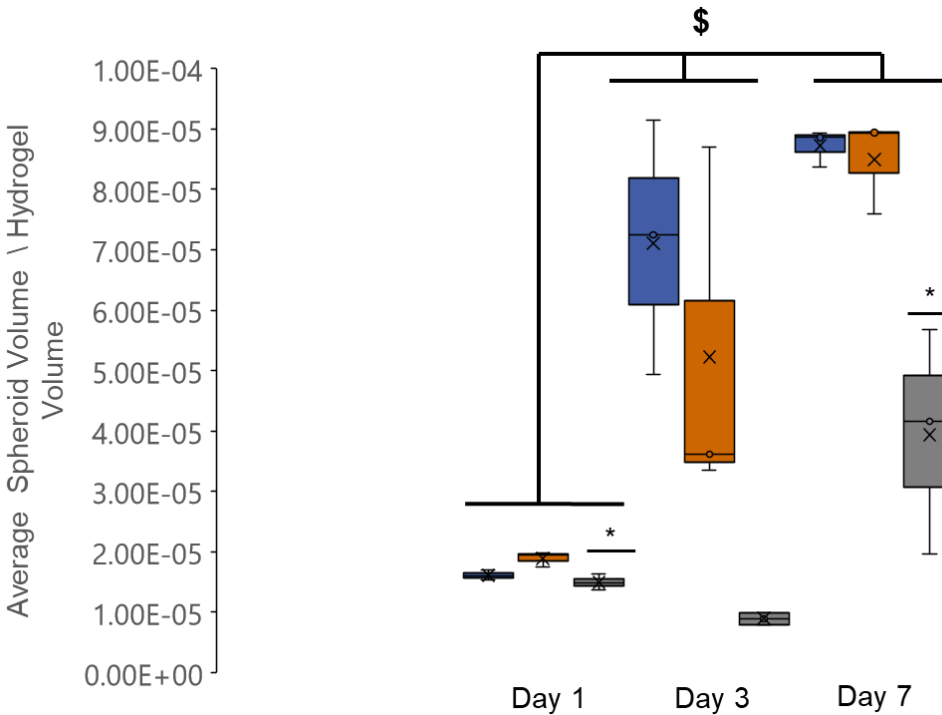


Figure 13 - MADM OPC line encapsulated at 1wt% (wt/v) NorHA, 1.5wt%, and 2wt% all showed increases in fraction of average spheroid volume over a period of 7 days.

\$ indicates significant difference in fraction of average spheroid volume at each time point ($\alpha < 0.05$). * indicates that 2wt% hydrogel sample type is significantly different from the other two weight percentages ($\alpha < 0.05$). (n=12) for all sample types.

It was found that weight percentage and day of culture influence the normalized average spheroid volume in a non-additive way (Figure 13). 1wt% and 1.5wt% were indistinguishable and were statistically different from 2wt% ($\alpha < 0.05$). All time points are statistically different from each other ($\alpha < 0.05$).

Russell et. al. reports an average cluster diameter of 21 μ m for ~600Pa stiffness and 10nm mesh size PEGDM hydrogels.¹⁶⁹ In this study, average cluster diameters of NorHA hydrogels were at least 1.5 fold greater in hydrogels of ~795Pa stiffness and 75 nm mesh size.

NorHA hydrogels of ~170Pa and 85nm mesh size had 2 - 2.5 fold greater cluster diameters than the ~600Pa stiffness and 10nm mesh size PEGDM hydrogels. These results validate the swelling study results. Larger mesh sizes lead to larger spheroid clusters. When normalized to hydrogel volume, 1wt% and 1.5wt% NorHA hydrogels are equivalent, but in terms of absolute value, 1wt% hydrogels did trend towards the largest spheroid volumes (Figure 14) after a 7 day culture period.

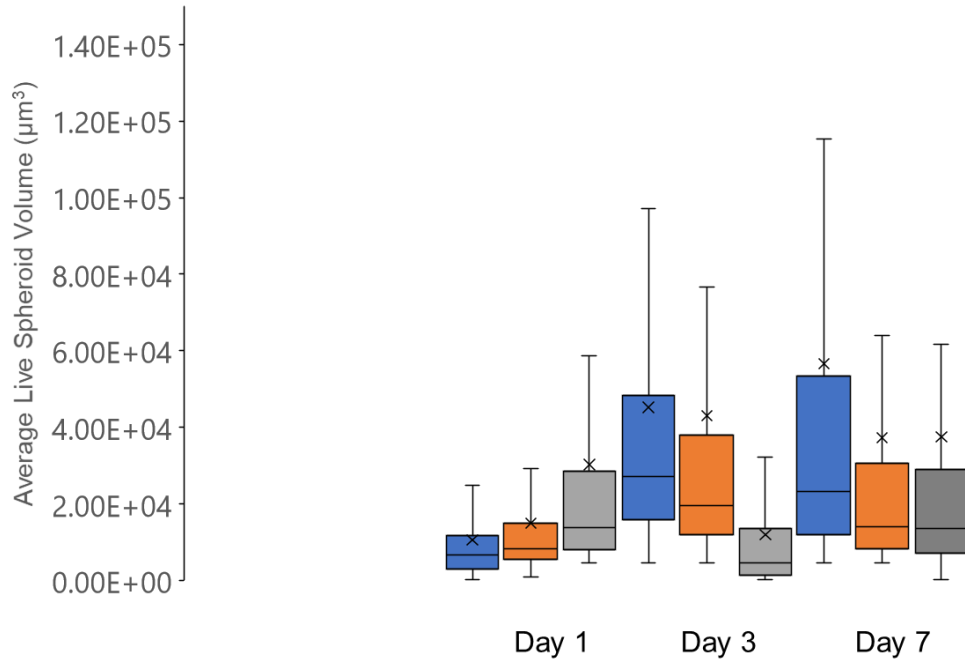


Figure 14 - Average live spheroid volume was determined by thresholding the images and automatically calculating the spheroid volume.

Number of spheroids counted were as follows: 1wt% day 1 (9755), 1.5wt% day 1 (8455), 2wt% day 1 (3613), 1wt% day 3 (8004), 1.5wt% day 3 (4993), 2wt% day 3 (5638), 1wt% day 7 (10359), 1.5wt% day 7 (14870), 2wt% day 7 (6132).

We hypothesized that 1wt% and 1.5wt% have a different number of cell clusters when measured in total (Figure 15) and wanted to determine how this affected the results. Time of culture affects the total spheroid volume, but the weight percentage does not. Only Day 1 and Day 7 were statistically different from each other ($\alpha < 0.05$). This suggests that the differences in

number of spheroids in different sample types are balanced by the average spheroid volume so that total spheroid volume is not a function of weight percentage of macromer. While more compliant hydrogels may have larger spheroids, they don't occupy more total space than those of stiffer hydrogels which supports the conclusions from the Pico Green assay that all hydrogels show about the same degree of proliferation.

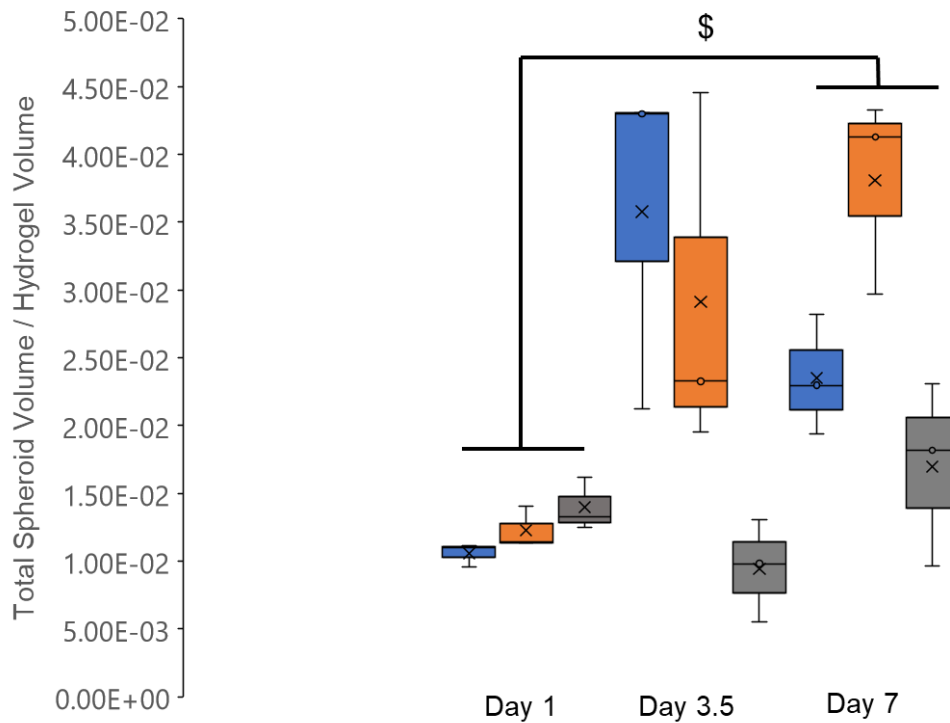


Figure 15 - MADM OPC line encapsulated at 1wt% (wt/v) NorHA, 1.5wt%, and 2wt% all showed increases in total spheroid volume over a period of 7 days.

\$ indicates significant difference in fraction of total spheroid volume at each time point ($\alpha < 0.05$). (n=12) for all sample types.

Representative max projections of hydrogel samples (Figure 12) visually show similarities between the 1wt% hydrogels and the 1.5wt% hydrogels over the 7 day period in comparison to the 2wt% hydrogels. Although cellular area was increased in all hydrogel sample stiffnesses, the vast majority of cells in these hydrogels exhibit rounded morphologies, which

supports Li et. al.'s conclusion that the number of processes of OPCs culture inside 3D hydrogels decreases significantly when the elastic modulus is $> 120 \text{ Pa}$.²⁰

Finally, to compare cell viability in these hydrogels to those of Leach et. al., we measured the total live spheroid volume to dead spheroid volume ratio (Figure 16). Leach et. al. reported values of 60-100% viability with the GMHA hydrogels nearing 100%.²⁶⁷ In these NorHA hydrogels we report a 6:1 ratio of live to dead cells on day 7 (85% viability) for the 1wt% samples, 4:1 ratio of live to dead for 1.5wt% on day 7 (80% viability), and 2.5:1 ratio of live to dead for the 2wt% on day 7 (71% viability).

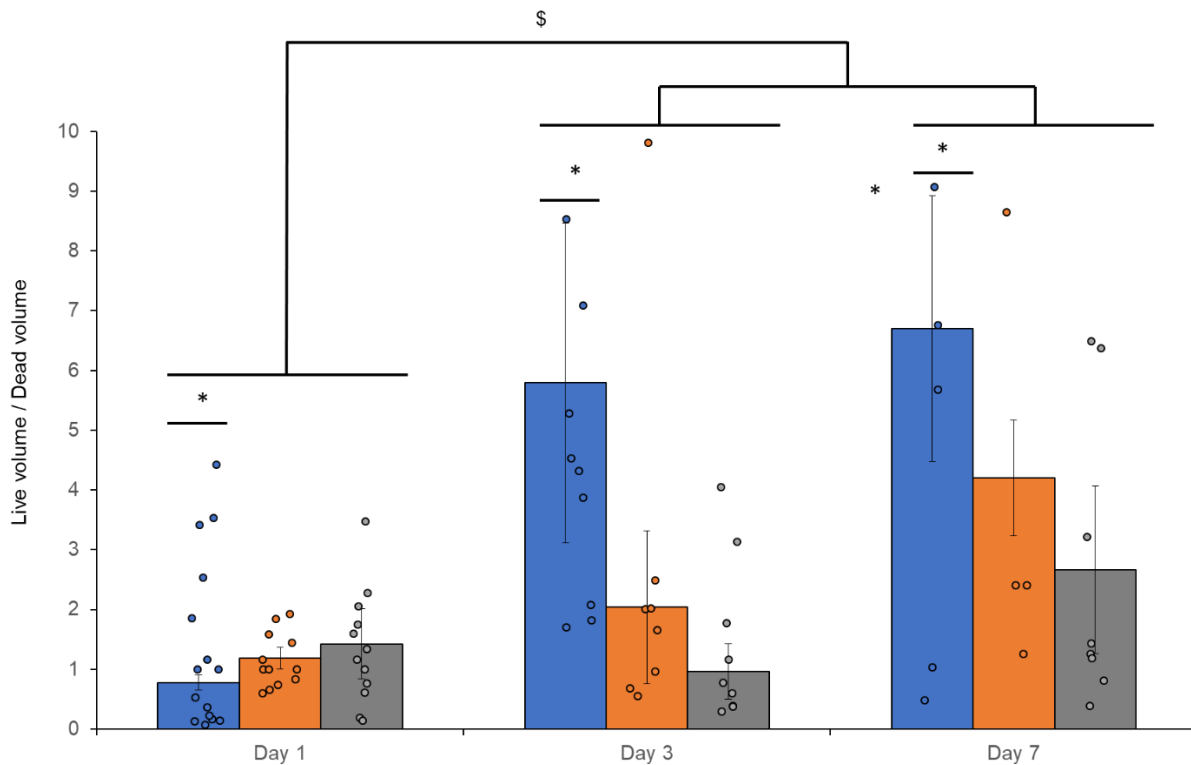


Figure 16 - The ratio of total live spheroid volume to dead spheroid volume was taken for all sample types.

(n = 13) for 1wt% day 1, (n=13) for 1.5wt% day 1, (n=12) for 2wt% day 1, (n=9) for 1wt% day 3, (n=8) for 1.5wt% day 3, (n=9) for 2wt% day 3, (n=8) for 1wt% day 7, (n=8) for 1.5wt% day 7, (n=8) for 2wt% day 7.

Conclusions:

NorHA hydrogels were synthesized with stiffness resembling CNS tissue. Mesh sizes calculated were larger than Russell et. al. but smaller than Leach et. al. Studies of NorHA hydrogels with OPCs and no fibers showed proliferation in all sample types over a 7 day period without any significant differences between them. ATP/DNA was largest in the lowest stiffness hydrogels followed by the medium stiffness and high stiffness hydrogels. Average spheroid volume per gel volume was greatest in the low and medium stiffness hydrogels in comparison to the high stiffness hydrogels. Total spheroid volume per gel volume was only a function of day of culture and not of stiffness. Due to larger mesh sizes in the NorHA hydrogels, average live spheroid volumes were greater than in PEGDM hydrogels. Viability of OPCs after 7 days of culture was greatest in the lowest stiffness hydrogels (85%) and lowest in the highest stiffness hydrogels (71%).

Chapter 3: Future Work: Fiber Encapsulation Studies with Hyaluronic Acid Hydrogels

Introduction:

Previous literature has simulated natural CNS development in vitro in 2D cultures. Chan et. al. were the first to incorporate axon mimics (polystyrene fibers) in 2D, showing structure property relationships such as myelin basic protein (MBP) expression as a function of fiber diameter.²²⁰ The 2D model lacks physiological relevance because tissues are 3D structures. Demyelination and remyelination have been observed in vivo in rat models, however challenges still remain in separating the mechanisms' pathology and forming structure property relationships.^{52,53} A 3D in-vitro model may be able to elucidate the important microenvironmental features for OPC survival, growth, and differentiation. Additionally, 3D in vitro models are not complicated by the presence of signaling factors from the surfaces of live axons. We hypothesized that cell behavior would be different in 3D, as now the cells have freedom to expand in all directions. There is already some evidence corroborating this, such as recent work from Seidlits et. al. that showed improved proliferation and differentiation in 3D human neural stem cell cultures in hyaluronic acid hydrogels compared to in 2D.²⁵⁵ Evidence of axon mimic encapsulation in 3D is yet to be discovered.

Materials & Methods:

Electrospinning:

Electrospinning solution was made in 3mL batches consisting of 2wt% MeHA, 3wt% PEO,²⁶⁸ 0.05wt% I2959, 5.55×10^{-8} wt% methacryloxyethylthiocarbamoyl rhodamine B in DI water solvent. Fibers were spun in a Spraybase electrospinning apparatus with conditions set at 30- 40% relative humidity, 45°C chamber temperature, 10-15 kV voltage, 21 cm distance to collecting plate, 11.9 mm diameter Cadence syringe of 5 mL volume, 0.4 mL/hr solution flow rate, class E electrospinning tubing from Spraybase, and 20 gauge nozzle oriented vertically downwards towards the collecting plate. The collecting plate was covered with either aluminum foil. Collected fibers were placed in Ziploc storage bags under nitrogen and crosslinked under UV light using 14 mW/cm² light intensity (365 nm) for 15 minutes.

Fiber Preparation:

After weighing the dried fiber mass, crosslinked MeHA fibers were suspended in PBS at 0.4wt%. Fiber solution was mixed through inversion for 10 minutes. Fibers were broken up using a 20 gauge needle followed by pipetting with a 5 mL pipet tip and a P1000 pipet tip. Fiber solution was sterilized in a petri dish under UV light for 4 hours in the TC hood. Fiber solution was then pipetted in hydrogels at 0.18wt%.

Mechanics of hydrogels with fibers

MeHA fiber webs were electrospun into mats, crosslinked under UV light, and suspended in PBS at 0.4wt%. Under the scanning electron microscope (SEM), individual fibers can be observed (Figure 17).

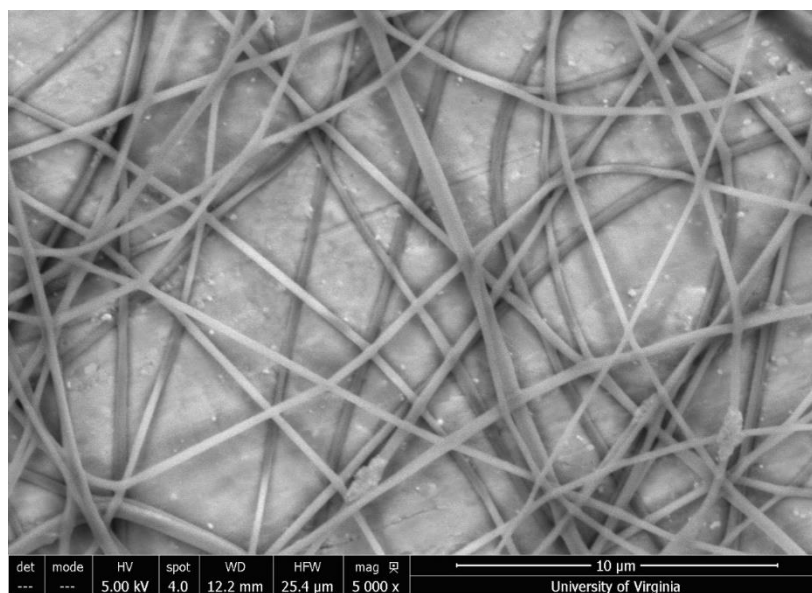


Figure 17 - SEM imaging of fiber mats shows individual fibers with consistent cross section and no signs of webbing between fibers.

This indicates that individual threads were pulled through the electric field with sufficiently high solution viscosity and conductivity. Fiber diameter was measured manually to be $0.316 \pm 0.035 \mu\text{m}$.

After crosslinking, the fibers resemble large sheets that can then be hydrated without dissolution. The fibers can be cut into individual strands using a cryostat (Figure 18), but these showed poor viability in cell encapsulation studies. One possible reason is that these hydrophilic fibers retained too much of the OCT media used to freeze the sample even after rinsing thoroughly and lyophilizing. A more reserved approach was to force the hydrated fiber mats into an 18 gauge needle syringe to break them up. The distribution of fiber sizes was still large. MeHA hydrated fiber mats absorb several times their weight in water and become sponge-like, making them difficult to separate without heavy force.

Encapsulations with fibers showed sample heterogeneity. Future work could mitigate this issue by thinly slicing dry MeHA fibers followed by soaking and pushing through the needle. Areas with fibers were imaged (Figure 19) and compared to samples without fibers and samples with 2mM RGD. We hypothesized that process extension would be encouraged by adhesive ligands, so the comparison between hydrogels with fibers and hydrogels with RGD definitely makes a statement about the kind of benefits the fibers provide.

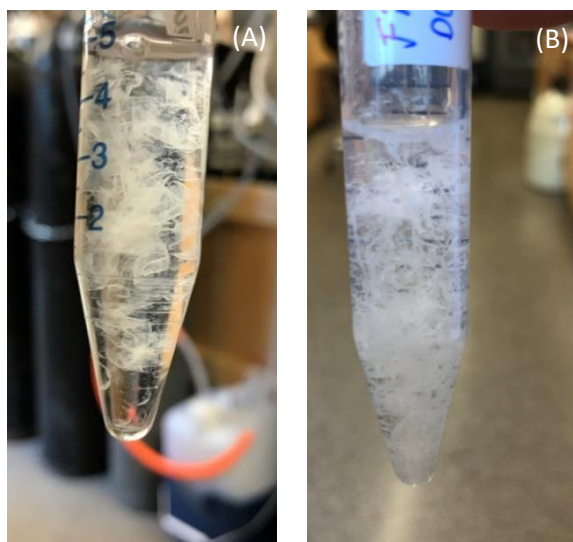


Figure 18 - (A) Fiber mats were electrospun on aluminum foil, gently scraped off the aluminum foil, and suspended in solution. (B) Using the cryostat, the fibers are shorter and more uniform in shape.

Electrospun fibers are long soaked sheets that are elastic in nature and difficult to cut precisely. For cryosectioned fibers, exposure to tissue cutting media (OCT media), highly unsterilized cutting surfaces, and opaque nature of the fibers may have made them difficult to sterilizing under the UV light.

Cell morphology on Day 1 and Day 3 was no different from the encapsulations without fibers. Day 7, however, showed significant process extension and cell cluster development. The formation of processes in all sample type hydrogels is an indication that the mesh size of all hydrogels (Table 1) are compatible for cell-fiber interactions. Regions of hydrogels with heavy fiber presence may have altered mechanical properties (i.e. mesh size and stiffness)

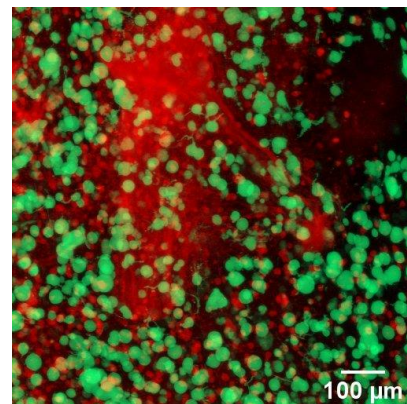
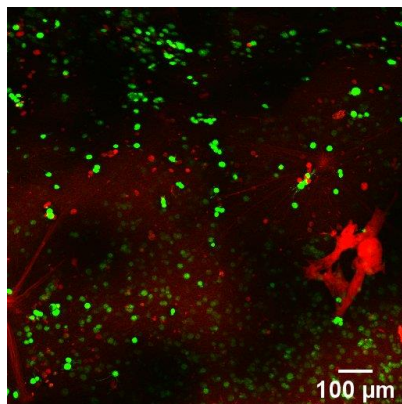
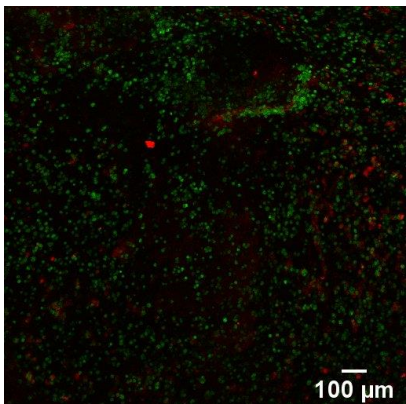
since crosslinks may not be uniform in those regions (i.e. a spoon embedded in a cylindrical piece of jello). Li et. al's conclusion of no process extension in hydrogels with stiffness > 120 Pa seems to be refuted when fibers are present. Oscillatory shear rheology on hydrogels with fibers (0.18wt%) is needed to see if mechanical properties had changed.

Day 1

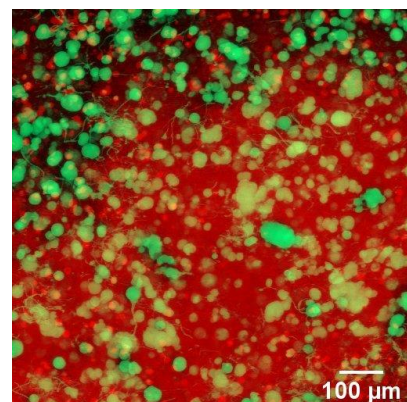
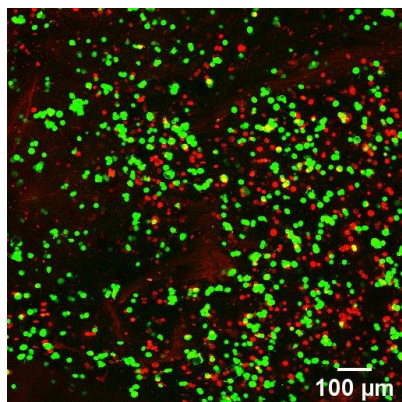
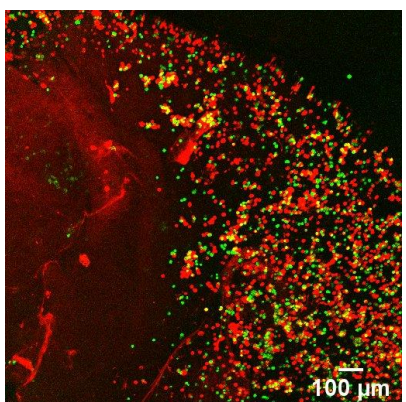
Day 3.5

Day 7

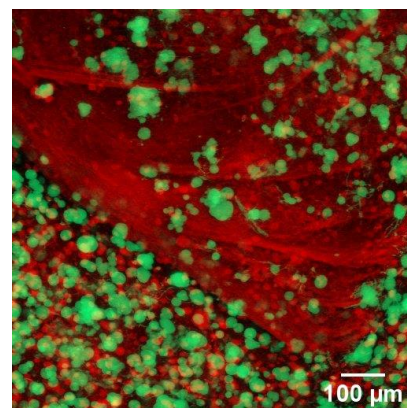
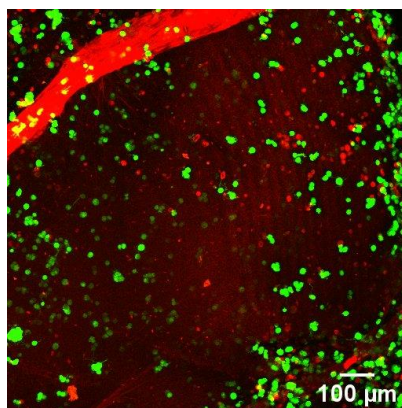
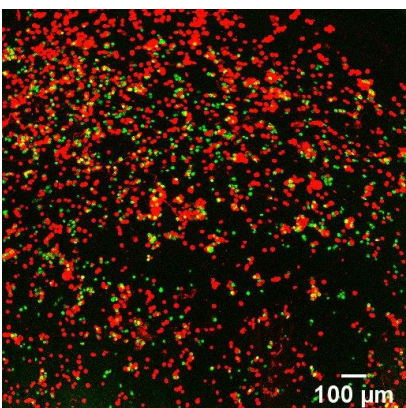
1wt% w/fibers



1.5wt% w/fibers



2wt% w/fibers



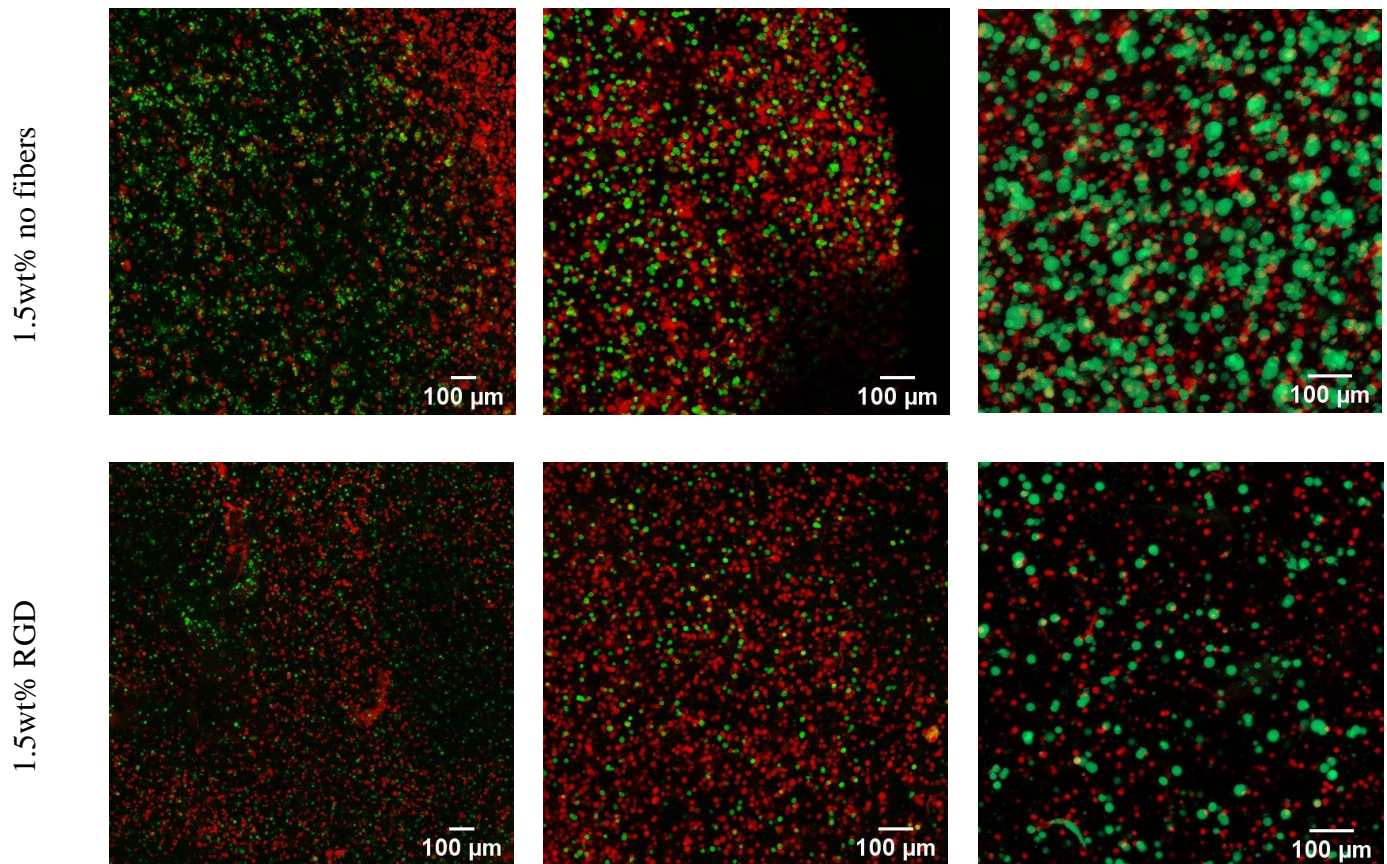


Figure 19 - 10 μm slices of NorHA hydrogels with 0.18wt% MeHA fibers.

Portrait (1,1) 390 μm depth (1,2) 300 μm depth (1,3) 320 μm depth (1,4) 1297 μm depth (1,5) 828 μm depth (2,1) 250 μm depth (2,2) 280 μm depth (2,3) 350 μm depth (2,4) 280 μm depth (2,5) 450 μm depth (3,1) 1150 μm depth (3,2) 910 μm depth (3,3) 900 μm depth (3,4) 1520 μm depth (3,5) 1330 μm depth

Effects of encapsulated fibers on OPC proliferation and metabolic activity

Fibers were encapsulated at 0.18wt% with OPCs in 1-2wt% NorHA hydrogels. Comparisons were made to hydrogels without fibers and hydrogels with RGD adhesive peptide. Preliminary results show promise that hydrogels with fibers encapsulated may actually improve the overall metabolic activity according to Alamar Blue in comparison to hydrogels without fibers and hydrogels with RGD. The significant jump in fraction of Alamar Blue reduced on day 7 may

just be an artifact of over-exposure to ambient light before reading cell-induced reduction fluorescence values, however the trend between sample types is clear. The data supports the conclusion that the MeHA fibers promote OPC maturation to a greater degree than RGD does. The cells may be using the fibers as mechanical cues with thicker fibers inducing greater maturation (and more complex process extensions), but there is possibility that the fibers could also be used like an adhesive ligand. Perhaps with the larger mesh sizes in comparison to PEGDM hydrogels, OPCs are able to reach the critical population densities needed to mature. Further studies on MBP expression and myelin oligodendrocyte glycoprotein expression in hydrogels with fibers are needed to distinguish between maturity, ensheathment, and concentric wrapping of fibers.

Surprisingly, RGD which is supposed to support cell adhesion (something that is needed in 3D encapsulations), has more of a negative impact on overall cell metabolic activity. Perhaps other concentrations of RGD may be more beneficial. Russell et. al. found that incorporation of Laminin I did not have any effect on OPCs in 3D PEGDM hydrogels.²⁶⁷ Seidlits et. al. found that Laminin I had no effect on fate of neural stem progenitor cells in 3D hyaluronic acid hydrogels.²⁵³ Hyaluronic acid methyl cellulose hydrogels (HAMC) modified with RGD and PDGF-A showed enhanced OPC survival when compared to HAMC with only PDGF-A or HAMC alone in vitro.¹⁵⁷ In vivo data showed improved migration of OPCs from the injection site to the lesion site at two weeks post rat spinal cord injury with the RGD-modified biomaterial.¹⁵⁷ As there are mixed results, the effects of RGD vs Laminin on OPC cultures in 3D are not really clear at this point. Perhaps the use of MeHA crosslinked with RGD in encapsulation studies may be worthwhile to enhance the adhesive properties of the fibers and promote greater maturation towards myelination.

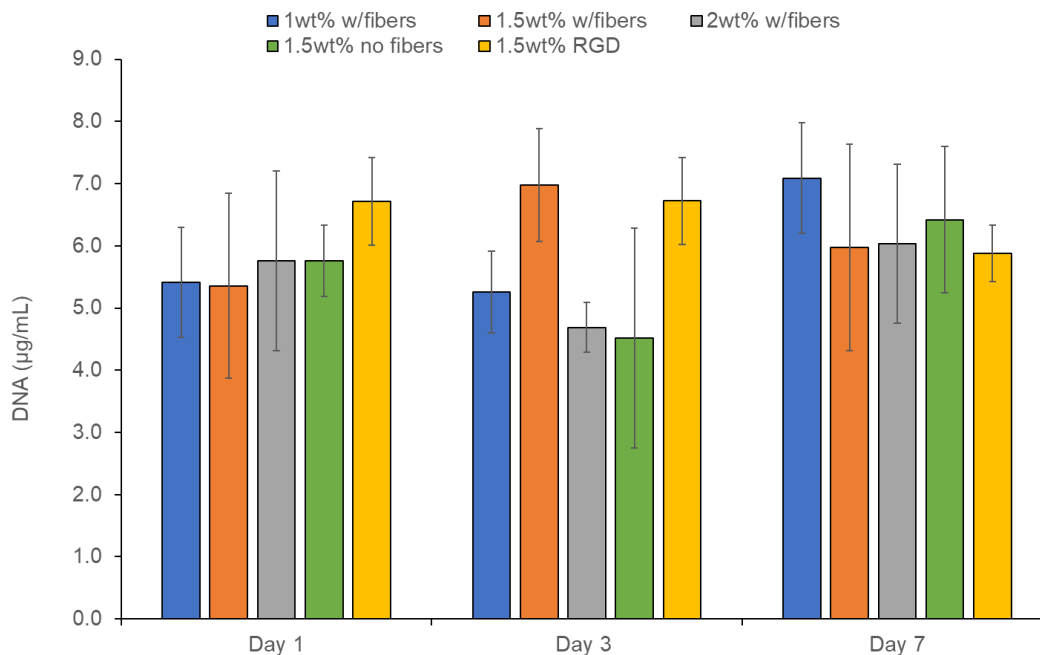


Figure 20 - Pico Green assay for experimentation with fibers shows inconclusive results. (n=3) for each sample type.

Pico Green assay results are inconclusive after 7 days of culture (Figure 20), but with the trends in Alamar Blue (Figure 21), Cell Glo (Figure 22), and ATP/DNA (Figure 23) it is reasonable to hypothesize that the same trends observed in hydrogels without fibers will be observed in hydrogels with fibers when referring to OPC behavior as a function of stiffness and

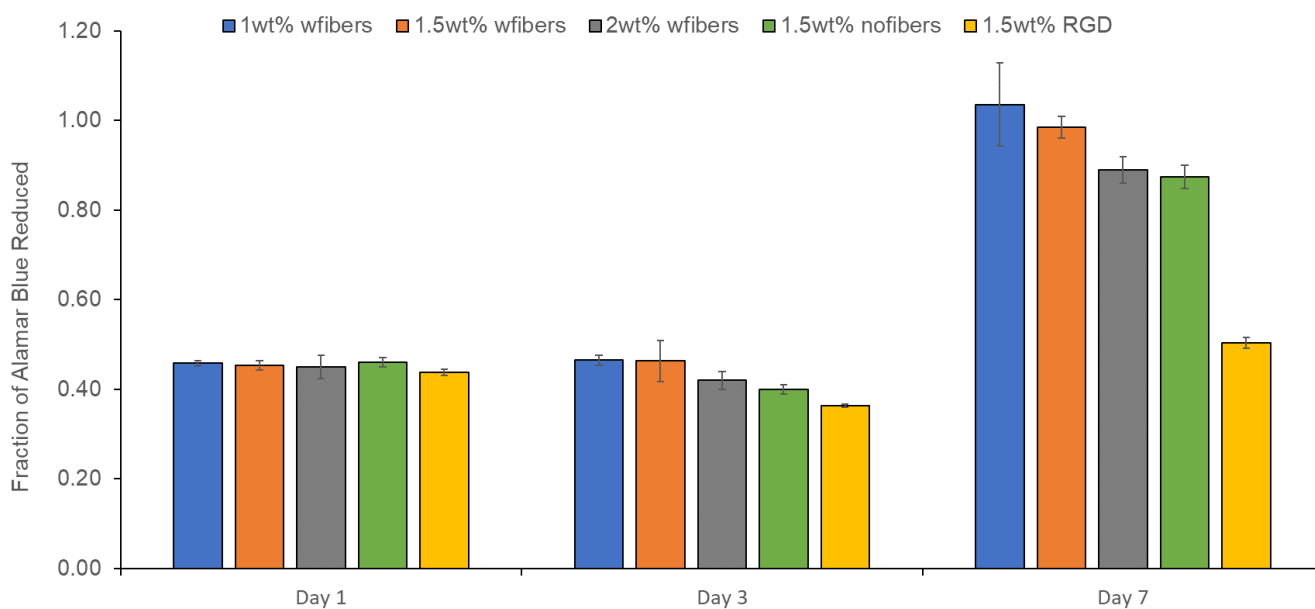


Figure 21 - Alamar Blue assay on hydrogels with and without fibers. (n=3) for all sample types. Fraction reduction values about 1.00 may be due to over-exposure of samples to ambient light.

mesh size. The notable difference may be that the fibers could very well improve the metabolic activity of OPCs in comparison to no fiber conditions and RGD conditions.

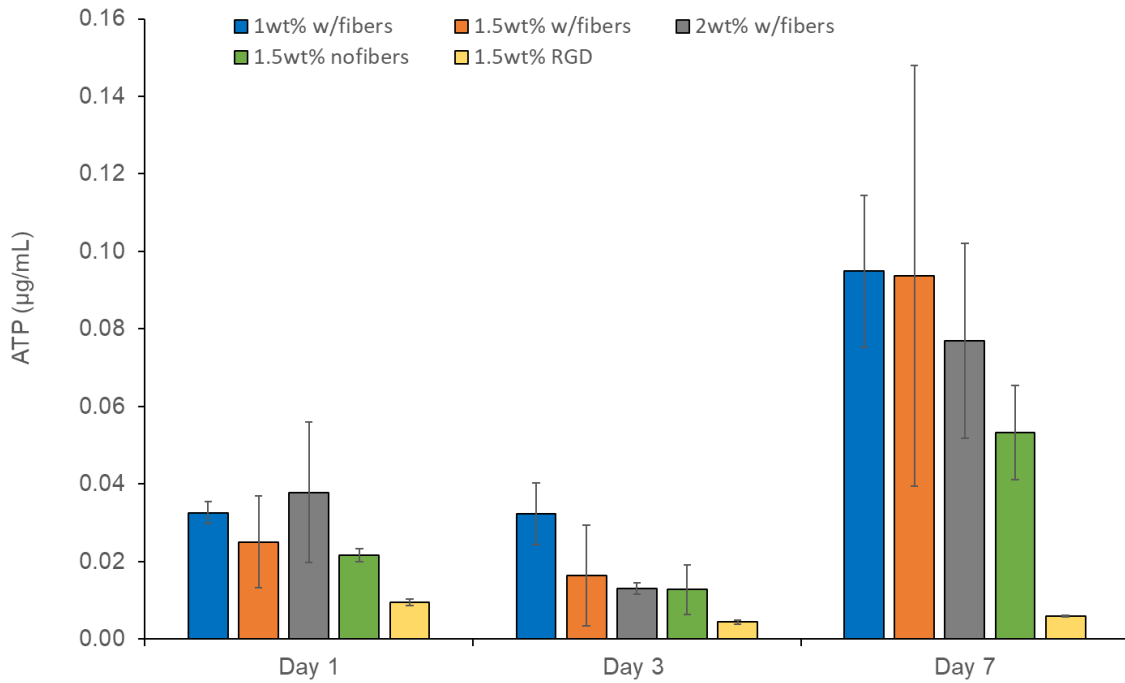


Figure 22 - Cell Glo assay shows similar trends to no fiber experiments when referring to ATP concentration as a function of stiffness. (n=3) for all time points.

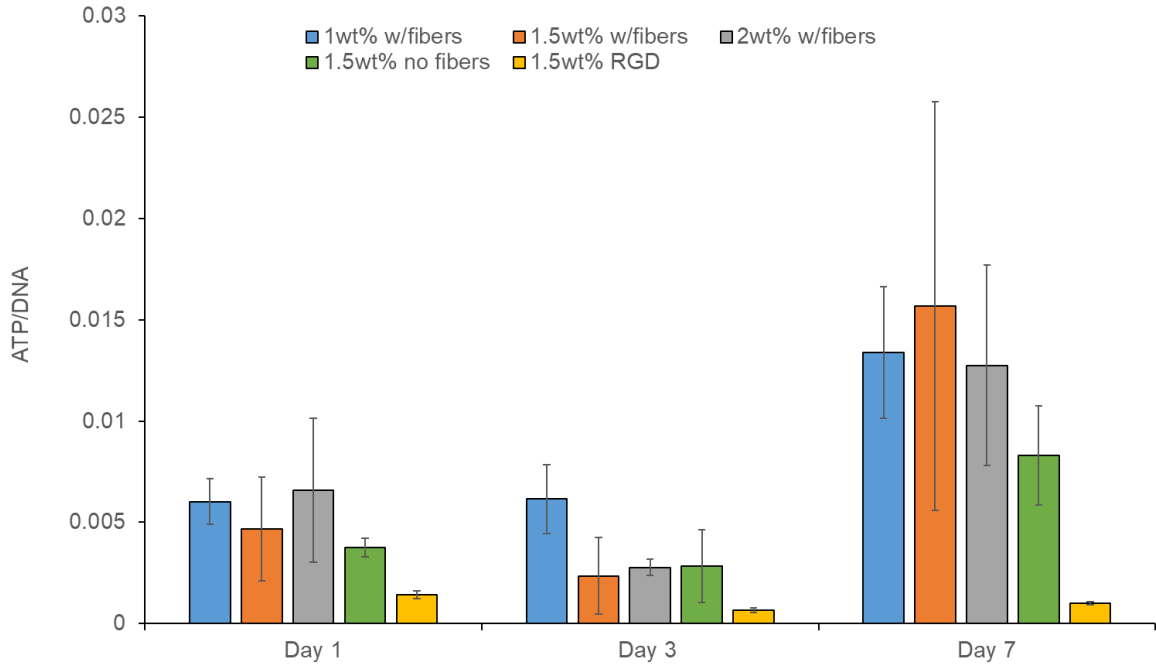


Figure 23 - ATP/DNA shows similar trends to no fiber experiments when referring to ATP concentration as a function of stiffness. (n=3) for all time points.

Appendix

Appendix 1: MeHA HNMR spectrum, HA-TBA, and NorHA HNMR spectrum

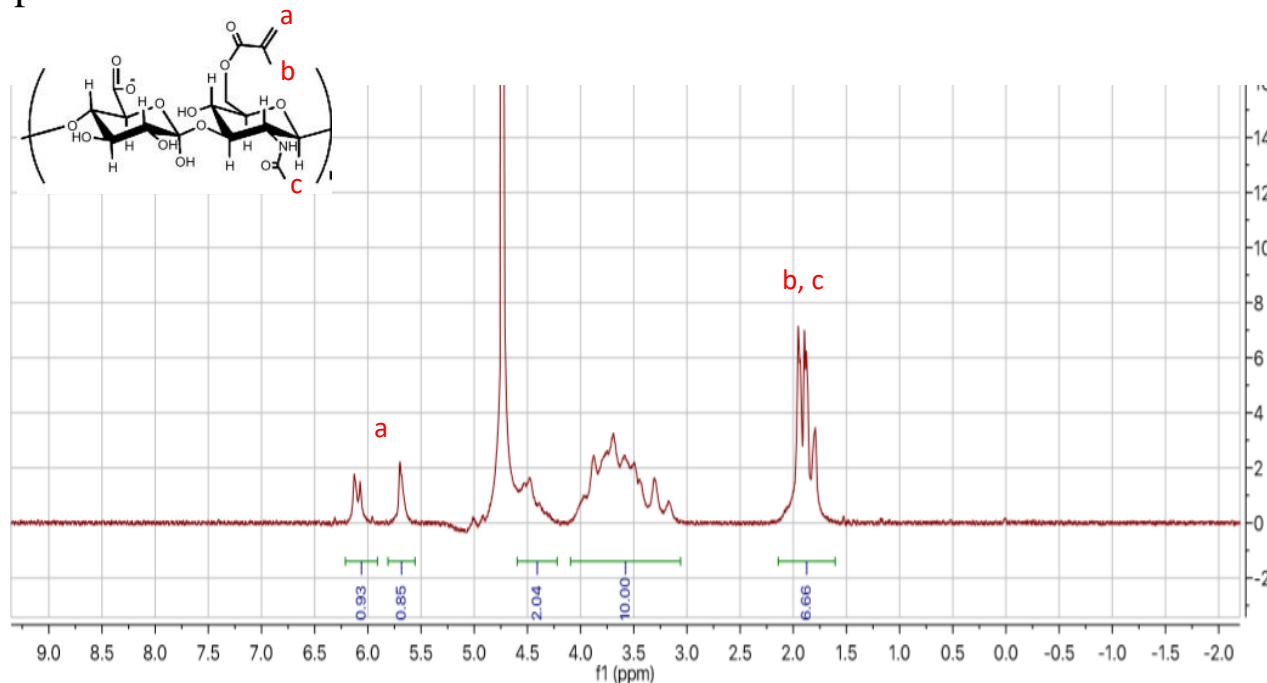


Figure 24 - MeHA HNMR spectrum for 90% methacrylation efficiency.

Integrated peaks are normalized to the HA backbone between 3.0 ppm and 4.0 ppm. Peaks at 5.7 and 6.2 are averaged to get the methacrylation efficiency.

The methacrylation efficiency is determined by setting the hyaluronic acid polysaccharide backbone peaks to 10 and then integrating the peaks at (a). The average of the

two peaks (a) is taken.

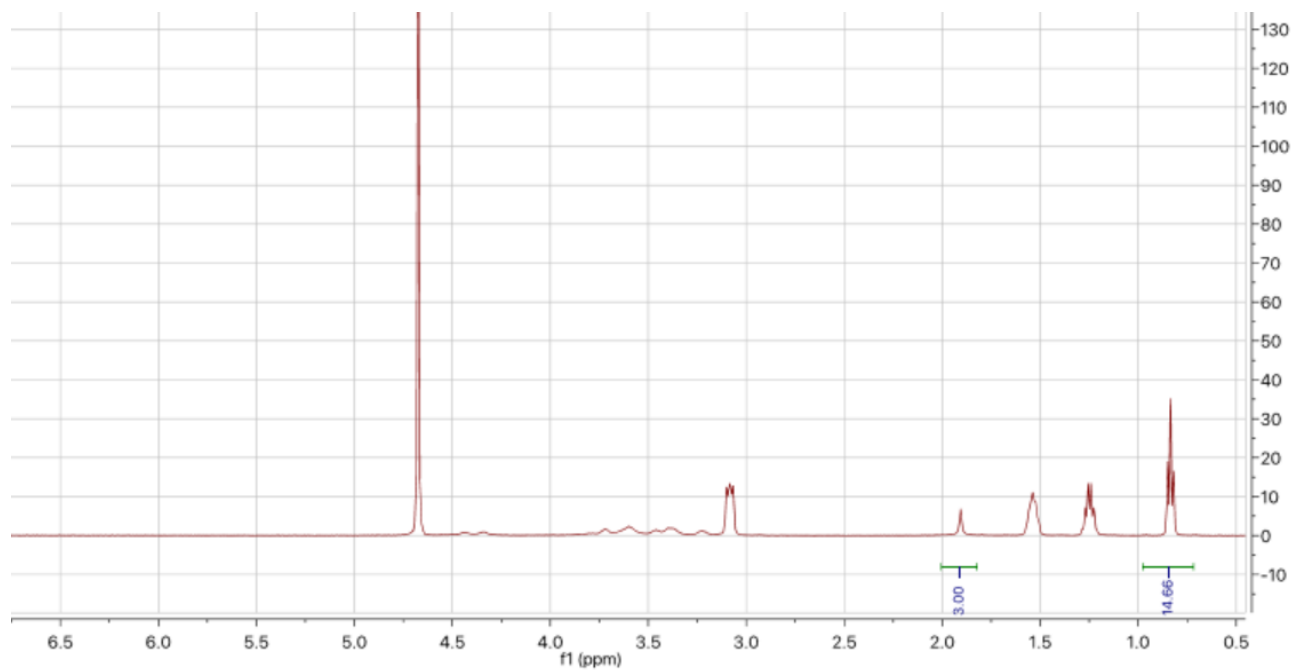


Figure 25 - HA-TBA HNMR spectrum.

The hyaluronic acid backbone carbons are seen again from 3.2 – 3.7 ppm however they are not important for integration. The methyl peak is the standard again at 1.8 ppm. The value of the tetra-butyl ammonium peak at 0.7ppm is used in the calculations to determine the amount of Nor-amine and BOP needed for making NorHA.

The HA-TBA spectrum is normalized to the methyl peak at ~1.8 ppm. This is set to 3.00. Then the peak at 0.6 ppm is integrated and the value is used in calculations for amount of nor amine and BOP to use in the coupling reaction. This value changes depending on the ratio of HA-TBA to sodium hyaluronate that results from the titration.

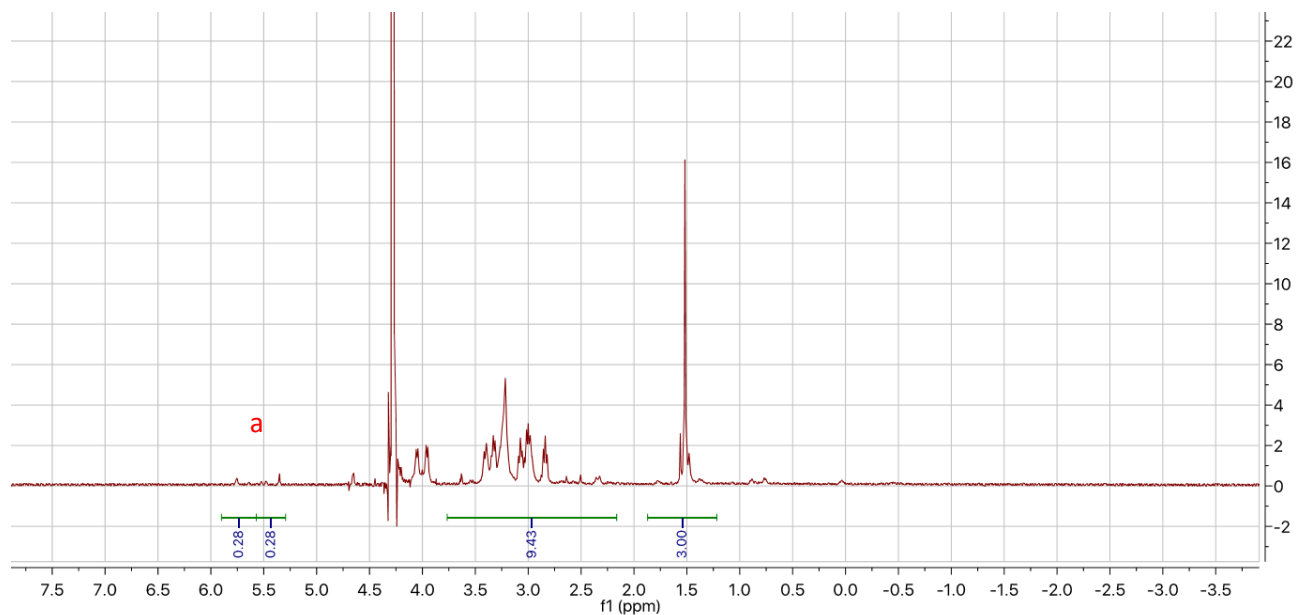


Figure 26 - NorHA HNMR spectrum.

The methyl peak is again the integration standard (1.5 ppm). The norbornene peaks at 5.2 and 5.7 ppm are averaged to get the functionalization efficiency.

For the NorHA spectrum, first the methyl peak at 1.5 is integrated and set to 3. Then the peaks at 5.3 and 5.7 are integrated to get the norbornene functionalization efficiency. The average of the peaks is taken at (a). Note how the hyaluronic acid backbone at 2.5 – 3.5 ppm is ~10 since as was the case for the MeHA spectrum.

Appendix 2: Protocols

Appendix 2-1: Flask preparation for OPC MADM cells in the Lampe Lab:

1. Prepare poly-ornithione covered T-75 flasks (TC hood).
 - a. Open a 5-pack of T-75 flasks in the TC hood.
 - b. Coat with polyornithione (10 $\mu\text{g}/\text{mL}$) at 5 mL per flask
 - c. Incubate for at least 30 minutes at 37°C incubator
2. Prepare OPC proliferation media (TC hood) consisting of:
 - a. 40 mL DMEM (with 4.5 g/L D-glucose, L-glutamine, and 110 mg/L sodium pyruvate)
 - b. 400 μL pen-strep (aliquots are same concentration as stock solution)
 - c. 800 μL B-27 supplement
 - d. 400 μL N-2 supplement
3. Wash the polyornithione-covered plates (TC hood).
 - a. Wash 3x with 5 mL each of DPBS without Ca^{2+} and Mg^{2+}
 - i. Aspirate the PBS out of the flask carefully with a 200 μL pipet tip on the glass pipet. Do not touch the inside surfaces of the T-75 flasks with the pipet tip or the extension of the glass pipet.
4. Coat T-75 flasks with OPC proliferation media (8 mL per flask).
 - a. Do not touch the 10 mL pipet tip to the inside surfaces of the flask. The pipet will project the fluid into the flask from a distance.
5. Seed OPCs at 5.00×10^5 cells/plate.
6. Change media after two days.
7. Passage cells after a total of four days of culture. They should be confluent at this point.

Appendix 2-2: Passaging on T-75 flasks in the Lampe Lab:

1. Flasks should be prepared according to Appendix 2-1. This protocol will instruct how to seed OPCs at 5.00×10^5 cells/plate.
2. Aspirate media from confluent plates (TC hood).
3. Replace contents of confluent flasks with 5 mL DPBS (without Ca^{2+} and Mg^{2+}) and 250 μL of trypsin (10x concentration in aliquots) (TC hood).
4. Swirl plates thoroughly and allow trypsinization to occur for 6 minutes (TC hood).
5. Pipet out the DPBS with trypsin and cells into a 10 mL Falcon tube (TC hood).
6. Rinse the T-75 flasks with 5 mL of DPBS to collect any remaining cells and pipet into the Falcon tube (TC hood).
7. Seal the Falcon tube and centrifuge the cell solution at 1000 RPM for 5 minutes (balance the centrifuge with appropriate blank volumes).
8. Aspirate out the supernatant (TC hood). A white cell pellet should remain at the bottom of the flask.
9. Add 500 – 1000 μL of OPC proliferation media to the Falcon tube (TC hood) depending on how concentrated the cell solution should be.
 - a. Triturate the solution with a P1000 pipet tip. Be careful not to introduce too many bubbles. The cell solution should mix completely with the media to form a suspension.
10. Pipet 10 μL of cell solution into a mini Eppendorf tube. This tube will be taken out of the hood for cell counting.
11. Pipet 90 μL of Trypan Blue solution into the mini Eppendorf tube. Mix the solution thoroughly.

12. Pipet 10 μL of the cell/trypan blue solution into the hemocytometer with the special glass coverslip on top of the gridded area. Angle the pipet tip up towards the glass coverslip in order to encourage the liquid to settle in the gridded area.
13. Using the microscope, count the cells in the four quadrants. Take an average for the four quadrants to get cell count.
14. Multiple the cell count by 10^5 to get the concentration of cells in the solution (cells/mL).
 - a. One plate should be able to yield 1×10^7 cells/mL under the best growth conditions but less than that is often observed.
15. Using the cell solution in the TC hood, seed the T75 flasks at 5.00×10^5 cells/plate (TC hood).

EX:
$$\frac{5.00 \times 10^5 \frac{\text{cells}}{\text{plate}}}{1 \times 10^7 \frac{\text{cells}}{\text{mL}}} = 0.050 \text{ mL} = 50 \mu\text{L}$$

Therefore if you end up with 1×10^7 cells/mL you will need to add 50 μL of the cell solution to the flask to get the right seeding density.

16. Swirl the plate with cells thoroughly in order to get proper distribution of cells on the plate (TC hood). Label the flask with the passage number, date, and name.

Appendix 2-3: Freezing cells down:

1. Leftover cell solution from an experiment can be frozen down. The orange lid cryogenic tubes should be used for this. Use a concentration of 1×10^7 cells/mL for freezing and add 10% by volume DMSO (in the TC hood). Label the cryogenic tube with the passage number, date and name.
2. After sealing the cryogenic tube, place in the $-80\text{ }^\circ\text{C}$ freezer overnight. This is so the cells will not get temperature shocked when put in LN2.
3. Place the cryogenic tube in the LN2 dewar after freezing overnight.

Appendix 2-4: Seeding frozen cells:

1. Remove the cryogenic tube from the LN2 dewar and allow to thaw at room temperature.
2. Prepare T-75 flasks according to protocol Appendix 2-1.
3. Pipet one tube's worth of solution per flask (TC hood). Swirl thoroughly. Many of the cells will die overnight because of the presence of DMSO.
4. After one day of culture, change media in the T-75 flask to remove the toxic DMSO.
5. Culture cells as normal according to procedure Appendix 2-1.
6. Passage cells as normal according to procedure Appendix 2-2. Do not use the cells from this passage in an experiment. Wait until the next passage to use cells in an experiment.

Appendix 2-5: MeHA macromer synthesis in the Caliri Lab:

1. Weigh 4g of sodium hyaluronate (65 kDa).
2. Secure the round bottom flask in a clamp resting on a cork based while sitting on top of a stir plate. Place the football-shaped stir bar in the flask.
3. Add the sodium hyaluronate to the round bottom flask.
4. Add 200 mL of distilled water to the round bottom flask. Stir vigorously until fully dissolved.
5. Calculate the amount of methacrylic anhydride (MA) needed for the reaction using the following formula.

$$\frac{4g \text{ NaHA}}{1} * \frac{1 \text{ mol}}{65,000 \text{ g}} * \frac{65,000 \frac{g}{\text{mol}}}{385 \frac{g}{\text{mol}}} (\text{number of reaction sites}) * 0.9 (\text{functionalization efficiency desired})$$
$$* 12.3 (\text{excess MA}) * \frac{154.2 \text{ g}}{\text{mol}} \text{MA} * \frac{1.04 \text{ mL}}{\text{g}}$$

6. Place the dissolved HA solution in an ice bath within a crystallization dish and continue to stir.
7. Calibrate the pH probe using the buffer solutions. Then insert the pH probe in the crooked leg of the flask. Make sure that it is anchored properly and away from the stir bar so the stir bar can operate freely.
8. Monitor the pH. It should be around 7 in the dissolved HA solution.
9. Add 1 mL of MA slowly to the stirring solution. Bubbles should form. The pH needs to be adjusted to be 8-9.
10. Add NaOH solution to maintain pH. Only a few drops should be needed.
11. Wait 5 minutes for the pH to stabilize and then add another 1 mL of MA. Again, maintain the pH to be around 8-9.

12. Repeat step 9 until all the MA has been added. By the end of the reaction, the solution should look like a colloidal suspension. This ensures that the organic phase and aqueous phase have mixed and can behave like a stable suspension.
13. The ice bath can be removed. Continue stirring the solution overnight so that excess methacrylic anhydride degrades. Place rubber stoppers over the legs of the flask to prevent evaporation of fluid.
14. After overnight stirring, place the solution in DI water dialysis for 5 days switching out the water twice a day. Cloudiness should disappear quickly. If there are excess bubbles in the solution for the organic phase, they can be popped by centrifugation.
15. ^1H NMR with D_2O . Scale the integration to the hyaluronic acid backbone at $\sim 2.5 - 3.5$ ppm (integration value of 3.00).

Appendix 2-6: NorHA macromer synthesis in the Caliri Lab:

A. HA-TBA Synthesis

1. Dissolve 5g NaHA in 250 mL DI water 1-neck, 500mL RBF. (can scale to any batch size needed, just increase H₂O and resin accordingly). If converting polymer (MeHA, NorHA, etc) back to TBA salt vortex in DI water, then add to RBF.
2. Add Dowex 50W x 200 (15g resin; 3g resin/1g HA) to HA solution (Dowex Resin will exchange sodium ion for hydrogen ion, making the resulting solution very acidic)
3. Stir for ~2 hours.
4. Stop stirring and let resin settle to the bottom of flask, then filter HA/resin mix w/ #2 filter paper by vacuum filtration. Repeat filtering if necessary until solution is clear.
5. Set aside ~ 10 mL HA solution in case titration is over-shot
6. Titrate by TBA OH to ~pH 5 (will need a lot of TBA OH to do this, at least 10 mL for 5 g)
7. Titrate slowly and carefully by TBA OH (1:1 w/ DI water) to ~pH 7
8. Titrate by TBA OH (1:5 w/ DI water) to ~ pH 7.02-7.05
*if you overshoot pH, just add a bit of the HA solution set aside.
9. Once neutral, partition to 50 mL tubes and freeze @ -80 C. Lyophilize dry. Purge tubes with N₂ and store at -20 °C.
10. Glassware can be rinsed thoroughly in sink and washed, since it is water based
11. ¹H NMR with D₂O. Normalize to the hyaluronic acid backbone chain (integration value of 10) at 3.0 – 3.5 ppm.

B. NorHA synthesis

1. Allow the HA-TBA to come to room temperature. Use about 4g of HA-TBA for the conversion to NorHA to allow for space for fluid in the round bottom flask.

2. Remove the one-necked RBF from the oven, equipped with the football shaped stir bar. Stopper immediately. The reaction is anhydrous so the flask needs to be devoid of moisture.
3. Once cooled add the HA-TBA and nor-amine. Nor-amine amount to be added should be calculated using the spreadsheet on the Caliari lab drive. Inputs on the spreadsheet are the TBA methyl peak integration, the mass of HA-TBA used, and the functionalization efficiency desired.
4. Attach the round bottom flask to the ring stand above the stir plate in the hood and set the stirrer to ~350 rpm.
5. Add anhydrous DMSO (~5 mL per 0.1g of HA-TBA) to round bottom flask via cannulation.
6. Once the HA is fully dissolved, mass the BOP (according to the calculation spreadsheet) into a separate 25 mL round bottom flask and stopper.
 - a. Add ~20 mL of DMSO via cannulation, dissolve, and cannulate the solution into the reaction.
 - b. Rinse cannula with acetone and return to oven.
7. React for ~2hrs at room temperature.
8. Quench the reaction with DI water (~ 10mL) and transfer to pre-soaked dialysis tubing.
9. Perform dialysis for 5 days at room temperature (for first 3 days, include ~5g of NaCl in the dialysis water). Change water twice daily.
10. Filter to remove side-products from BOP coupling. (If large precipitates have formed, transfer to 50 mL tubes, centrifuge, then filter.
11. Return to dialysis for 3-5 days.

12. Transfer to 50 mL tubes, freeze at $-80\text{ }^{\circ}\text{C}$, and lyophilize.
13. H^1 NMR with D_2O . Scale the integration to the methyl peak at $\sim 1.5\text{ppm}$ (integration value of 3.00).

Appendix 2-7: Hydrogel without fibers preparation for 3D encapsulations

1. Usually 1mL of hydrogel precursor solution per sample type is a reasonable volume. With each hydrogel at 40 μL , this yields 25 hydrogels, enough for several different kinds of assays. Prepare a 6 mg/mL DTT solution, a 23 mM LAP solution, and a 8wt% NorHA solution. Sterile filter each of these solutions. Then prepare precursor solution formulations (without cells) as follows (TC hood) assuming a 1mL total volume per sample type:
 - a. 1wt%
 - i. 125 μL NorHA solution
 - ii. 48.5 μL LAP solution (0.0328wt%)
 - iii. 38.3 μL DTT (0.315 thiol / norbornene ratio)
 - b. 1.5wt%
 - i. 187.5 μL NorHA solution
 - ii. 48.5 μL LAP solution
 - iii. 57.8 μL DTT solution
 - c. 2wt%
 - i. 250 μL NorHA solution
 - ii. 48.5 μL LAP solution
 - iii. 77 μL DTT solution
2. The cell volume needed will vary depending on the concentration of cells available in the cell solution. It is wise to create a concentrated cell solution (i.e. 1mL at $\sim 2 \times 10^7$ cells/mL) so that there are enough cells for at least 3 sample types if not 4 (which is needed for fiber experiments) as well as cells to seed onto new T75 plates. Also, by creating a concentrated cell solution, the volume added to the gel precursor solutions is minimized, thus allowing

room for other components (fibers, RGD, etc...). There is only 1mL total volume allotted for each sample type.

- a. EX: cell solution concentration (2×10^7 cells/mL with 1mL solution). Cell volume to be added is 250 μ L per sample type to establish a concentration of 5×10^6 cells/mL in the precursor solution.
3. Fill the remaining volume of the precursor solutions with sterile PBS (TC hood).

Appendix 2-8: Hydrogel with fibers preparation for 3D encapsulations

1. Follow the formulations without cells in section Appendix 2-7.
2. Add cell solution (needs to be extra concentrated to allow room for fiber solution).
3. Add pre-made fiber stock solution. Fiber stock solution should be prepared according to A2-9, and it is 0.4wt%. Usually 450 μL of this solution is added (TC hood) to create a 0.18wt% concentration in the gel precursor solution.

Appendix 2-9: Fiber stock solution preparation (where cell viability was present)

1. After electrospinning a dry mat of fibers on aluminum foil (section A2-11), place the mat in a large Ziploc bag and purge the air inside the bag with nitrogen.
2. Crosslink the dry mat of fibers at 14 mW/cm^2 (365 nm) for 15 minutes. There is a timer on the UV light in the Caliri lab. Calibrate the light through the inside of the Ziploc bag. Repurge with nitrogen if needed.
3. Scrape the fibers gently off the aluminum foil. Use gloved fingers or the back of a razor blade (not the sharp end). Fibers should come off relatively easily.
4. Weigh the dry fibers to get a dry mass.
 - a. (optional) cutting the dry fibers into half centimeter bits may help with the breaking up of fibers following suspension.
5. Suspend the fibers in PBS at 0.4wt%.
6. Use an 18 gauge needle to break up the fibers in solution into smaller sections. Ideally fibers sizes should change based on needle gauge according to the Burdick paper abstract. These fibers may be difficult to separate when wet.
7. Sterilize the fiber solution under the UV light for at least 4hours. If a large volume of fiber solution is made (20 mL or so) then the fiber solution can be put into an open petri dish. Evaporation will not be an issue since the volume is large.

8. Add the fiber solution to gel precursor solution according to A2-8.

Appendix 2-10: Fiber stock solution preparation (where cell viability was not present)

1. Electrospin fibers, crosslink them, and suspend them in solution according to Appendix 2-9.
2. Centrifuge the solution at 5000 RPM for 5 minutes. A fiber pellet should form.
3. Remove supernatant.
4. Add ~2mL of OCT media to the wet fibers.
5. Go to the Deppmann cryostat on the 4th floor of PLSB.
6. Pour a layer or two of OCT media over an aluminum mount in the cryostat. This will provide support for the fiber solution. Allow the layer to freeze in the cryostat.
7. Pour the viscous OCT solution with fibers onto the layers of OCT media carefully so as to get as many fibers as possible oriented towards the blade. Allow the solution to freeze.
8. Place the aluminum mount in the cryostat and cut the fibers into 200 μm sections.
9. Use tweezers to collect the cut fibers into a conical tube.
10. Bring the cut fibers back to the Caliri lab. Rinse the fibers 3 times with DI water. Each rinse should have a 15 minute incubation period.
11. Refill the conical tube with DI water (enough for lyophilization). The DI water should be clear and void of any cloudiness from OCT media.
12. Freeze the conical tube at $-80\text{ }^{\circ}\text{C}$ freezer overnight.
13. Lyophilize the frozen fiber stock.
14. Upon drying of fibers weigh them to get a dry mass. They should all be clumped together.
15. Moisten the fibers with 70% ethanol (not soak) and place under the UV light for 4 hours.
The fibers should still remain clumped together.

16. Rinse the fibers 3x with sterile PBS (15 minute incubations per rinse). Keep track of the volume of PBS used. The fiber solution should be 0.4wt% at this point.
17. Suspend the fibers in 1x solution consisting of DMEM and Pen-strep (based on OPC proliferation media) overnight. Keep the fiber solution at 0.4wt%.
18. Use fibers in experiment according to Appendix 2-8.

Appendix 2-11: Electrospinning

1. Prepare electrospinning precursor solution. 3mL batches usually work best. A 23 mM I2959 solution and a 30 μ M methacrylated rhodamine B solution will be needed. Solution should be prepared as follows (assuming 3mL batches).
 - a. 60 mg MeHA
 - b. 90 mg PEO (900 kDa)
 - c. 500 μ L methacrylated rhodamine B solution
 - d. 304 μ L I2959 solution
 - e. 2196 μ L DI water
2. Allow the solution to mix over an hour or two in the 4 °C fridge. Cover with aluminum foil if desired.
3. Use a 5mL cadence syringe and a 20 gauge electrospinning needle to withdraw the solution into the syringe. There will be bubble formation.
4. Take this filled syringe, a piece of aluminum foil to wrap around the conducting plate, a Ziploc bag, and an extra 5mL cadence syringe with you to the Spraybase device.
5. Use the vertical electrospinning apparatus to spin fibers onto the aluminum foil at the following conditions:
 - a. 25% relative humidity
 - b. 45 °C
 - c. 8-16 kV
 - d. 21 cm collecting distance
 - e. 0.4 mL/hr solution flow rate
 - f. ~2-3 hours of spinning
6. Follow Appendix 2-9 or Appendix 2-10 for preparation of fibers to put into hydrogels.

Appendix 2-12: Oscillatory shear rheology

1. Use the glass plate for time sweeps. Replace the existing plate with the glass plate if needed.
2. Make sure the rheometer is level.
3. Using the settings to adjust the motor and the drive inertia. These calibrate the instrument.
4. Install the 25mm cone plate with smooth surface.
5. Zero gap the instrument with the cone plate.
6. Calibrate the UV light to $4\text{mW}/\text{cm}^2$ while the light is inserted underneath the glass plate.
7. Copy the NorHA test template to run a new set of tests with the same protocol.
8. Use $50\ \mu\text{L}$ volume when running a sample on the rheometer.

Appendix 2-13: Alamar Blue

1. Keep the stock Alamar blue solution protected from light in the 4 °C fridge. The Alamar blue solution is sterile.
2. Create a 10% (by volume) Alamar blue in OPC proliferation media solution (TC hood). If you have 9 hydrogels to test, you will need 400 μ L per gel plus 400 μ L for the blank (4mL total). Add media to Alamar blue, not the other way around.
3. Put the samples in the 37 °C incubator for 4 hours.
4. After four hours, remove the hydrogels from the reduced Alamar blue solution and continue culturing the hydrogels as needed for the experiment (TC hood)
5. Take the remaining Alamar blue solutions and pipet into the 96 well plate. Three pipet replicates of 100 μ L for each sample type.
6. Run the Alamar blue test on the Lampe Lab plate reader. Settings should all be set there except the layout of the 96 well plate which can be customized to each reading. Take fluorescence and absorbance readings.

Appendix 2-14: Pico Green

1. Samples from each time point should have already been collected in Eppendorf tubes and stored in the $-80\text{ }^{\circ}\text{C}$ freezer for at least a day. Three hydrogels per sample per time point is usually enough. That means a total of 27 hydrogels to be run on the assay.
2. Place all the gel samples on ice to thaw for at least 45 minutes.
3. Make 40mL of 1x TE buffer from the 20x stock.
4. Prepare the dye solution (50 μL Pico green dye / 10mL 1x TE buffer). Dye can be found in the $-20\text{ }^{\circ}\text{C}$ freezer.
5. Prepare the DNA standards according to the procedure below. DNA aliquots of 5.5 μL can be found in the $-20\text{ }^{\circ}\text{C}$ freezer.

a. Std 1:	5 μL stock DNA	495 μL TE buffer
b. Std 2:	250 μL std. 1	250 μL TE buffer
c. Std 3:	250 μL std. 2	250 μL TE buffer
d. Std 4:	250 μL std. 3	250 μL TE buffer
e. Std 5:	25 μL std. 4	225 μL TE buffer
f. Std. 6:	25 μL std. 5	225 μL TE buffer
g. Std 7:	25 μL std. 6	225 μL TE buffer
h. Blank	0	250 μL TE buffer

6. When the time comes to make the DNA standard curve, it should be calibrated as follows:
 - a. Std. 1 1000 ng/mL
 - b. Std. 2 500 ng/mL
 - c. Std. 3 250 ng/mL
 - d. Std. 4 125 ng/mL
 - e. Std. 5 12.5 ng/mL

f. Std. 6	1.25 ng/mL
g. Std. 7	0.125 ng/mL
h. Blank	0

7. Homogenize each of the gel samples while in the Eppendorf tube for 10 seconds using the handheld homogenizer. Clean the tip with ethanol after each gel.
8. Place the sonicating tip in the middle of the Eppendorf tube without touching the sides or bottom of the tube. Sonicate each of the gel samples while in the Eppendorf tube for 10 seconds at a low enough amplitude that bubbles don't form. Mixing can be heard and observed visibly in the tube. Wipe the tip of the sonicator with ethanol after each gel.
9. Use a black 384 well plate to prepare the assay. A single pipet or repeater pipet can be used to fill the plate.
 - a. Standards at 20 μ L with three pipet replicates
 - b. Gel samples at 5 μ L with 15 μ L TE buffer with three pipet replicates
 - c. Be careful to keep track of the wells in the 384 well plate. Skipping rows or columns to separate sample types may be a useful practice.
10. Add 20 μ L of dye solution to all the standards and samples.
11. Incubate for 10 minutes.
12. Read the fluorescence in the plate reader using the Pico Green settings already established.

Change the layout of the 384 well plate as needed.
13. Create a standard curve of fluorescence readings vs DNA concentrations.
14. Convert all gel fluorescence readings to DNA concentrations.

Appendix 2-15: Cell Glo

1. Usually this is done at the same time as the Pico Green assay with the same samples.

Samples from each time point should have already been collected in Eppendorf tubes and stored in the -80°C freezer for at least a day. Three hydrogels per sample per time point is usually enough. That means a total of 27 hydrogels to be run on the assay.

2. Place all the gel samples on ice to thaw for at least 45 minutes.
3. Take out 4-5 aliquots of CellTiter-Glo reagent (already premixed with buffer and substrate). Each aliquot is 1mL.
4. Prepare the ATP standards according to the procedure below. ATP aliquots of $0.5\ \mu\text{L}$ can be found in the -80°C freezer.

a. Std 1:	0.5 μL stock ATP	250 μL PBS
b. Std 2:	250 μL std. 1	250 μL PBS
c. Std 3:	250 μL std. 2	250 μL PBS
d. Std 4:	250 μL std. 3	250 μL PBS
e. Std 5:	250 μL std. 4	250 μL PBS
f. Std. 6:	250 μL std. 5	250 μL PBS
g. Std 7:	250 μL std. 6	250 μL PBS
h. Std 8:	250 μL std. 7	250 μL PBS
i. Std 9:	250 μL std. 8	250 μL PBS
j. Std 10:	250 μL std. 9	250 μL PBS
k. Std 11:	250 μL std. 10	250 μL PBS
l. Std 12:	250 μL std. 11	250 μL PBS

5. When the time comes to make the DNA standard curve, it should be calibrated as follows:

a. Std. 1	9 $\mu\text{g/mL}$
b. Std. 2	4.5 $\mu\text{g/mL}$
c. Std. 3	2.25 $\mu\text{g/mL}$
d. Std. 4	1.125 $\mu\text{g/mL}$
e. Std. 5	0.5625 $\mu\text{g/mL}$
f. Std. 6	0.2813 $\mu\text{g/mL}$
g. Std. 7	0.1406 $\mu\text{g/mL}$
h. Std. 8	0.0703 $\mu\text{g/mL}$
i. Std. 9	0.0352 $\mu\text{g/mL}$
j. Std. 10	0.0176 $\mu\text{g/mL}$
k. Std. 11	0.0088 $\mu\text{g/mL}$
l. Std. 12	Blank

6. Homogenize each of the gel samples while in the Eppendorf tube for 10 seconds using the handheld homogenizer. Clean the tip with ethanol after each gel.
7. Place the sonicating tip in the middle of the Eppendorf tube without touching the sides or bottom of the tube. Sonicate each of the gel samples while in the Eppendorf tube for 10 seconds at a low enough amplitude that bubbles don't form. Mixing can be heard and observed visibly in the tube. Wipe the tip of the sonicator with ethanol after each gel.
8. Use a white 384 well plate to prepare the assay. A single pipet or repeater pipet can be used to fill the plate.
 - a. Standards at 25 μL with three pipet replicates
 - b. Gel samples at 5 μL with 20 μL PBS with three pipet replicates

- c. Be careful to keep track of the wells in the 384 well plate. Skipping rows or columns to separate sample types may be a useful practice.
9. Add 25 μL of cell glo reagent to all the standards and samples.
10. Incubate for 10 minutes.
11. Read the luminescence in the plate reader using the Cell Glo settings already established.
Change the layout of the 384 well plate as needed.
12. Create a standard curve of luminescence readings vs ATP concentrations.
13. Convert all gel luminescence readings to ATP concentrations.

Appendix 2-16: Spheroid Volume Measurements

1. Load z-stacks from the confocal into ImageJ. The GFP and ethidium homodimer channels will probably be separated. Do not convert the confocal files into any other format or you will lose the micron to pixel scaling.
2. The red and green channels should be kept separated and counted separately.
3. Use “3D object counter” module in ImageJ to threshold the image and separate background as much as possible from the actual cell spheroids.
4. Select all of the options when prompted to select which data is being requested. Then execute the counter.

The first column that shows up will be the volume of the spheroid. Collect all the spheroid volumes and store in an Excel sheet for plotting.

Appendix 2-17: Primary OPC extraction

***The following instructions are for three P5-7 rat pups. If more pups are to be panned, then scale the dishes accordingly.**

***All of the plate coating biochemicals are in the 4°C fridge.**

Day 1:

1. Coat 10 cm petri dish with 22.5 μ L of goat anti-mouse IgM in 10 mL of 50 mM Tris-HCL pH 9.5, incubate overnight at 4 degrees. The primary antibody changes the surface of the dish and creates affinity for O4. Addition of O4 will occur on day 2 before the rat work.
2. Solid DNase is 400 units/mg. The stock solution needs to dissolve and be sterile filtered the day before immunopanning. You don't want to add DNase to the panning buffer until the cells are spun down at 1200 RPM. DNase solution needs to be 0.125 mg/mL to reach a concentration of 50 units/mL. For a 10 mL solution, that means 1.25 mg.
3. Make 40 mL lectin: Dilute lectin (2.5 mg/mL stock) in D-PBS with $\text{Ca}^{2+}/\text{Mg}^{2+}$ at 1:1000, vortex, and add to two 15 cm petri dishes (20 mL/dish). Incubate overnight at 4°C. These dishes will be rinsed while the cells are spinning in step 10 of Day 2 protocol.
4. 2D Tissue Culture Step (if needed): Dilute laminin (1.2 mg/mL stock) in Poly-L-lysine (100 μ g/mL stock) at 1:120, vortex, and add to tissue culture plate. Incubate overnight at 4°C.
 - a. Wash 3x with sterile DI water and completely air dry before plating cells.
 - b. If expanding OPCs use one well of a 12-well plate.
 - i. 1 mL to cover 12-well plate well.

Day 2:

1. Make 0.2% BSA solution: 19 mL D-PBS with $\text{Ca}^{2+}/\text{Mg}^{2+}$ + 1 mL 4% BSA.

2. Aspirate liquid off day 1 10 cm petri dish, wash 3x with D-PBS with $\text{Ca}^{2+}/\text{Mg}^{2+}$, and add O4 antibody. Coat 1 x 10 cm plate from day 1 with 3.75 μL of O4 antibody plus 5 mL of 0.2% BSA. Incubate at room temperature for > 2 hrs.
3. Add 10 mL HBSS (no $\text{Ca}^{2+}/\text{Mg}^{2+}$), 100 μL pen strep, and 1x DNase (units/mL) to a petri dish. The HBSS can be bought as 10x and diluted with DI water to 1x. The pen strep is for killing of the excess bacteria from euthanizing the animals. The DNase breaks down the polymerized DNA and makes the solution less viscous. Some cells die so you need DNase to remove those cells.
4. Thaw 5 mL accutase in cold room or room temperature, do not thaw at 37°C . Protect from light.
5. Inside the laminar flow hood, remove the brain from the mouse pups, remove the meninges, and remove the cerebellum.
 - a. With #10 scalpel blade cut a V into the ventral brain to remove subcortical structures from the cortex.
 - b. Add cortical hemispheres to aliquot of accutase + 1x of DNase (3 pup brains in 5 mL accutase).
6. Pipette brains up and down with a 5 mL pipette to break up tissue.
7. Incubate for 45 minutes @ 37°C , pipetting up and down every 15 minutes
 - a. Minute 15: use 5 mL pipette. Do rinsing of 15 cm plate while cells are incubating.
 - b. Minute 30: use P1000 pipette set to 1 mL and gently pipette up and down to break up chunks.
 - i. Make 15 mL panning buffer: 13.5 mL HBSS with $\text{Ca}^{2+}/\text{Mg}^{2+}$ + 1.5 mL 0.2% BSA + 18.8 μL insulin. This is the panning buffer.

- ii. Do not add DNase yet
 - iii. Equilibrate in tissue culture incubator until you use it
 - c. Minute 45: use P1000 pipette set to 1 mL and gently pipette up and down to break up any chunks leftover
 - i. There should be no snot in this suspension. If there is, the right concentration of DNase was not added and cell viability will be poor. There should be a one cell suspension at this point.
- 8. Add an equal volume of HBSS with $\text{Ca}^{2+}/\text{Mg}^{2+}$, and spin down at 1200 rpm for 5 minutes. HBSS solution will make the cells happier. Too long in accutase leads to cell death.
- 9. While cells are spinning, wash 1st big petri dish 3x with 15 mL D-PBS with $\text{Ca}^{2+}/\text{Mg}^{2+}$
 - a. Leave the last wash on the plate.
- 10. Add DNase to the panning buffer and gently mix by inverting tube a few times. Vortexing will create bubbles and you don't want that. Panning buffer is different from the cell pellet. Instructions for panning buffer is in 7bi.
- 11. Aspirate HBSS⁺⁺⁺ accutase, leaving cell pellet. Remember this is from the section where brains were collected, not from the section about panning buffer.
- 12. Resuspend cell pellet in 10 mL of panning buffer, making sure to break up clumps. Instead of passing through a cell filter, we can just triturate up and down several times.
- 13. Aspirate 1st 15 cm petri dish.
- 14. Add cell suspension to 1st 15 cm petri dish. Shake up/down and left/right gently. Incubate at room temperature for 15 minutes.
- 15. Around 10-13 minutes wash 2nd 15 cm petri dish 3x with 15 mL D-PBS with $\text{Ca}^{2+}/\text{Mg}^{2+}$ and leave third wash until next step. Wash 2nd set of plate 3x with D-PBS.

16. Aspirate 2nd 15 cm petri dish and add supernatant from 1st plate. Incubate at room temperature for 15 minutes.
17. Around 10-13 minutes wash O4 plate 3x with 5 mL of D-PBS with Ca/Mg and lead third wash until next step.
18. Aspirate last wash in O4 plate and add supernatant, and incubate at room temperature for 45 minutes. Gently shake up/down and left/right every 15 minutes. O4 plates should have been incubating for > 2 hrs by the time you get to this step. Then you can do the wash.
 - a. Minute 30: pre-warm trypsin and DMEM⁺⁺⁺ + FBS in water bath
19. Aspirate supernatant and wash O4 plate gently 3x with 10 mL D-PBS with Ca²⁺/Mg²⁺. The divalent cations help with adhesion.
20. We have 2x trypsin, so that needs to be diluted to 2 mL trypsin, 2 mL PBS (1x). Add 4 mL of trypsin and incubate for 10 minutes in the tissue culture incubator.
21. Neutralize trypsin by adding 4 mL of DMEM⁺⁺⁺ + 10% FBS solution.
22. Using a P1000 pipette up 1 mL of supernatant and spray it from the outside edge of the dish to the center of the dish, going around the whole dish.
 - a. Make sure this doesn't take too much time, less than 4 minutes.
 - b. Make sure you spray the edges.
 - c. Check plate periodically to know if your cells have detached.
 - i. If they have not detached, use a cell scraper.
23. Pipette mixture into a 15 mL conical and spin down at 1200 RPM for 8 minutes
24. Aspirate off most of the supernatant, resuspend in 1 mL OPC media or 500 μ L, gently pipette up and down, plate in one well of a 12-well plate, perform a short spin, and place in tissue incubator.

25. Change media every two days

- a. When cells have adopted a healthy OPC morphology and have expanded they are ready to use.

Appendix 2-18: Surface modification of glass substrates using trimethoxysilane-based coatings

Overview: creates oxidized groups on the surface of glass which can be bonded to trimethoxysilane groups (which in turn polymerize with neighbors) to create a surface functionalized with whatever functionality (e.g., methacrylate, thiol) is bonded to the trimethoxysilane.

1. Turn on oven and set to 100°C.
2. Fill larger Petri dish(es) with 10M NaOH (400 g/L) (found in the base cabinet under the fume hood) and immerse cover glasses (22x22) for 20 min. Press down to make sure they're fully submerged. The side facing up will be the side that is modified.
3. Carefully pour NaOH back into bottle (NaOH solution can be reused several times) and then rinse cover glasses with ultrapure water by pouring water in the Petri dish, swirling, then pouring out. Rinse 3 times, bringing back slides in fresh DI water.
4. Lift each coverglass with forceps and dab edge of slide on Kimwipe. Stand upright in slide box and allow to air dry for 15-30 min (remember which side is the top side).
5. Cover lunch tray in aluminum foil (helps with even cooking in the baking step). Place glass pieces on the covered tray (leave some space in between).
6. Add the coating material dropwise to the top of each cover glass (found in the 4°C fridge). Make sure the entire top surface is covered by dropping the coating material carefully at the corners and around the top (you can use the tip of the syringe/pipette to help evenly spread). Each coverglass will need between 100-200 μL
 - a. Methacrylated: 3-(Trimethoxysilyl)propyl methacrylate
 1. Use syringe.
 - b. Thiolated: (3-Mercaptopropyl)trimethoxysilane
 1. Use 200 μL pipette.

7. Bake for 1 hour @ 100°C
8. Turn up oven to 120°C at the end of the hour for an additional 10 min
9. Remove slides from oven and place in fume hood to cool/decrease fumes
10. Wash coverslips
 - a. Methacrylated: Ethanol (in Petri dish) then ultrapure water (in Petri dish)
 - b. Thiolated: DCM (fill small beaker and dip), ethanol (in Petri dish), ultrapure water (in Petri dish)
11. Dry both sides of glass using Kimwipe and use within 2-3 days (methacrylated) or 24 hours (thiolated; can store under nitrogen)

Appendix 2-19: 2D NorHA experiments

1. Make 1wt%, 1.5wt%, and 2wt% NorHA solutions as you would in Appendix 2-7 (before adding cells). These solutions do not need to be sterile.
2. Add the desired amount of RGD to the solutions. ($40\ \mu\text{L} = 2\text{mM}$ when the total volume is 1 mL). This will be necessary to get the cells to adhere.
3. Fill the remaining volume of each sample type with PBS. The volume per sample type should be 1 mL total.
4. Using the thiolated cover slips (Appendix 2-18), pipet $50\ \mu\text{L}$ of sample solution onto the center of the thiolated surface of the cover slip. You can place 3-4 cover slips under the UV light for curing so pipet batches of 3-4 at a time.
5. Using tweezers, cover the 22 x 22mm cover slip with an 18 x 18 mm coverslip. There will be portions of the underneath coverslip that will be exposed, however the fluid should be caught between the two coverslips.
6. Cure the coverslips under UV light (again 3-4 at a time) using $4\ \text{mW}/\text{cm}^2$ (365 nm) for 2 minutes.
7. Wait 20 minutes after curing is complete. This will help the gel to adhere better to the thiolated cover slip.
8. Carefully flip the top (18 x 18mm) coverslip off of the 22 x 22mm coverslip, exposing the gel. The gel should be mostly intact and adhered to the 22 x 22mm coverslip.
9. Soak the coverslips in PBS overnight to swell them (a 6 well non tissue culture treated plate should be fine).
10. Sterilize the coverslips in the 6 well plate under the UV light for 2.5 hours with the lid of the 6 well plate off (TC hood). Spray the cover of the 6 well plate and surface of the bottom of the 6 well plate with ethanol to ensure that all contamination sources are eliminated.

11. Once the cover of the 6 well plate is put on top and the plate is removed from the TC hood, it is sterile. Use it in an experiment.
12. Cells should be seeded onto the coverslips at the same concentration as seeding on a T75 flask (0.5×10^4 cells/cm²). This way you are more likely to get single cell attachment on the hydrogels.
 - a. Mix all of the cells needed in a conical tube with the total amount of media needed. Mix thoroughly to get a single cell suspension.
 - b. Pipet 3 mL of cell solution per cover slip. Swirl the plates to mix further.
 - c. Incubate the plates for 24 hours in the cell incubator.
13. After 1 day of incubation, aspirate out the media. Using sterile sharp tip tweezers, move the coverslips to new non tissue culture treated 6 well plates. This will remove any of the loose cells that will make the data noisy. Replace the media in the plates. 3 mL per well should be enough.
14. Image the coverslips under the Lampe lab fluorescent microscope (10x works well). The entire 6 well plate can be put under the microscope without compromising sterility. Make sure the coverslips are resting on the bottom surface of the well plate so that images will show clearly on the microscope.
15. Be careful about imaging cells on the exposed 22 x 22mm coverslip portions. They will most likely be more strongly adhered there than to the gel on the coverslip and they will also probably have more process extension. These cells are not the cells that will give you good data.
16. The experiment should last 3 days in order to get process extension as a function of stiffness and culture time.

Appendix 2-20: Fixing and staining of 2D hydrogels at end of experiment

1. Move gels to new 6-well plates and rinse gels with PBS (2 mL per well) to remove media/dead cells.
2. Fix cells in formalin for 15 min. Remove formalin with pipette (do not aspirate!) and transfer to appropriate formalin waste container. Rinse with PBS and proceed to next steps or store at 4°C
3. Permeabilize cells in 0.1% Triton X100 in PBS for 10 min.
4. Block gels in 3% BSA in PBS for at least 1 h at room temperature. BSA is in fridge; allow to warm before weighing. Make enough BSA blocking solution for both days (~2.5 mL per gel). Lift the gels to insure BSA blocking solution gets under gel coverslips too.
5. Add 500 uL rhodamine phalloidin (1:600 dilution) in 3% BSA per well. Mix well, then flip gels face down into well and incubate in dark at room temperature for 1-2 h.
6. Rinse 3 times with PBS (use the shaker at the lowest speed for 5 min each time).
7. Add 2 mL DAPI (1:10000 dilution in PBS, located in 4C box with antibodies) to each gel for 1 min.
8. Rinse twice with PBS. Store gels in dark at 4°C or proceed to imaging.

Appendix 3: Supplemental Data

Fiber Washing Experiments

The degree of leaching of PEO from the MeHA fibers was investigated over a 3 day period over three individual trials. Dry MeHA fibers were massed right after crosslinking, then washed with DI water and gently stirred overnight. Time points were taken every 24 hrs with an additional wash occurring at each new time point. Dry fibers were lyophilized and massed.

Trial	Day 0 Dry Weight (mg)	Day 1 Dry Weight (mg)	Day 2 Dry Weight (mg)	Day 3 Dry Weight (mg)	Percent Change from Original
1	45.3	39.4			- 13.0%
1	19.5		14.4		- 26.2%
1	25.8			18.3	- 29.1%
2	23.5	21.9			- 6.9%
2	15.5		14.9		- 3.9%
2	25.0			17.7	- 29.2%
3	23.3	16.3			- 30.0%
3	30.1		14.0		- 53.6%
3	67.3			44.2	- 34.3%

Table 2 - Fiber washing experiments were intended to determine how much of the PEO was leaching from the electrospun fibers over a period of 3 days with dry masses taken every 24 hrs.

The data suggests that about 30% of fiber mass is lost over a period of three days (neglecting the outliers in yellow). It is not clear why this is the case. PEO accounts for 3/5 of the total dry mass with MeHA serving the other 2/5. To lose all the PEO would mean a mass loss of 60%. None of the data points show an excess of 60% mass loss, however at the same time we cannot say that PEO is only being lost in the washes. There could be some heterogeneity in how the fiber mats are laid which would lead to heterogeneity in entanglements/crosslinks and thus variable tendencies of leaching to occur. It is recommended that a single batch of electrospun fibers be split into three groups of about 20mg in weight for washing. This eliminates heterogeneities

between samples. The washing should suspend the fibers in the same concentration of DI water for each trial and each sample type.

2D Hydrogel on Coverslips

The goal of 2D experimentation was to develop an understanding of process extension length as a function of stiffness and number of processes per cell as a function of stiffness. Differences were marginal and the collected data may have been compromised by too many cell clusters forming on the hydrogels with a high seeding density (Figure 22). Obtaining single cell attachment on the cover slips at 24 hrs was a challenge. Having a portion of the cells be individual adhesions is not enough. The vast majority of the cells need to be single attachments. Preliminary results were obtained indicating that process extension increased with increased stiffness and the number of processes extended decreased with increased stiffness (Figures 23 and 24).

After curing, the hydrogels would sometimes not remain fully attached to the thiolated cover slips when flipping off the 18 x 18 mm cover slip which is why the incubation time was extended for 2 minutes to 20 minutes. Even with the extended wait period, there could be bad batches of coverslips due to NaOH solutions being contaminated or over-used (the solution is

reused to modify the coverslip surfaces). Sometimes it would seem as if there was no reason at all for the hydrogels to not form correctly but it would still happen.

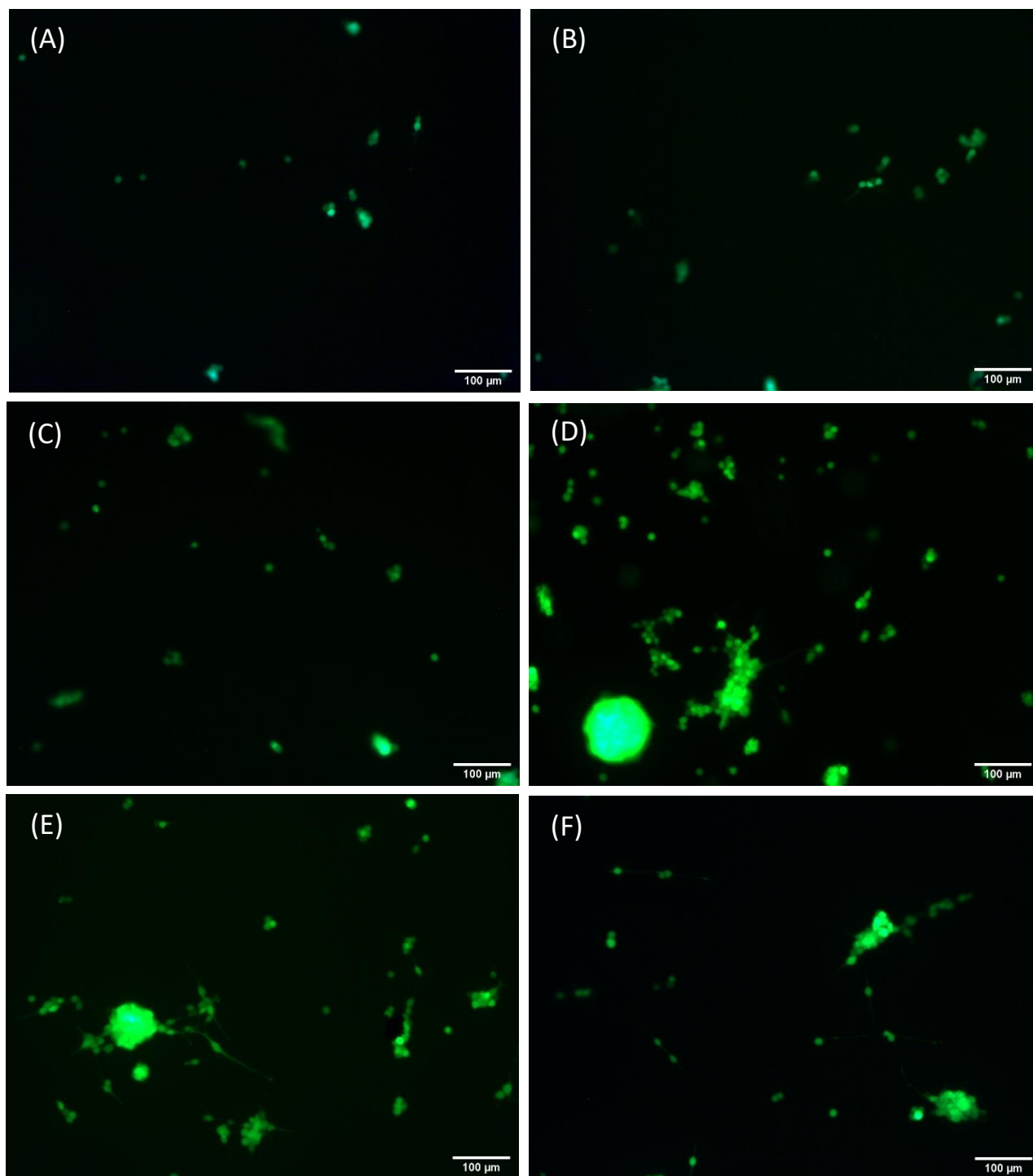


Figure 27 - Representative 2D experiment images with NorHA hydrogels.

(A) 1wt% 24hrs (B) 1.5wt% 24hrs (C) 2wt% 24 hrs (D) 1wt% 48 hrs (E) 1.5wt% 48 hrs (F) 2wt% 48 hrs

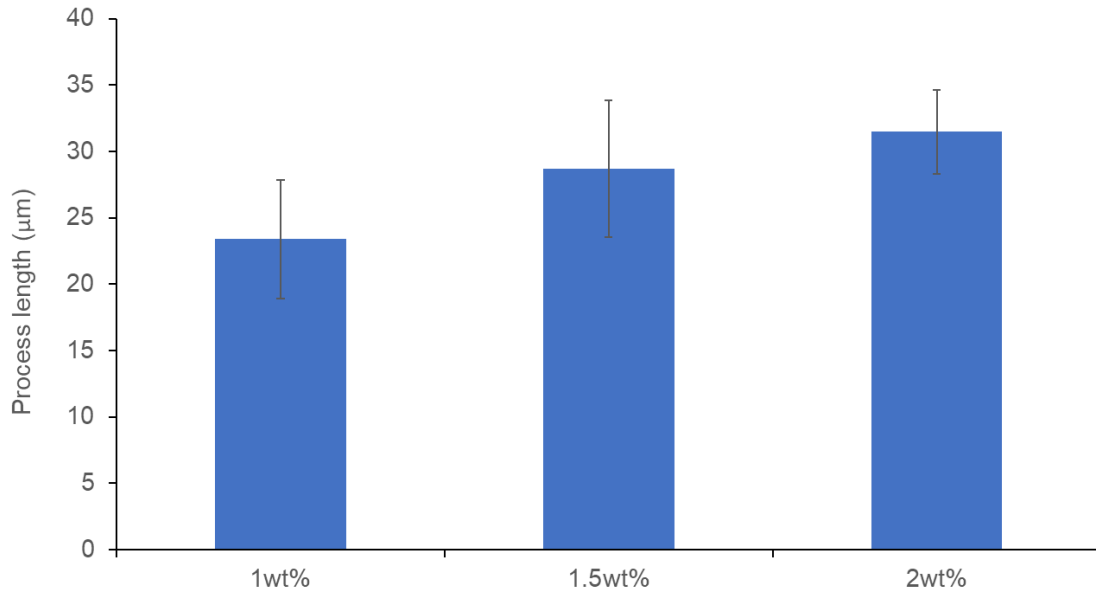


Figure 28 - Process extensions were measured after 72 hours of culture in 2D coverslip experiments.

The general trend was that the stiffer the material, the longer the process extensions. Processes were measured manually using NeuronJ plugin in Fiji. (n=8) for 1wt% and 1.5wt%. (n=11) for 2wt%.

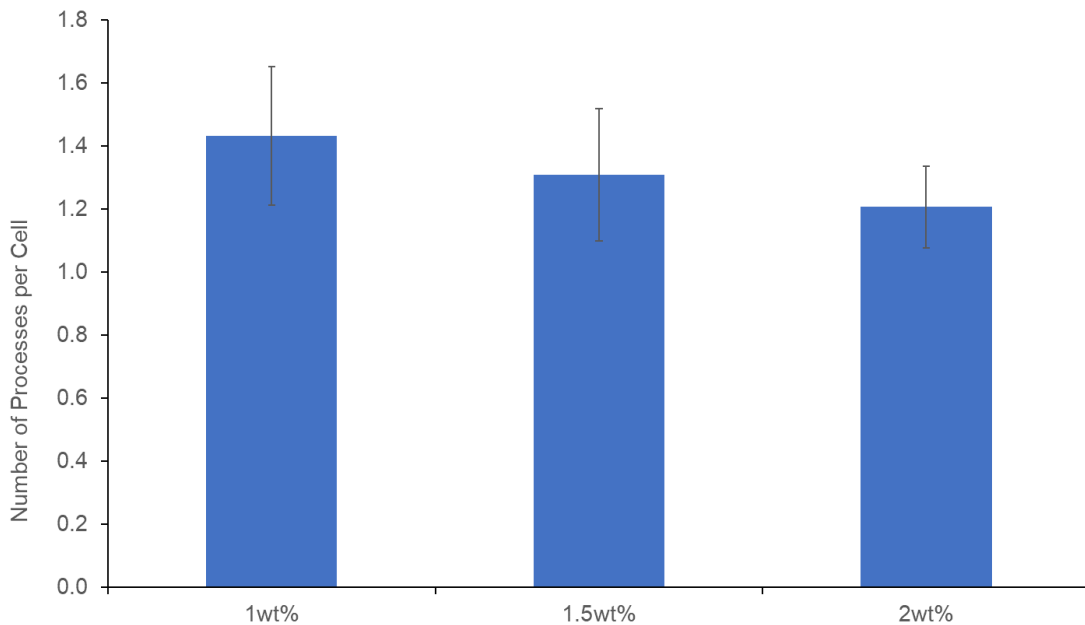


Figure 29 - Number of processes per cell were counted manually.

Any connecting processes between multiple cells were assigned to the cell with more processes. (n=8) for 1wt% and 1.5wt%. (n=11) for 2wt%.

Manually measuring process extensions using NeuronJ was time-consuming but also the simplest method to get accurate data (Figure 25). Using the original image files from the microscope kept the appropriate scaling for taking measurements in micron instead of pixels. Process extensions were attempted to be measured automatically using CellProfiler's line-by-line module system. The program did capture cells with GFP⁺ signal, however the processes were not separated from the cells adequately. The difference in pixel intensity between the cell bodies and the processes was not noticeably different, so the program would overestimate the region occupied by processes (Figure 26). The use of an F-actin stain would overlap with the GFP signal and is also an end-point assay, so it is difficult to incorporate that in middle time points. All signals are converted to grayscale so identification is more a function of pixel intensity than it is color. There are programs that separate images by color, however attempting to teach the software to recognize the difference between a DAPI and GFP stain was not a simple task considering the overlapping spectra.

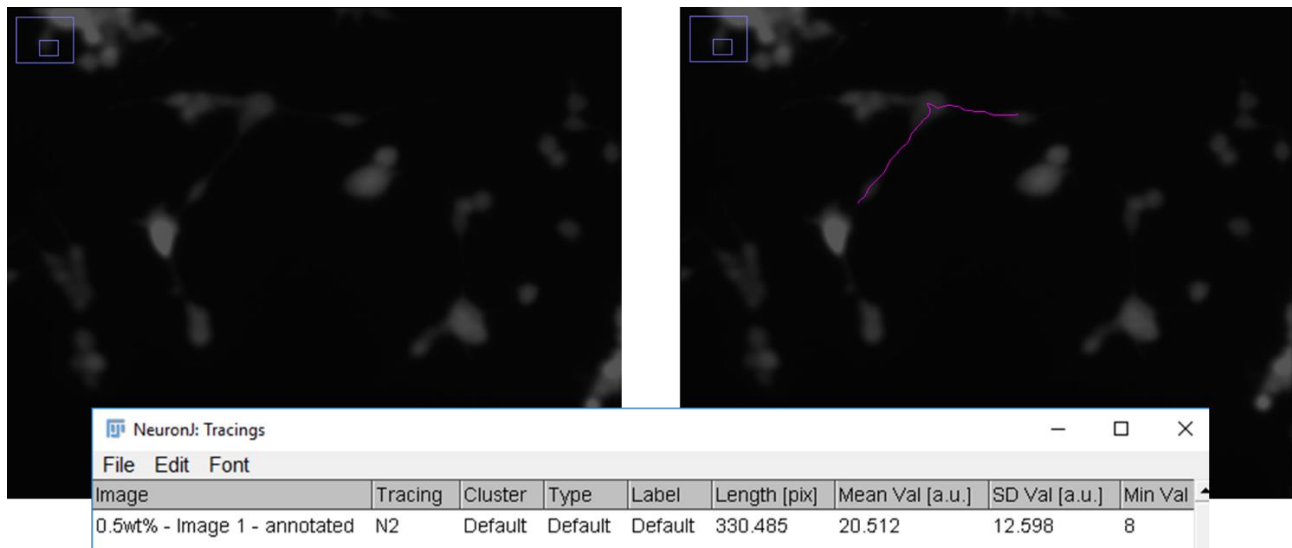
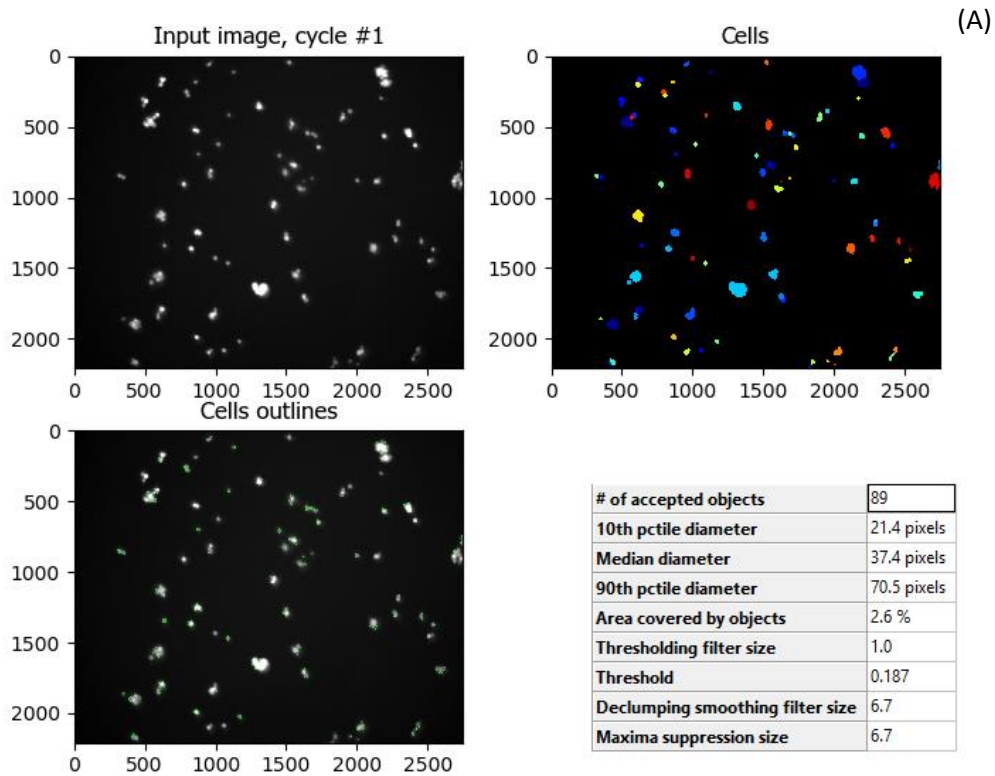


Figure 30 - NeuronJ plugin in Fiji was used to trace process extensions and measure their lengths.

Each process would be measured manually but the tracing algorithm was efficient at separating the background from the process extension. NeuronJ has a couple files to upload into the Fiji software so be sure to copy all the files in the right places in order to use the plugin.

2D hydrogels were also fixed and stained with DAPI and F-actin at the end of experimentation to elucidate process extension from the rest of the cell body (Figure 27). Separating background from stained cells was challenging on the fluorescent widefield microscope. Also cells did not respond well to fixing. Once large cells shriveled under the microscope.



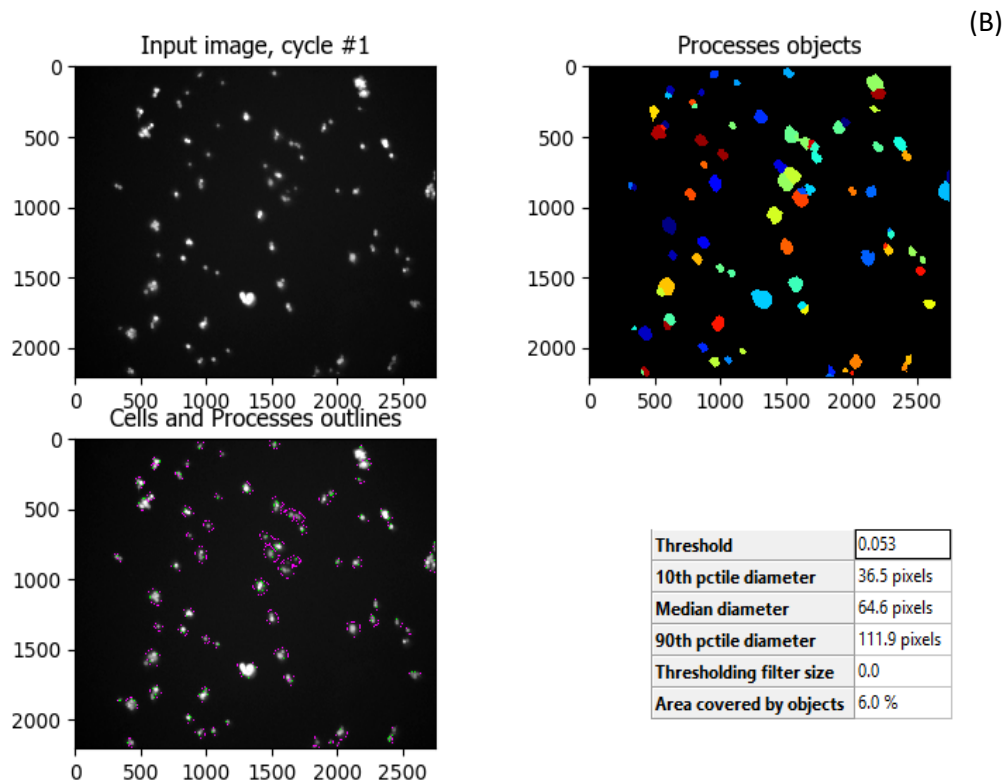


Figure 31 - (A) Cells were counted as primary objects in Cell Profiler using the appropriate module. It was hypothesized that the best way to count process extensions would be as secondary objects (B) that were based on the profiles of the cell bodies. There is a separate module for counting secondary objects.

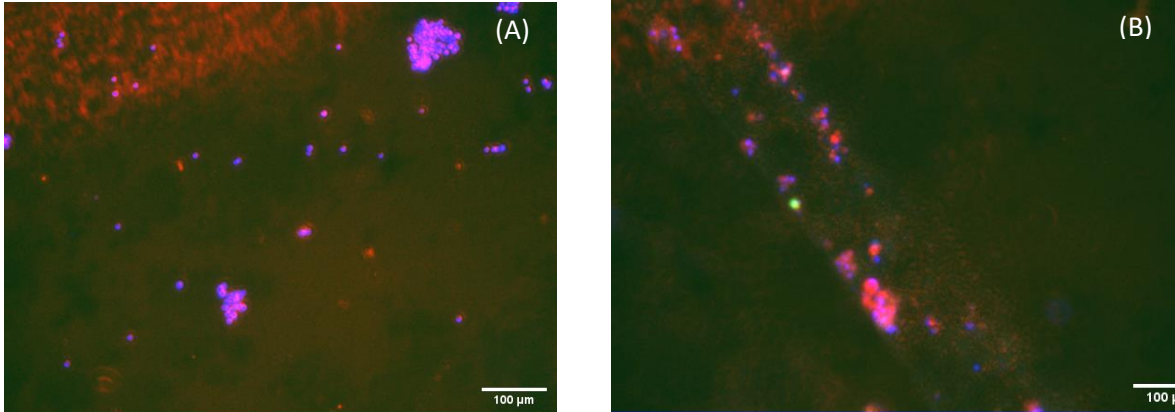


Figure 32 - GFP+ transfected MADM OPC cells with F-actin stain (red) and DAPI stain (blue). Large process extension was not observed after fixing these cells even though before fixing the cells seemed healthy and active.

Works Cited

1. Purves, D.; Augustine, G.J.; Fitzpatrick, D.; Hall, W.C.; LaMantia, A-S.; Mooney, R.D.; Platt, M.L.; White LE. *Neuroscience, Sixth Edition.*; 2018.
2. Kramer-Albers, Eva-Maria.; Bretz, N.; Tenzer, S.; Winterstein, C.; Mobius, W.; Berger, H.; Nave, K.A.; Schild, H.; Trotter J. Oligodendrocytes secrete exosomes containing major myelin and stress-protective proteins: Trophic support for axons? *Proteomics-Clinical Appl.* 2007;1(11):1446-1461.
3. Simons, M.; Trajkovic K. Neuron-glia communication in the control of oligodendrocyte function and myelin biogenesis. *J Cell Sci.* 2006;119:4381-4389.
4. Kramer, E-M.; Schardt, A.; Nave K-A. Membrane traffic in myelinating oligodendrocytes. *Microsc Res Tech.* 2001;52(6):656-671.
5. Funschilling, U.; Supplie, L.M.; Mahad, D.; Boretius, S.; Saab, A.S.; Edgar, J.; Brinkmann, B.G.; Kassmann, C.M.; Tzvetanova, I.D.; Movius, W.; Diaz F. Glycolytic oligodendrocytes maintain myelin and long-term axonal integrity. *Nature.* 2012;485(7399):517.
6. Rosenbluth, J.; Nave, K.A.; Mierzwa, A.; Schiff R. Subtle myelin defects in PLP-null mice. *Glia.* 2006;54(3):172-182.
7. Griffiths, I.; Klugmann, M.; Anderson, T.; Thomson, C.; Vouyiouklis, D.; Nave KA. Current concepts of PLP, its role in the nervous system. *Microsc Res Tech.* 1998;41(5):344-358.
8. Griffiths, I.; Klugmann, M.; Anderson, T.; Yool, D.; Thomson, C.; Schwab, M.H.; Schneider, A.; Zimmermann, F.; McCulloch, M.; Nadon, N.; Nave KA. Axonal swellings and degeneration in mice lacking the major proteolipid of myelin. *Science (80-).* 1998;280(5369):1610-1613.
9. Nave KA. Myelination and the trophic support of long axons. *Nat Rev Neurosci.* 2010;11(4):275.
10. Butt, A.M.; Colquhoun, K.; Berry M. Confocal imaging of glial cells in the intact rat optic nerve. *Glia.* 1994;10(4):315-322.
11. Orthmann-Murphy, J.L.; Freidin, M.; Fischer, E.; Scherer, S.S.; Abrams CK. Two distinct heterotypic channels mediate gap junction coupling between astrocyte and oligodendrocyte connexins. *J Neurosci.* 2007;27(51):13949-13957.
12. Hampson, E.C.; Munro, M.N.; Vaney DI. Unidirectional coupling of gap junctions between neuroglia. *Science (80-).* 1993;262(5136):1072-1074.

13. Felts, P.A.; Baker, T.A.; Smith KJ. Conduction in segmentally demyelinated mammalian central axons. *J Neurosci.* 1997;17(19):7267-7277.
14. Franklin, R.J.M.; French-Constant C. Remyelination in the CNS: from biology to therapy. *Nat Rev Neurosci.* 2008;9:839-855.
15. Stadelmann, C.; Wegner, C.; Bruck W. Inflammation, demyelination, and degeneration - Recent insights from MS pathology. *Biochim Biophys Acta.* 2011;18(12):275-282.
16. Henderson, A.P.; Barnett, M.H.; Parratt, J.D.; Prineas J. Multiple sclerosis: distribution of inflammatory cells in newly forming lesions. *Ann Neurol Off J Am Neurol Assoc Child Neurol Soc.* 2009;66(6):739-753.
17. Barnett, M.H.; Henderson, A.P.; Prineas JW. The macrophage in MS: just a scavenger after all? Pathology and pathogenesis of the acute MS lesion. *Mult Scler J.* 2006;12(2):121-132.
18. Bung, M.B.; Bunge, R.P.; Ris H. Ultrastructural study of remyelination in an experimental lesion in adult cat spinal cord. *J Cell Biol.* 1961;10(1):67-94.
19. Patrikios, P.; Stadelmann, C.; Kutzelnigg, A.; Rauschka, H.; Schmidbauer, M.; Laursen, H.; Sorensen, P.S.; Bruck, W.; Lucchinetti, C.; Lassmann H. Remyelination is extensive in a subset of multiple sclerosis patients. *Brain.* 2006;129(12):3165-3172.
20. Li, X.; Liu, X.; Cui, L.; Brunson, C.; Zhao, W.; Bhat, N.R.; Zhang, N.; Wen X. Engineering an in situ Crosslinkable Hydrogel for Enhanced Remyelination. *FASEB J.* 2013;27(3):1127-1136.
21. Macklin, W.B.; Weill, C.L.; Deininger PL. Expression of myelin proteolipid and basic protein mRNAs in cultured cells. *J Neurosci Res.* 1986;16:203-217.
22. Korn, M.J.; Cramer KS. Distribution of glial-associated proteins in the developing chick auditory brainstem. *Dev Neurobiol.* 2008;68:1093-1106.
23. Judge, S.I.; Smith, P.J.; Stewart, P.E.; Bever CTJ. Potassium channel blockers and openers as CNS neurologic therapeutic agents. *Recent Pat CNS Drug Discov.* 2007;2:200-228.
24. Basso, A.S.; Frenkel, D.; Quintana, F.J.; Costa-Pinto, F.A.; Petrovic-Stojkovic, S.; Puckett, L.; Monsonego, A.; Bar-shir, A.; Engel, Y.; Gozin, M.; Weiner HL. Reversal of axonal loss and disability in a mouse model of progressive multiple sclerosis. *J Clin Invest.* 2008;118(4):1532-1543.
25. Ludwin, S.K.; Sternberger NH. An immunohistochemical study of myelin proteins during remyelination in the central nervous system. *Acta Neuropathol.* 1984;63:240-248.

26. Morell, P.; Barrett, C.V.; Mason, J.L.; Toews, A.D.; Hostettler, J.D.; Knapp, G.W.; Matsushima GK. Gene expression in brain during cuprizone-induced demyelination and remyelination. *Mol Cell Neurosci.* 1998;12(4-5):220-227.
27. Capello, E.; Voskuhl, R.R.; McFarland, H.F.; Raine CS. Multiple sclerosis: re-expression of a developmental gene in chronic lesions correlates with remyelination. *Ann Neurol.* 1997;41:797-805.
28. Sim, F.J.; Hinks, G.L.; Franklin RJM. The re-expression of the homeodomain transcription factor Gtx during remyelination of experimentally-induced demyelinating lesions in young and old rat brain. *Neuroscience.* 2000;100:131-139.
29. Franklin RJM. Why does remyelination fail in multiple sclerosis. *Nat Rev.* 2002;3(9):705.
30. Blakemore WF. Pattern of remyelination in the CNS. *Nature.* 1974;249(5457):577.
31. Prineas JKJC. The neuropathology of multiple sclerosis. *Handb Clin Neurol demyelinating Dis.* 1985;47:337-395.
32. Ozawa, K.; Suchanek, G.; Breitschopf, H.; Bruck, W.; Budka, H.; Jellinger K. Patterns of oligodendroglia pathology in multiple sclerosis. *Brain.* 1994;117:1311-1322.
33. Lucchinetti, C.; Bruck, W.; Parisi, J.; Scheithauer, B.; Rodriguez, M.; Lassmann H. A quantitative analysis of oligodendrocytes in multiple sclerosis lesions. *Brain.* 1999;122:2279-2295.
34. Wolswijk G. Oligodendrocyte survival, loss and birth in lesions of chronic-stage multiple sclerosis. *Brain.* 2000;123:105-115.
35. Frohman, E.; Racke, M.K.; Raine CS. Multiple sclerosis - the plaque and its pathogenesis. *North Engl J Med.* 2006;354:942-955.
36. Prineas, J.W.; Barnard, R.O.; Revesz, T.; Kwon, E.E.; Sharer, L.; Cho ES. Multiple Sclerosis. Pathology of recurrent lesions. *Brain.* 1993;116:681-693.
37. Albert, M.; Antel, J.; Bruck, W.; Stadelmann C. Extensive cortical remyelination in patients with chronic multiple sclerosis. *Brain Pathol.* 2007;17:129-138.
38. Prayoonwiwat, N.; Rodriguez M. The potential for oligodendrocyte proliferation during demyelinating disease. *J Neuropathol Exp Neurol.* 1993;52(1):55-63.
39. Gensert, J.M.; Goldman JE. Endogenous progenitors remyelinate demyelinated axons in the adult CNS. *Neuron.* 1997;19:197-203.

40. Carroll, W.M.; Jennings AR. Early recruitment of oligodendrocyte precursors in CNS remyelination. *Brain*. 1994;117:563-578.
41. Zhang, S.C.; Ge, B.; Duncan ID. Adult brain retains the potential to generate oligodendroglial progenitors with extensive myelination capacity. *Proc Natl Acad Sci*. 1999;96(7):4089-4094.
42. Wang, Z.; Colognato H. Contrasting effects of mitogenic growth factors on myelination in neuron-oligodendrocyte co-cultures. *Glia*. 2007;55(5):537-545.
43. Patani, R.; Balaratnam, M.; Vora, A.; Reynolds R. Remyelination can be extensive in multiple sclerosis despite a long disease course. *Neuropathol Appl Neurobiol*. 2007;33(3):277-287.
44. Bramow, S.; Frischer, J.M.; Lassmann, H.; Koch-Henriksen, N.; Lucchinetti, C.F.; Sorensen, P.S.; Laursen H. Demyelination versus remyelination in progressive multiple sclerosis. *Brain*. 2010;133(10):2983-2998.
45. Lassmann, H.; Bradl M. Multiple sclerosis: experimental models and reality. *Acta Neuropathologica*. 2016;133(2):233-244.
46. Blakemore WF. Demyelination of the Superior Cerebellar Peduncle in the Mouse Induced by Cuprizone. *J Neurol Sci*. 1973;20:63-72.
47. Ludwin SK. Central nervous system demyelination and remyelination in the mouse: an ultrastructural study of cuprizone toxicity. *Lab Investig a J Tech methods Pathol*. 1978;39(6):597-612.
48. Matsushima, G.K.; Morell P. The neurotoxicant, cuprizone, as a model to study demyelination and remyelination in the central nervous system. *Brain Pathol*. 2001;11:107-116.
49. Stidworthy, M.F.; Genoud, S.; Suter, U.; Mantei, N.; Franklin RJ. Quantifying the Early Stages of Remyelination Following Cuprizone-induced Demyelination. *Brain Pathol*. 2003;13(3):329-339.
50. Hiremath, M.M.; Sait, Y.; Knapp, G.W.; Ting, J.P-Y; Suzuki, K. Matsushima GK. Microglial/macrophage accumulation during cuprizone-induced demyelination in C57BL/6 mice. *J Neuroimmunol*. 1998;92(1-2):38-49.
51. Crawford, A.H.; Chambers, C.; Franklin RJM. Remyelination: the true regeneration of the central nervous system. *J Comp Pathol*. 2013;149(2-3):242-254.
52. Skripuletz, T.; Hackstette, D.; Bauer, K.; Gudi, V.; Pul, R.; Voss, E.; Berger, K.; Kipp, M.; Baumgartner, W.; Stangel M. Astrocytes Regulate Myelin Clearance Through Recruitment of Microglia During Cuprizone-Induced Demyelination. *Brain*. 2012;136(1):147-167.

53. Manrique-Hoyos, N. Jurgens, T.; Gronborg, M.; Kreutzfeldt, M; Schedensack, M.; Kuhlmann, T.; Schrick, C.; Bruck, W.; Urlaub, H.; Simons, M.; Merkler D. Late Motor Decline After Accomplished Remyelination: Impact for Progressive Multiple Sclerosis. *Ann Neurol.* 2012;71(2):227-244.
54. Weltzien HU. Cytolytic and membrane-perturbing properties of lysophosphatidylcholine. *Biochim Biophys Acta - Rev Biomembr.* 1979;559(2-3):259-287.
55. Ngwenya, B.Z.; Yamamoto N. Activation of peritoneal macrophages by lysophosphatidylcholine. *Biochim Biophys Acta - Gen Subj.* 1985;839(1):9-15.
56. Huang YH et. al. Lysophosphatidylcholine (LPC) induces proinflammatory cytokines by a platelet-activating factor (PAF) receptor-dependent mechanism. *Clin Exp Immunol.* 1999;116(2):326.
57. Schilling T. et. al. Physiological mechanisms of lysophosphatidylcholine-induced de-ramification of murine microglia. *J Physiol.* 2004;557(1):105-120.
58. Kotter, M.R.; Setzu, A.; Sim FJ. Macrophage depletion impairs oligodendrocyte remyelination following lysolecithin-induced demyelination. *Glia.* 2001;35:204-212.
59. Blakemore, W.F.; Franklin RJ. *Remyelination in Experimental Models of Toxin-Induced Demyelination.*; 2008.
60. Ineichen, B.V.; Kapitzka, S.; Bleul, C.; Good, N.; Plattner, P.S.; Seyedsadr, M.S.; Kaiser, J.; Schneider, M.P.; Zorner, B.; Martin, R.; Linnebank, M.; Schwab ME. Nogo-A antibodies enhance axonal repair and remyelination in neuro-inflammatory and demyelinating pathology. *Acta Neuropathol.* 2017;134:423-440.
61. Pavelko, K.D.; Van Engelen, B.G.M.; Rodriguez M. Acceleration in the rate of CNS remyelination in lysolecithin-induced demyelination. *J Neurosci.* 1998;18(7):2498-2505.
62. Blakemore WF. Remyelination of the superior cerebellar peduncle in old mice following demyelination induced by cuprizone. *J Neurol Sci.* 1974;22(1):121-126.
63. Oskari, V.J.; Jacobson S. Viruses and multiple sclerosis. *CNS Neurol Disord - Drug Targets.* 2012;11(5):528-544.
64. Dziembowska, M.; Tham, T.N.; Lau, P.; Vitry, S.; Lazarini, F.; Dubois-Dalcq M. A role for CXCR4 signaling in survival and migration of neural and oligodendrocyte precursors. *Glia.* 2005;50(3):258-269.
65. Carbajal, K.S.; Schaumburg, C.; Strieter, R.; Kane, J.; Lane TE. Migration of engrafted neural stem cells is mediated by CXCL12 signaling through CXCR4 in a viral model of multiple sclerosis. *Proc Natl Acad Sci.*

- 2010;107(24):11068-11073.
66. Keough, M.B.; Jensen, S.K.; Yong VW. Experimental demyelination and remyelination of murine spinal cord by focal injection of lysolecithin. *J Vis Exp*. 2015;97:e52679.
 67. Fawcett JW, Asher RA. The glial scar and central nervous system repair. *Brain Res Bull*. 1999;49(6):377-391. doi:10.1016/S0361-9230(99)00072-6
 68. Raivich, G.; Bohatschek, M.; Kloss, C.U.A.; Werner, A.; Jones, L.J.; Kreutzberg GW. Neuroglial activation repertoire in the injured brain: graded response, molecular mechanisms, and cues to physiological function. *Brain Res Rev*. 1999;30(1):77-105.
 69. McPherson, C.A.; Merrick, B.A.; Harry GJ. In Vivo Molecular Markers for Pro-inflammatory Cytokine M1 Stage and Resident Microglia in Trimethyltin-Induced Hippocampal Injury. *Neurotox Res*. 2014;25(1):45-56.
 70. Schafer, D.P.; Stevens B. Microglia function in central nervous system development and plasticity. *Cold Spring Harb Perspect Biol*. 2015;7(10):a020545.
 71. Kotter, M.R.; Li, W.W.; Zhao, C.; Franklin RJ. Myelin impairs CNS remyelination by inhibiting oligodendrocyte precursor cell differentiation. *J Neuorscience*. 2006;26(1):328-332.
 72. Lampron, A.; Larochelle, A.; Laflamme, N.; Prefontaine, P.; Plante, M.M.; Sanchez, M.G.; Yong, W.; Stys, P.K.; Tremblay, M.E.; Rivest S. Inefficient clearance of myelin debris by microglia impairs remyelinating processes. *J Exp Med*. 2015;212(4):481-495.
 73. Ajami, B.; Bennett, J.L.; Krieger, C.; McNagny, K.M.; Rossi FM. Infiltrating monocytes trigger EAE progression, but do not contribute to the resident microglia pool. *Nat Neurosci*. 2011;14(9):1142.
 74. Olah, M.; Amor, S.; Brouwer, N.; Vinet, J.; Eggen, B.; Biber, K.; Hendrikus WGM. Identification of a microglia phenotype supportive of remyelination. *Glia*. 2012;60:306-321.
 75. Getts, D.R; Terry, R.L.; Getts, M.T.; Muller, M.; Rana, S.; Shrestha, B.; Radford, J.; Rooijen, N.V.; Campbell, I.L.; King NJC. Ly6c+ “inflammatory monocytes” are microglial precursors recruited in a pathogenic manner in West Nile virus encephalitis. *J Exp Med*. 2008;205(10):2319-2337.
 76. Lee, S.K.; Wolfe SW. Peripheral Nerve Injury and Repair. *JAAOS-Journal Am Acad Orthop Surg*. 2000;8(4):243-252.
 77. Kandel ER, Schwartz, James H, Jessell TM, Siegelbaum SA, Hudspeth AJ. *Principles Of Neural Science.*; 2013. doi:10.1036/0838577016

78. Massey, J.M.; Amps, J.; Viapiano, M.S.; Matthews, R.T.; Wagoner, M.R.; Whitaker, C.M.; Alilain, W.; Yonkof, A.L.; Khalyfa, A.; Cooper, N.G.F.; Silver, J.; Onifer SM. Increased chondroitin sulfate proteoglycan expression in denervated brainstem targets following spinal cord injury creates a barrier to axonal regeneration overcome by chondroitinase ABC and neurotrophin-3. *Exp Neurol*. 2008;209:426-445.
79. Jarius, S.; Wildemann B. The history of neuromyelitis optica. *J Neuroinflammation*. 2013;10(8).
80. Prineas, J.W.; Lee S. Multiple Sclerosis: Destruction and Regeneration of Astrocytes in Acute Lesions. *J Neuropathol Exp Neurol*. 2019;78(2):140-156.
81. Brown, A.W.; Brierley JB. Anoxic-ischaemic cell change in rat brain light microscope and fine-structural observations. *J Neurol Sci*. 1972;16(1):59-84.
82. Schreiner, B.; Romanelli, E.; Liberski P. et al. Astrocyte depletion impairs redox homeostasis and triggers neuronal loss in the adult. *Cell Rep*. 2015;12:1377-1384.
83. Fitch, M.T.; Silver J. Activated macrophages and the blood-brain barrier: inflammation after CNS injury leads to increase in putative inhibitory molecules. *Exp Neurol*. 1997;148(2):587-603.
84. Pindzola, R.R.; Doller, C.; Silver J. Putative inhibitory extracellular matrix molecules at the dorsal root entry zone of the spinal cord during development and after root and sciatic nerve lesions. *Dev Biol*. 1993;156(1):34-48.
85. Jones, L.L.; Margolis, R.U.; Tuszynski MH. The chondroitin sulfate proteoglycans neurocan, brevican, phosphacan, and versican are differentially regulated following spinal cord injury. *Exp Neurol*. 2003;182:399-411.
86. Jones, L.L.; Sajed, D.; Tuszynski MH. Axonal regeneration through regions of chondroitin sulfate proteoglycan deposition after spinal cord injury: a balance of permissiveness and inhibition. *J Neurosci*. 2003;23:9276-9288.
87. Ray, S.K.; Dixon, C.E.; Banik N. Molecular mechanisms in the pathogenesis of traumatic brain injury. *Histol Histopathol*. 2002;17(4):1137-1152.
88. Galtrey, C.M.; Fawcett JW. The role of chondroitin sulfate proteoglycans in regeneration and plasticity in the central nervous system. *Brain Res Rev*. 2007;54(1):1-18.
89. Fidler, P.S.; Schuette, K.; Asher, R.A.; Dobbertim, A.; Thornton, S.R.; Calle-Pantino Y. et. al. Comparing astrocytic cell lines that are inhibitory or permissive for axon growth: the major axon-inhibitory proteoglycan

- is NG2. *J Neurosci.* 1999;19(20):8778-8788.
90. Correale, J.; Farez MF. The role of astrocytes in multiple sclerosis progression. *Front Neurol.* 2015;6:180.
 91. Tom, V.J.; Steinmetz, M.P.; Miller, J.H.; Doller, C.M.; Silver J. Studies on the development and behavior of the dystrophic growth cone, the hallmark of regeneration failure, in an in vitro model of the glial scar and after spinal cord injury. *J Neurosci.* 2004;24:6531-6539.
 92. Fitch MT, Silver J. CNS injury, glial scars, and inflammation: Inhibitory extracellular matrices and regeneration failure. *Exp Neurol.* 2008;209(2):294-301. doi:10.1016/j.expneurol.2007.05.014
 93. Schizas N, Rojas R, Kootala S, et al. Hyaluronic acid-based hydrogel enhances neuronal survival in spinal cord slice cultures from postnatal mice. *J Biomater Appl.* 2014;28(6):825-836. doi:10.1177/0885328213483636
 94. Anderson MA, Burda JE, Ren Y, et al. Astrocyte scar formation AIDS central nervous system axon regeneration. *Nature.* 2016;532(7598):195-200. doi:10.1038/nature17623
 95. Hara M et. al. Interaction of reactive astrocytes with type I collagen induces astrocytic scar formation through the integrin-N-cadherin pathway after spinal cord injury. *Nat Med.* 2017;23(7):818.
 96. Adams, K.L.; Gallo V. The diversity and disparity of the glial scar. *Nat Neurosci.* 2018;21:9-15.
 97. Abu-Rub, M.; Miller RH. Emerging Cellular and Molecular Strategies for Enhancing Central Nervous System (CNS) Remyelination. *Brain Sci.* 2018;8(6):111.
 98. Kessaris, N.; Fogarty, M.; Iannarelli, P.; Grist, M.; Wegner, M.; Richardson WD. Competing waves of oligodendrocytes in the forebrain and postnatal elimination of an embryonic lineage. *Nat Neurosci.* 2006;9:173-179.
 99. Richardson, W.D.; Kessaris, N.; Pringle N. Oligodendrocyte wars. *Nat Rev Neurosci.* 2006;7:11-18.
 100. Tripathi, R.B.; Clarke, L.E.; Burzomato V. et. al. Dorsally and ventrally derived oligodendrocytes have similar electrical properties but myelinate preferred tracts. *J Neurosci.* 2011;31:6809-6819.
 101. de Castro, F.; Ana, B.; Ortega MC. Regulation of oligodendrocyte precursors migration during development, in adulthood and in pathology. *Cell Mol life Sci.* 2013;70(22):4355-4368.
 102. Barres, B.A.; Hart, I.K.; Coles, H.S.R.; Burne, J.F.; Voyvodic, J.T.; Richardson, W.D.; Raff MC. Cell death and control of cell survival in the oligodendrocyte lineage. *Cell.* 1992;70(1):31-46.
 103. Miller, R.H.; Dinsio, K.; Wang, R.; Geertman, R.; Maier, C.E.; Hall AK. Patterning of spinal cord

- oligodendrocyte development by dorsally derived BMP4. *J Neurosci Res.* 2004;76:9-19.
104. Orenta, D.M.; Hayes, J.E.; Dyer, K.L.; Miller RH. Sonic hedgehog signaling is required during the appearance of spinal cord oligodendrocyte precursors. *Development.* 1999;126:2419-2429.
105. Rowitch DH. Glial specification in the vertebrate neural tube. *Nat Rev Neurosci.* 2004;5(5):409.
106. Kuhlbrodt, K.; Herbarth, B.; Sock, E.; Hermans-Borgmeyer, I.; Wegner M. Sox10, a novel transcriptional modulator in glial cells. *J Neurosci.* 1998;18:237-250.
107. Zhao, X.; He, X.; Han, X.; Yu, Y.; Ye, F.; Chen, Y.; Hoang, T.; Xu, X.; Mi, Q.S.; Xin M et. al. MicroRNA-mediated control of oligodendrocyte differentiation. *Neuron.* 2010;65:612-626.
108. Fancy, S.P.; Zhao, C.; Franklin RJ. Increased expression of Nkx2.2 and Olig2 identifies reactive oligodendrocyte progenitor cells responding to demyelination in the adult CNS. *Mol Cell Neurosci.* 2004;27:247-254.
109. Karadottir, R.; Cavelier, P.; Bergensen, L.H.; Attwell D. NMDA receptors are expressed in oligodendrocytes and activated in ischaemia. *Nature.* 2005;438:1162-1166.
110. Karadottir, R.; Attwell D. Neurotransmitter receptors in the life and death of oligodendrocytes. *Neuroscience.* 2007;145:1426-1438.
111. Karadottir, R.; Hamilton, N.B.; Bakiri, Y.; Attwell D. Spiking and nonspiking classes of oligodendrocyte precursor glia in CNS white matter. *Nat Neurosci.* 2008;11:450-456.
112. Ziskin, J.L.; Nishiyama, A.; Rubio, M.; Fukaya, M.; Bergles DE. Vesicular release of glutamate from unmyelinated axons in white matter. *Nat Neurosci.* 2007;10:321-330.
113. Mangin, J.M.; Li, P.; Scafidi, J.; Gallo V. Experience-dependent regulation of NG2 progenitors in the developing barrel cortex. *Nat Neurosci.* 2012;15:1192-1194.
114. Tsai, H.H.; Niu, J.; Munji, R.; Davalos, D.; Chang, J.; Zhang, H.; Tien, A.C.; Kuo, C.J.; Chan, J.R.; Daneman, R.; Fancy SP. Oligodendrocyte precursors migrate along vasculature in the developing nervous system. *Science (80-).* 2016;351(6271):379-384.
115. Fancy, S.P.; Baranzini, S.E.; Zhao, D.I.; Yuk, K.A.; Irvine, S.; Kaing, N.; Sanai, R.J.; Franklin, D.; Rowitch H. Dysregulation of the Wnt pathway inhibits timely myelination and remyelination in the mammalian CNS. *Genes Dev.* 2009;23(13):1571-1585.
116. Kirby, B.B.; Takada, N.; Latimer, A.J.; Shin, J.; Carney, T.J.; Kelsh, R.N.; Appel B. In vivo time-lapse

- imaging shows dynamic oligodendrocyte progenitor behavior during zebrafish development. *Nat Neurosci.* 2006;9(12):1506.
117. Plemel, J.R.; Liu, W.Q.; Yong VW. Remyelination therapies: a new direction and challenge in multiple sclerosis. *Nat Rev Drug Discov.* 2017;16:617-634.
118. Marques, S.; Zeisel, A.; Codeluppi, S.; van Bruggen, D.; Falcao, A.M.; Xiao, L.; Huiliang L. Oligodendrocyte heterogeneity in the mouse juvenile and adult central nervous system. *Science (80-).* 2016;352(6291):1326-1329.
119. Tomassy, G.S.; Berger, D.R.; Chen, H.H.; Kasthuri, N.; Hayworth, K.J.; Vercelli A et. al. Distinct profiles of myelin distribution along single axons of pyramidal neurons in the neocortex. *Science (80-).* 2014;344:319-324.
120. Hughes, E.G.; Kang, S.H.; Fukaya, M.; Bergles DE. Oligodendrocyte progenitors balance growth with self-repulsion to achieve homeostasis in the adult brain. *Nat Neurosci.* 2013;16:668-676.
121. Rosenberg, S.S.; Kelland, E.E.; Tokar, E.; Asia, R.; Chan JR. The geometric and spatial constraints of the microenvironment induce oligodendrocyte differentiation. *Proc Natl Acad Sci.* 2008.
122. Bogler, O.; Wren, D.; Barnett, S.C.; Land, H.; Noble M. Cooperation between two growth factors promotes extended self-renewal and inhibits differentiation of oligodendrocyte-type-2 astrocyte (O-2 A) progenitor cells. *Proc Natl Acad Sci.* 1990;87(16):6368-6372.
123. Gautier, H.O.B.; Evans, K.A.; Volbracht, K.; James, R.; Sitnikov, S.; Lundgaard, I.; James, F.; Lao-Peregrin, C.; Reynolds, R.; Franklin, R.J.M.; Karadottir RT. Neuronal activity regulates remyelination via glutamate signalling to oligodendrocyte progenitors. *Nat Commun.* 2015;6:8518.
124. Sim, F.J.; Zhao, C.; Penderis, J.; Franklin RJM. The age-related decrease in CNS remyelination efficiency is attributable to an impairment of both oligodendrocyte progenitor recruitment and differentiation. *J Neurosci.* 2002;22:2451-2459.
125. Kuhlmann T et. al. Differentiation block of oligodendroglial progenitor cells as a cause for remyelination failure in chronic multiple sclerosis. *Brain.* 2008;131:1749-1758.
126. Wang, Y.; Cheng, X.; He, Q.; Zheng, Y.; Kim, D.H.; Whittemore, S.R.; Cao QL. Astrocytes from the contused spinal cord inhibit oligodendrocyte differentiation of adult oligodendrocyte precursor cells by increasing the expression of bone morphogenetic proteins. *J Neurosci.* 2011;31(16):6053-6058.

127. Altman, J.; Das GD. Autoradiographic and histological evidence of postnatal hippocampal neurogenesis in rats. *J Comp Neurol*. 1965;124(3):319-335.
128. Altman J. Autoradiographic and histological studies of postnatal neurogenesis. IV. Cell proliferation and migration in the anterior forebrain, with special reference to persisting neurogenesis in the olfactory bulb. *J Comp Neurol*. 1969;137(4):433-457.
129. Reynolds, B.A.; Weiss S. Generation of neurons and astrocytes from isolated cells of the adult mammalian central nervous system. *Science (80-)*. 1992;255(5052):1707-1710.
130. Richards, L.J.; Kilpatrick, T.J.; Bartlett PF. De novo generation of neuronal cells from the adult mouse brain. *Proc teh Natl Acad Sci*. 1992;89(18):8591-8595.
131. Zuchero, J.B.; Barres BA. Intrinsic and extrinsic control of oligodendrocyte development. *Curr Opin Neurobiol*. 2013;23(6):914-920.
132. Zuchero, J.B.; Barres BA. Glia in mammalian development and disease. *Development*. 2015;142(22):3805-3809.
133. Teng, Y.D.; Liao, W.L.; Choi H. et. al. Physical activity-mediated functional recovery after spinal cord injury: potential roles of neural stem cells. *Regen Med*. 2006;1(6):763-776.
134. Coutts, M.; Keirstead HS. Stem cells for the treatment of spinal cord injury. *Exp Neurol*. 2008;209(2):368-377.
135. Liu, S.; Qu, Y.; Stewart TJ et. al. Embryonic stem cells differentiate into oligodendrocytes and myelinate in culture and after spinal cord transplantation. *Proc Natl Acad Sci*. 2009;97(11):6126-6131.
136. Deshpande, D.M.; Kim, Y.S.; Martinez T et. al. Recovery from paralysis in adult rats using embryonic stem cells. *Ann Neurol*. 2006;60(1):32-44.
137. Nishikawa, S.; Goldstein, R.A.; Nierras CR. The promise of human induced pluripotent stem cells for research and therapy. *Nat Rev Mol Cell Biol*. 2008;9(9):725-729.
138. Parr, A.M.; Kulbatski, I.; Tator CH. Transplantation of adult rat spinal cord / progenitor cells for spinal cord injury. *J Neurotrauma*. 2007;24(5):835-845.
139. Nandoe, T.R.D.; Levi, H.A.; Grotenhuis, J.A.; Oudega M. Bone marrow stromal cells for repair of the spinal cord: towards clinical application. *Cell Transplant*. 2006;15(7):563-577.
140. Takami, T.; Oudega, M.; Bates, M.L.; Wood, P.M.; Kleitman, N.; Bunge MB. Schwann cell but not olfactory

- ensheathing glia transplants improve hindlimb locomotor performance in the moderately contused adult rat thoracic spinal cord. *J Neurosci*. 2002;22(15):6670-6681.
141. Raisman, G.; Li Y. Repair of neural pathways by olfactory ensheathing cells. *Nat Rev Neurosci*. 2007;8(4):312-319.
 142. Ramon-Cueto A. Olfactory ensheathing glia transplantation into the injured spinal cord. *Prog Brain Res*. 2000;128:265-272.
 143. Hu, J.; Deng, L.; Wang, X.; Xu XM. Effects of extracellular matrix molecules on the growth properties of oligodendrocyte progenitor cells in vitro. *J Neurosci Res*. 2009;87(13):2854-2862.
 144. Douvaras, P.; Wang, J.; Zimmer, M.; Hanchuk, S.; O'Bara, M.A.; Sadiq, S.; Sim, F.J.; Goldman, J.; Fossati V. Efficient generation of myelinating oligodendrocytes from primary progressive multiple sclerosis patients by induced pluripotent stem cells. *Stem cell reports*. 2014;3(2):250-259.
 145. Torrente, Y.; Belicchi, M.; Marchesi, C.; D'antona, G.; Cogiamanian, F.; Pisati, M.; Gavina, M.; Giordano, R.; Tonlorenzi, R.; Fagiolari, G.; Lamperti C. Autologous transplantation of muscle-derived CD133+ stem cells in Duchenne muscle patients. *Cell Transplant*. 2007;16(6):563-577.
 146. Crigler, L.; Robey, R.C.; Asawachaicharn, A.; Gaupp, D.; Phinney DG. Human mesenchymal stem cell subpopulations express a variety of neuro-regulatory molecules and promote neuronal cell survival and neuritogenesis. *Exp Neurol*. 2006;198(1):54-64.
 147. Ankeny, D.P.; McTigue, D.M.; Jakeman LB. Bone marrow transplants provide tissue protection and directional guidance for axons after contusive spinal cord injury in rats. *Exp Neurol*. 2004;190(1):17-31.
 148. Bai, L.; Lennon, D.P.; Eaton, V.; Maier, K.; Caplan, A.I.; Miller, S.D.; Miller RH. Human bone marrow-derived mesenchymal stem cells induce Th2-polarized immune response and promote endogenous repair in animal models of multiple sclerosis. *Glia*. 2009;57:1192-1203.
 149. Tam, R.Y.; Fuehrmann, T.; Mitrousis, N.; Shoichet MS. Regenerative therapies for central nervous system diseases: a biomaterials approach. *Neuropsychopharmacology*. 2014;39:169-188.
 150. Zimmermann, D.R.; Dours-Zimmermann MT. Detailed review describing the composition of the extracellular matrix of the CNS. *Histochem Cell Biol*. 2008;130:635-653.
 151. Khaing ZZ, Seidlits SK. Hyaluronic acid and neural stem cells: implications for biomaterial design. *J Mater Chem B*. 2015;3(40):7850-7866. doi:10.1039/C5TB00974J

152. Li X, Katsanevakis E, Liu X, Zhang N, Wen X. Engineering neural stem cell fates with hydrogel design for central nervous system regeneration. *Prog Polym Sci.* 2012;37(8):1105-1129. doi:10.1016/j.progpolymsci.2012.02.004
153. Zhu, J.; Marchant RE. Design properties of hydrogel tissue-engineering scaffolds. *Expert Rev Med Devices.* 2011;8(5):607-626.
154. Tibbitt, M.W.; Anseth KS. Hydrogels as extracellular matrix mimics for 3D cell culture. *Biotechnol Bioeng.* 2009;103:655-663.
155. Drury, J.L.; Mooney DJ. Hydrogels for tissue engineering scaffold design variable and applications. *Biomaterials.* 2003;24:4337-4351.
156. Tang, J.D.; Lampe KJ. From de novo peptides to native proteins: advancements in biomaterial scaffolds for acute ischemic stroke repair. *Biomed Mater.* 2018;13(3):034103.
157. Fuhrmann, T.; Tam, R.Y.; Ballarin, B.; Coles, B.; Donague, I.E.; van der Kooy, D.; Nagy, A.; Tator, C.H.; Morshead, C.M.; Shoichet MS. Injectable hydrogel promotes early survival of induced pluripotent stem cell-derived oligodendrocytes and attenuates longterm teratoma formation in a spinal cord injury model. *Biomaterials.* 2016;83:23-36.
158. Gudz, T.I.; Komuro, H.; Macklin WB. Glutamate stimulates oligodendrocyte progenitor migration mediated via an av integrin/myelin proteolipid protein complex. *J Neurosci.* 2006;26(9):2458-2466.
159. Carson, A.E.; Barker TH. Emerging concepts in engineering extracellular matrix variants for directing cell phenotype. *Regenerative Med.* 2009;4(4):593-600.
160. Barker TH. The role of ECM proteins and protein fragments in guiding cell behavior in regenerative medicine. *Biomaterials.* 2011;32(18):4211-4214.
161. Bellis SL. Advantages of RGD peptides for directing cell association with biomaterials. *Biomaterials.* 2011;32(18):4205-4210.
162. Mothe, A.J.; Tam, R.Y.; Zahir, T.; Tator, C.H.; Shoichet M. Repair of the injured spinal cord by transplantation of neural stem cells in a hyaluronan-based hydrogel. *Biomaterials.* 2013;34(15):3775-3783.
163. Itosaka, H.; Kuroda, S.; Shichinohe, H.; Yasuda, H.; Yano, S.; Kamei, S.; Kawamura, R.; Hida, K.; Iwasaki Y. Fibrin matrix provides a suitable scaffold for bone marrow stromal cells transplanted into injured spinal cord: a novel material for CNS tissue engineering. *Neuropathology.* 2009;29(3):248-257.

164. Hejcl, A.; Sedy, J.; Kapcalova, M.; Toro, D.A.; Amemori, T.; Lesny, P.; Likavcanova-Masinova K. et. al. HPMA-RGD hydrogels seeded with mesenchymal stem cells improve functional outcome in chronic spinal cord injury. *Stem Cells Dev.* 2010;19(10):1535-1546.
165. Kleinman, H.K.; Martin GR. Matrigel basement membrane matrix with biological activity. *Semin Cancer Biol.* 2005;15(5):378-386.
166. Hoffman-Kim, D.; Mitchel, J.A.; Bellamkonda RV. Topography, cell response, and nerve regeneration. *Annu Rev Biomed Eng.* 2010;12:203-231.
167. Flemming, R.G.; Murphy, C.J.; Abrams, G.A.; Goodman, S.L.; Nealey PF. Effects of synthetic micro- and nano- structure surfaces on cell behavior. *Biomaterials.* 1999;20:573-588.
168. Medberry, C.J.; Crapo, P.M.; Siu, B.F.; Carruthers, C.A.; Wolf, M.T.; Nagarkar, S.P.; Agrawal, V.; Jones, K.E.; Kelly, J.; Johnson, S.A.; Velankar, S.S.; Watkins, S.C.; Modo, M.; Badylak SF. Hydrogels derived from central nervous system extracellular matrix. *Biomaterials.* 2013;34(4):1033-1040.
169. Russell LN, Lampe KJ. Oligodendrocyte Precursor Cell Viability, Proliferation, and Morphology is Dependent on Mesh Size and Storage Modulus in 3D Poly(ethylene glycol)-Based Hydrogels. *Acs Biomater Sci Eng.* 2017;3(12):3459-3468. doi:10.1021/acsbomaterials.7b00374
170. King, V.R.; Alovskaya, A.; Wei, D.Y.; Brown, R.A.; Priestley JV. The use of injectable forms of fibrin and fibronectin to support axonal ingrowth after spinal cord injury. *Biomaterials.* 2010;31(15):4447-4456.
171. Piltti, K.M.; Funes, G.M.; Avakian, S.N.; Salibian, A.A.; Huang, K.I.; Carta, K.; Kamei, N.; Flanagan, L.A.; Monuki, E.S.; Uchida, N.; Cummings, B.J.; Anderson AJ. Increasing human neural stem cell transplantation dose alters oligodendroglial and neuronal differentiation after spinal cord injury. *Stem Cell Reports.* 2017;8(6):1534-1548.
172. Nisbet, D.R.; Forsythe, J.S.; Shen, W.; Finkelstein, D.I.; Horne MK. A review of the cellular response on electrospun nanofibers for tissue engineering. *J Biomater Appl.* 2009;24(1):7-29.
173. Lampe, K.J.; Mooney, R.G.; Bjugstad, K.B.; Mahoney MJ. Effect of macromer weight percent on neural cell growth in 2D and 3D nondegradable PEG hydrogel culture. *J Biomed Mater Res Part A.* 2010;94(4):1162-1171.
174. Gaillard, P.J.; Appeldoorn, C.C.M.; Rip, J.; Dorland, R.; van der Pol, S.M.A.; Kooij, G.; Vries, H.E. de; Reijerkerk A. Enhanced brain delivery of liposomal methylprednisolone improved therapeutic efficacy in a

- model of neuroinflammation. *J Control Release*. 2012;164:364-369.
175. Zimmermann, D.R.; Dours-Zimmermann MT. Extracellular matrix of the central nervous system: From neglect to challenge. *Histochem Cell Biol*. 2008;130(4):635-653.
176. Moshayedi, P.; Carmichael ST. Hyaluronan neural stem cells and tissue reconstruction after acute ischemic stroke. *Biomatter*. 2013;3(1):e23863.
177. Back, S.A.; Tuohy, T.M.; Chen, H.; Wallingford, N.; Craig, A.; Struve, J.; Luo NL. Hyaluronan Accumulates in Demyelinated Lesions and Inhibits Oligodendrocyte Progenitor Maturation. *Nat Med*. 2005;11(9):966.
178. Preston, M.; Gong, X.; Su, W.; Matsumoto, S.G.; Banine, F.; Winkler, C.; Foster S. Digestion Products of the PH20 Hyaluronidase Inhibit Remyelination. *Ann Neurol*. 2013;73(2):266-280.
179. Shrestha, B.; Coykendall, K.; Li, Y.; Moon, A.; Priyadarshani, P.; Yao L. Repair of injured spinal cord using biomaterial scaffolds and stem cells. *Stem Cell Res Ther*. 2014;5(4):91.
180. Jiang, D.; Liang, J.; Noble P w. Hyaluronan in tissue injury and repair. *Annu Rev Cell Dev Biol*. 2007;23:435-461.
181. Kubinova, S.; Horak, D.; Kozubenko, N.; Vanecek, V.; Proks, V.; Price, J.; Cocks, G.; Sykova E. The use of superporous Ac-CGGASIKVAVS-OH-modified PHEMA scaffolds to promote cell adhesion and the differentiation of human fetal neural precursors. *Biomaterials*. 2010;31(23):5966-5975.
182. Tysseling-Mattiace, V.M.; Sahni, V.; Niece, K.L.; Birch, D.; Czeisler, C.; Fehlings, M.G.; Stupp, S.I.; Kessler JA. Self-assembling nanofibers inhibit glial scar formation and promote axon elongation after spinal cord injury. *J Neurosci*. 2008;28(14):3814-3823.
183. Sun, Y.; Li, W.; Wu, X.; Zhang, N.; Zhang, Y.; Ouyang, S.; Song X. et. al. Functional self-assembling peptide nanofiber hydrogels designed for nerve degeneration. *ACS Appl Mater Interfaces*. 2016;8(3):2348-2359.
184. Tang, J.D.; Mura, C.; Lampe KJ. A stimuli-responsive, pentapeptide, nanofiber hydrogel for tissue engineering. *J Am Chem Soc*. 2019.
185. Tang, J.D.; Roloson, E.B.; Amelung, C.D.; Lampe KJ. Rapidly assembling pentapeptides for injectable delivery (RAPID) hydrogels as cytoprotective cell carriers. *ACS Biomater Sci Eng*. 2019.
186. Elkin, B.S.; Ilankovan, A.; Morrison B. Age-dependent regional mechanical properties of the rat hippocampus and cortex. *J Biomech Eng*. 2010;132(1):011010.
187. Budday, S.; Sommer, G.; Birkl, C.; Langkammer, C.; Haybaeck, J.; Kohnert, J.; Bauer, M.; Paulsen, F.;

- Steinmann, P.; Kuhl, E.; Holzapfel GA. Mechanical characterization of human brain tissue. *Acta Biomater.* 2017;48:319-340.
188. Chatelin, S.; Constantinesco, A.; Willinger R. Fifty years of brain tissue mechanical testing: from in vitro to in vivo investigations. *Biorheology.* 2017;47(5-6):255-276.
189. Franze, K.; Janmey, P.A.; Guck J. Mechanics in neuronal development and repair. *Annu Rev Biomed Eng.* 2013;15:227-251.
190. Rashid, B.; Destrade, M.; Gilchrist MD. Mechanical characterization of brain tissue in tension at dynamic strain rates. *J Mech Behav Biomed Mater.* 2014;33:43-54.
191. Mihai, L.A.; Chin, L.K.; Janmey, P.A.; Goriely A. A comparison of hyperelastic constitutive models applicable to brain and fat tissues. *J R Soc interface.* 2015;12:20150486.
192. Weickenmeier, J.; Rooij, R.; Budday, S.; Ovaert, T.C.; Kuhl E. The mechanical importance of myelination in the central nervous system. *J Mech Behav Biomed Mater.* 2017;76:119-124.
193. Chirst, A.F.; Franze, K.; Gautier, H.; Moshayedi, P.; Fawcett, J.; Franklin, R.J.; Karadottir, R.T.; Guck J. Mechanical difference between white and gray matter in the rat cerebellum measured by scanning force microscopy. *J Biomech.* 2010;43(15):2986-2992.
194. Feng, Y.; Clayton, E.H.; Chang, Y.; Okamoto, R.J.; Bayly PV. Viscoelastic properties of the ferret brain measured in vivo at multiple frequencies by magnetic resonance elastography. *J Biomech.* 2013;46:863-870.
195. Kruse, S.A.; Rose, G.H.; Glaser, K.J.; Manduca, A.; Felmlee, J.P.; Jack, C.R.; Ehman RL. Magnetic resonance elastography of the brain. *Neruoimage.* 2008;39:231-237.
196. Weickenmeier, J.; de Rooij, R.; Budday, S.; Steinmann, P.; Ovaert, T.C.; Kuhl E. Brain stiffness increases with myelin content. *Acta Biomater.* 2016;42:265-272.
197. Cunha, C.; Panseri, S.; Villa, O.; Silva, D.; Gelain F. 3D culture of adult mouse neural stem cells within functionalized self-assembling peptide scaffolds. *Int J Nanomedicine.* 2011;6:943-955.
198. Janmey, P.A.; Winer, J.P.; Murray, M.E.; Wen Q. The hard life of soft cells. *Cell Motil Cytoskeleton.* 2009;66(8):597-605.
199. Saha, K.; Keung, A.J.; Irwin, E.F.; Li, Y.; Little, L.; Schaffer DV. Substrate modulus directs neural stem cell behavior. *Biophys J.* 2008;95:4426-4438.
200. Balgude, A.P.; Yu, X.; Szymanski, A.; Bellamkonda RV. Agarose gel stiffness determines rate of DRG neurite

- extension in 3D cultures. *Biomaterials*. 2001;22:1077-1084.
201. Baumann, N.; Pham-Dinh D. Biology of oligodendrocyte and myelin in the mammalian central nervous system. *Physiol Rev*. 2001;81(2):871-927.
 202. Pek, Y.S.; Wan, A.C.A.; Ying JY. The effect of matrix stiffness on mesenchymal stem cell differentiation in a 3D thixotropic gel. *Biomaterials*. 2010;31(3):385-391.
 203. Lampe, K.J.; Bjugstad, K.B.; Mahoney MJ. Impact of degradable macromer content in a poly(ethylene glycol) hydrogel on neural cell metabolic activity, redox state, proliferation, and differentiation. *Tissue Eng Part A*. 2010;16(6):1857-1866.
 204. Keung, A.J.; Asuri, P.; Kumar, S.; Schaffer DV. Soft microenvironments promote the early neurogenic differentiation but not self-renewal of human pluripotent stem cells. *Integr Biol*. 2012;4(9):1049-1058.
 205. Urbanski, M.M.; Kingsbury, L.; Moussouros, D.; Kassim, I.; Mehjabeen, S.; Paknejad, N.; Melendez-Vasquez CV. Myelinating glia differentiation is regulated by extracellular matrix elasticity. *Sci Rep*. 2016;6:33751.
 206. Yao, L.; Phan, F.; Yongchao L. Collagen microsphere serving as a cell carrier supports oligodendrocyte progenitor cell growth and differentiation for neurite myelination in vitro. *Stem cell Res Ther*. 2013;4(5):109.
 207. Niu, J.; Mei, F.; Wang, L.; Liu, S.; Tian, Y.; Mo, W.; Li, H.; Lu, Q.R.; Xiao L. Phosphorylated olig1 localizes to the cytosol of oligodendrocytes and promotes membrane expansion and maturation. *Glia*. 2012;60(9):1427-1436.
 208. Buttery, P.C.; French-Constant C. Laminin-2/integrin interactions enhance myelin membrane formation by oligodendrocytes. *Mol Cell Nanosci*. 1999;14:199-212.
 209. Lourenco, T.; DeFaria, J.P.; Bippes, C.A.; Maia, J.; Lopes-da-Silve, J.A.; Relvas, J.B.; Graos M. Modulation of oligodendrocyte differentiation and maturation by combined biochemical and mechanical cues. *Sci Rep*. 2016;6:21583.
 210. Jagielska, A.; Norman, A.L; Whyte, G.; Van Vilet, K.J.; Guck. J.; Franklin RJM. Mechanical environment modulates biological properties of oligodendrocyte progenitor cells. *Stem Cells Dev*. 2012;21(16):2905-2914.
 211. Leipzig, N.D.; Shoichet MS. The effect of substrate stiffness on adult neural stem cell behavior. *Biomaterials*. 2009;30:6867-6878.
 212. Rinholm, J.E.; Hamilton, N.B.; Kessaris, N.; Richardson, W.D.; Bergersen, L.H.; Attwell D. Regulation of oligodendrocyte development and myelination by glucose and lactate. *J Neurosci*. 2011;31(2):538-548.

213. Smith, J.; Ladi, E.; Mayer-Proschel, M.; Noble M. Redox state is a central modulator of the balance between self-renewal and differentiation in a dividing glial precursor cell. *Proc Natl Acad Sci.* 2000;97(18):10032-10037.
214. Christopherson, G.T.; Song, H.; Mao HQ. The influence of fiber diameter of electrospun substrates on neural stem cell differentiation and proliferation. *Biomaterials.* 2009;30(4):556-564.
215. Shah, S.; Yin, P.T.; Uehara, T.M.; Chueng, S.T.D.; Yang, L.; Lee KB. Guiding stem cell differentiation into oligodendrocytes using graphene-nanofiber hybrid scaffolds. *Adv Mater.* 2014;26(22):3673-3680.
216. Schaub, N.J.; Johnson, C.D.; Cooper, B.; Gilbert RJ. Electrospun fibers for spinal cord injury research and regeneration. *J Neurotrauma.* 2016;33(15):1405-1415.
217. Yang, F.; Murugan, R.; Wang, S.; Ramakrishna S. Electrospinning of nano/micro scale poly(L-lactic acid) aligned fibers and their potential in neural tissue engineering. *Biomaterials.* 2005;26:2603-2610.
218. Bullock, P.N.; Rome LH. Glass micro-fibers: a model system for study of early events in myelination. *J Neurosci Res.* 1990;27:383-393.
219. Howe CL. Coated glass and vicryl microfibers as artificial axons. *Cells Tissues Organs.* 2006;183:180-194.
220. Lee, S.; Leach, M.K.; Redmond, S.A.; Chong, S.C.; Mellon, S.H.; Tuck, S.J.; Chan JR. A culture system to study oligodendrocyte myelination processes using engineered nanofibers. *Nat Methods.* 2012;9(9):917.
221. Lee, S.; Chong, S.Y.; Tuck, S.J.; Corey, J.M.; Chan JR. A rapid and reproducible assay for modeling myelination by oligodendrocytes using engineered nanofibers. *Nat Protoc.* 2013;8(4):771.
222. Emery B. Transcriptional and post-transcriptional control of CNS myelination. *Curr Opin Neurobiol.* 2010;20:601-607.
223. Bhalala, O.G.; Srikanth, M.; Kessler JA. The emerging roles of microRNAs in CNS injuries. *Nat Rev Neurol.* 2013;9:328-339.
224. He, X.; Yu, Y.; Awatramani, R.; Lu QR. Unwrapping myelination by microRNAs. *Neurosci.* 2012;18(1):45-55.
225. Zhao, X.; He, X.; Han, X.; Yu, Y.; Ye, F.; Chen Y et. al. MicroRNA-mediated control of oligodendrocyte differentiation. *Neuron.* 2010;65:612-626.
226. Diao, H.J.; Low, W.C.; Lu, Q.R.; Chew SY. Topographical effects on fiber-mediated microRNA delivery to control oligodendroglial precursor cells development. *Biomaterials.* 2015;70:105-114.

227. Diao, H.J.; Low, W.C.; Milbreta, U.; Lu, Q.R.; Chew SY. Nanofiber-mediated microRNA delivery to enhance differentiation and maturation of oligodendroglial precursor cells. *J Control Release*. 2015;208:85-92.
228. Yau, W.W.; Long, H.; Gauthier, N.C.; Chan, J.K.; Chew SY. The effects of nanofiber diameter and orientation on siRNA uptake and gene silencing. *Biomaterials*. 2014;37C:94-106.
229. Milbreta, U.; Lin, J.; Pinese, C.; Ong, W.; Chin, J.S.; Shirahama, H.; Mi, R.; Williams, A.; Bechler, M.E.; Wang, J.; French-Constant, C.; Hoke, A.; Chew SY. Scaffold-mediated sustained, non-viral delivery of miR-219/miR-338 promotes CNS remyelination. *Mol Ther*. 2019;27(2):411-423.
230. Espinosa-Hoyos, D.; Jagielska, A.; Homan, K.A.; Du, H.; Busbee, T.; Anderson, D.G.; Fang, N.X.; Lewis, J.A.; Van Vliet KJ. Engineered 3D-printed artificial axons. *Sci Rep*. 2018;8(1):478.
231. Horner PJ, Gage FH. Regenerating the damaged central nervous system. *Nature*. 2000;407(6807):963-970.
232. Thomas, A.M.; Seidlits, S.K.; Goodman, A.G.; Kukushliev, T.V.; Hassani, D.M.; Cummings, B.J.; Anderson, A.J.; Shea LD. Sonic hedgehog and neurotrophin-3 increase oligodendrocyte numbers and myelination after spinal cord injury. *Integr Biol*. 2014;6(7):694-705.
233. Levesque, S.G.; Shoichet MS. Synthesis of cell-adhesive dextran hydrogels and macroporous scaffolds. *Biomaterials*. 2006;27:5277-5285.
234. Choi, S.K.; Park, J.K.; Lee, K.M.; Lee, S.K.; Jeon WB. Improved neural progenitor cell proliferation and differentiation on poly (lactide-co-glycolide) scaffolds coated with elastin-like polypeptide. *J Biomed Mater Res Part B Appl Biomater*. 2013;101(8):1329-1339.
235. Lampe, K.J.; Antaris, A.L.; Heilshorn SC. Design of three-dimensional engineered protein hydrogels for tailored control of neurite outgrowth. *Acta Biomater*. 2013;9:5590-5599.
236. Madl, C.M.; LeSavage, B.L.; Dewi, R.E.; Dinh, C.B.; Stowers, R.S.; Khariton, M.; Lampe, K.J.; Nguyen, D.; Chaudhuri, O.; Enejder, A.; Heilshorn SC. Maintenance of neural progenitor cell stemness in 3D hydrogels requires matrix remodeling. *Nat Mater*. 2017;16(12):1233.
237. Butt, A.M.; Berry M. Oligodendrocytes and the control of myelination in vivo: new insights from the rat anterior medullary velum. *J Neurosci Res*. 2000;59(4):477-488.
238. Schwarz, D.S.; Hutvagner, G.; Du, T.; Xu, Z.; Aronin, N.; Zamore PD. Asymmetry in the assembly of the RNAi enzyme complex. *Cell*. 2003;115(2):119-208.
239. Caplan, A.I.; Dennis JE. Mesenchymal stem cells as trophic mediators. *J Cell Biochem*. 2006;98(5):1076-

- 1084.
240. Pluchino, S.; Quattrini, A.; Brambilla, E.; Gritti, A.; Salani, G.; Dina, G.; Galli, R.; Del Carro, U.; Amadio, S.; Bergami, A.; Furlan R. Injection of adult neurospheres induces recovery in a chronic model of multiple sclerosis. *Nature*. 2003;422(6933):688.
241. Pezawas, L.; Meyer-Lindenberg, A.; Drabant, E.M.; Verchinski, B.A.; Munoz, K.E.; Kolachana, B.S.; Weinberger DR. 5-HTTLPR polymorphism impacts human cingulate-amygdala interactions: a genetic susceptibility mechanism for depression. *Nat Neurosci*. 2005;8(6):828.
242. Aharonowiz, M.; Einstein, O.; Fainstein, N.; Lassmann, H.; Reubinoff, B.; Ben-Hur T. Neuroprotective effect of transplanted human embryonic stem cell-derived neural precursors in an animal model of multiple sclerosis. *PLoS One*. 2008;3(9):e3145.
243. Victorio, S.C.S.; Havton, L.A.; Oliveira ALR. Absence of IFN gamma expression induces neuronal degeneration in the spinal cord of adult mice. *J Neuroinflammation*. 2010;7:77-90.
244. Zhang, L.; Ma, Z.; Smith, G.M.; Wen, X.; Pressman, Y.; Wood, P.M.; Xu XM. GDNF-enhanced axonal regeneration and myelination following spinal cord injury is mediated by primary effects on neurons. *Glia*. 2009;57(11):1178-1191.
245. Wylie, R.G.; Ahsan, S.; Aizawa, Y.; Maxwell, K.L.; Morshead, C.M.; Shoichet MS. Spatially controlled simultaneous patterning of multiple growth factors in three-dimensional hydrogels. *Nat Mater*. 2011;10(10):799.
246. Owen, S.C.; Fisher, S.A.; Tam, R.Y.; Nimmo, C.M.; Shoichet MS. Hyaluronic acid click hydrogels emulate the extracellular matrix. *Langmuir*. 2013;29:7393-7400.
247. Jain, A.; Kim, Y.T.; McKeon, R.J.; Bellamkonda RV. In situ gelling hydrogels for conformal repair of spinal cord defects, and local delivery of BDNF after spinal cord injury. *Biomaterials*. 2006;27(3):497-504.
248. Bechler, M.E.; Byrne, L.; Ffrench-Constant C. CNS myelin sheath lengths are an intrinsic property of oligodendrocytes. *Curr Biol*. 2015;25(18):2411-2416.
249. Popovic, N.; Brundin P. Therapeutic potential of controlled drug delivery systems in neurodegenerative diseases. *Int J Pharm*. 2006;314(2):120-126.
250. Fournier, E.; Passirani, C.; Montero-Menei, C.N.; Benoit JP. Biocompatibility of implantable synthetic polymeric drug carriers: focus on brain biocompatibility. *Biomaterials*. 2003;24(19):3311-3331.

251. Pinezich, M.R.; Russell, L.N.; Murphy, N.P.; Lampe KJ. Encapsulated oligodendrocyte precursor cell fate is dependent on PDGF-AA release kinetics in a 3D microparticle-hydrogel drug delivery system. *J Biomed Mater Res Part A*. 2018;106(9):2402-2411.
252. Egawa, N.; Shindo, A.; Liang, A.C.; Du, Y.; Xing, C.; Lo, E.K.; Itoh, K.; Kinoshita, H.; Maki, T.; Takahashi, R.; Sudo, R.; Spector, M.; Lok, J.; Arai K. A novel three-dimensional culture system for oligodendrocyte precursor cells. *Stem Cells Dev*. 2017;26(14):1078-1085.
253. Sedilits, S.K.; Liang, J.; Bierman, R.D.; Sohrabi, A.; Karam, J.; Holley, S.M.; Cepeda, C.; Walthers CM. Peptide-Modified, Hyaluronic Acid-Based Hydrogels as a 3D Culture Platform for Neural Stem / Progenitor Cell Engineering. *J Biomed Mater Res Part A*. 2019;107(4):704-718.
254. Xiao, W.; Wang, S.; Zhang, R.; Sohrabi, A.; Yu, Q.; Liu, S.; Ehsanipour, A.; Liang, J.; Bierman, R.D.; Nathanson, D.A.; Seidlits SK. Bioengineered scaffolds for 3D culture demonstrate extracellular matrix-mediated mechanisms of chemotherapy resistance in glioblastoma. *Matrix Biol*. 2019.
255. Wen, H.; Xiao, W.; Biswas, S.; Cong, Z.; Liu, X.M.; Lam, K.S.; Liao, Y.H.; Deng W. An alginate hydrogel modified with a ligand interacting with $\alpha 3\beta 1$ integrin receptor promotes the differentiation of 3D neural spheroids towards oligodendrocytes in vitro. *ACS Appl Mater Interfaces*. 2019.
256. Rodrigues GMC et. al. Defined and scalable differentiation of human oligodendrocyte precursors from pluripotent stem cells in a 3D culture system. *Stem cell reports*. 2017;8(6):1770-1783.
257. Hyysalo, A.; Ristola, M.; Joki, T.; Honkanen, M.; Vippola, M.; Narkilahti S. Aligned poly (e-caprolactone) nanofibers guide the orientation and migration of human pluripotent stem cell-derived neurons, astrocytes, and oligodendrocyte precursor cells in vitro. *Macromol Biosci*. 2017;17(7):1600517.
258. Unal, D.B.; Caliarì, S.R.; Lampe KJ. Engineering Biomaterial Microenvironments to Promote Myelination in the Central Nervous System. *Brain Res Bull*. 2019.
259. Asmani MN, Ai J, Amoabediny G, Noroozi A. Three-dimensional culture of differentiated endometrial stromal cells to oligodendrocyte progenitor cells (OPCs) in fibrin hydrogel. *Cell Biol Int*. 2013;37(12):1340-1349. doi:10.1002/cbin.10171
260. Tabesh, H.; Amoabediny, G.H.; Nik, N.S.; Heydari, M.; Yoesfifard, M.; Siadat, S.R.; Mottaghy K. The role of biodegradable engineered scaffolds seeded with Schwann cells for spinal cord regeneration. *Neurochem Int*. 2009;54(2):73-83.

261. Isa, I.L.; Srivastava, A.; Tiernan, D.; Owens, P.; Rooney, P.; Dockery, P.; Pandit A. Hyaluronic acid based hydrogels attenuate inflammatory receptors and neurotrophins in interleukin-1B induced inflammation model of nucleus pulposus cells. *Biomacromolecules*. 2015;16(6):1714-1725.
262. Zong Lab Research: Challenges in Cancer Biology. <https://mic.med.virginia.edu/zong/research/>.
263. Burdick, J.A.; Chung, C.; Xinqiao, J.; Randolph, M.A.; Langer R. Controlled degradation and mechanical behavior of photopolymerized hyaluronic acid networks. *Biomacromolecules*. 2005;1:386-391.
264. Gramlich, W.M.; Kim, I.L; Burdick JA. Synthesis and orthogonal photopatterning of hyaluronic acid hydrogels with thiol-norbornene chemistry. *Biomaterials*. 2013;34(38):9803-9811.
265. Widjaja, L.K.; Bora, M.; Chan, P.N.P.H.; Lipik, V.; Wong, T.T.; Venkatraman SS. Hyaluronic acid-based nanocomposite hydrogels for ocular drug delivery applications. *J Biomed Mater Res Part A*. 2014;102(9):3056-3065.
266. Yang T. Mechanical and swelling properties of hydrogels. 2012.
267. Leach, J.B.; Bivens, K.A.; Patrick, C.W.; Schmidt CE. Leach, J.B.; Bivens, K.A.; Patrick, C.W.; Schmidt, C. E. (2003). Photocrosslinked Hyaluronic Acid Hydrogels: Natural, Biodegradable Tissue Engineering Scaffolds. *Biotechnology and Bioengineering*, 82(5), 578–589. Photocrosslinked Hyaluronic Acid Hydrogels: *. Biotechnol Bioeng*. 2003;82(5):578-589.
268. Ifkovits, J.L.; Sundararaghavan, H.G.; Burdick JA. Electrospinning fibrous polymer scaffolds for tissue engineering and cell culture. *J Vis Exp*. 2009;32.
269. Rampersad SN. Multiple applications of Alamar Blue as an indicator of metabolic function and cellular health in cell viability bioassays. *Sensors*. 2012;12(9):12347-12360.
270. alamarBlue Assay. http://tools.thermofisher.com/content/sfs/manuals/PI-DAL1025-1100_TI_alarBlue_Rev1.1.pdf.
271. Alberts, B.; Johnson, A.; Lewis, J.; Raff, M.; Roberts, K.; Walter P. *Molecular Biology of the Cell, 5th Ed.*; 2008.
272. Erickson HP. Size and shape of protein molecules at the nanometer level determined by sedimentation, gel filtration, and electron microscopy. *Biol Proced Online*. 2009;11(1):32.